

**SYNTHESIS, CHARACTERIZATION AND CATALYTIC
APPLICATIONS OF DIOXIDOMOLYBDENUM (VI) AND
DIOXIDOURANIUM (VI) COMPLEXES**

Ph.D. THESIS

by

BEKELE MENGESHA DOGIE



**DEPARTMENT OF CHEMISTRY
INDIAN INSTITUTE OF TECHNOLOGY ROORKEE
ROORKEE-247 667 (INDIA)
JANUARY, 2019**

**SYNTHESIS, CHARACTERIZATION AND CATALYTIC
APPLICATIONS OF DIOXIDOMOLYBDENUM (VI) AND
DIOXIDOURANIUM (VI) COMPLEXES**

A THESIS

*Submitted in partial fulfilment of the
requirement for the award of the degree*

of

DOCTOR OF PHILOSOPHY

in

CHEMISTRY

by

BEKELE MENGESHA DOGIE



**DEPARTMENT OF CHEMISTRY
INDIAN INSTITUTE OF TECHNOLOGY ROORKEE
ROORKEE-247 667 (INDIA)
JANUARY, 2019**



**©INDIAN INSTITUTE OF TECHNOLOGY ROORKEE, ROORKEE-2019
ALL RIGHTS RESERVED**



INDIAN INSTITUTE OF TECHNOLOGY ROORKEE

CANDIDATE'S DECLARATION

I hereby certify that the work which is being presented in the thesis entitled “**SYNTHESIS, CHARACTERIZATION AND CATALYTIC APPLICATIONS OF DIOXIDOMOLYBDENUM (VI) AND DIOXIDOURANIUM (VI) COMPLEXES**” in partial fulfillment of the requirements for the award of the Degree of Doctor of Philosophy and submitted in the Department of Chemistry of the Indian Institute of Technology Roorkee is an authentic record of my own work carried out during a period from July,2015 to January,2019 under the supervision of Dr. Mannar R. Maurya, Professor, Department of Chemistry, Indian Institute Of Technology Roorkee, Roorkee.

The matter presented in the thesis has not been submitted by me for the award of any other degree of this or any other Institute.

Signature of the Candidate

This is to certify that the above statement made by the candidate is correct to the best of my (our) knowledge.

Signature of Supervisor (s)

The Ph. D. Viva-Voce Examination Bekele Mengesha Dogie, Research Scholar, has been held on 12 April,2019.

Chairman, SRC

Signature of External Examiner

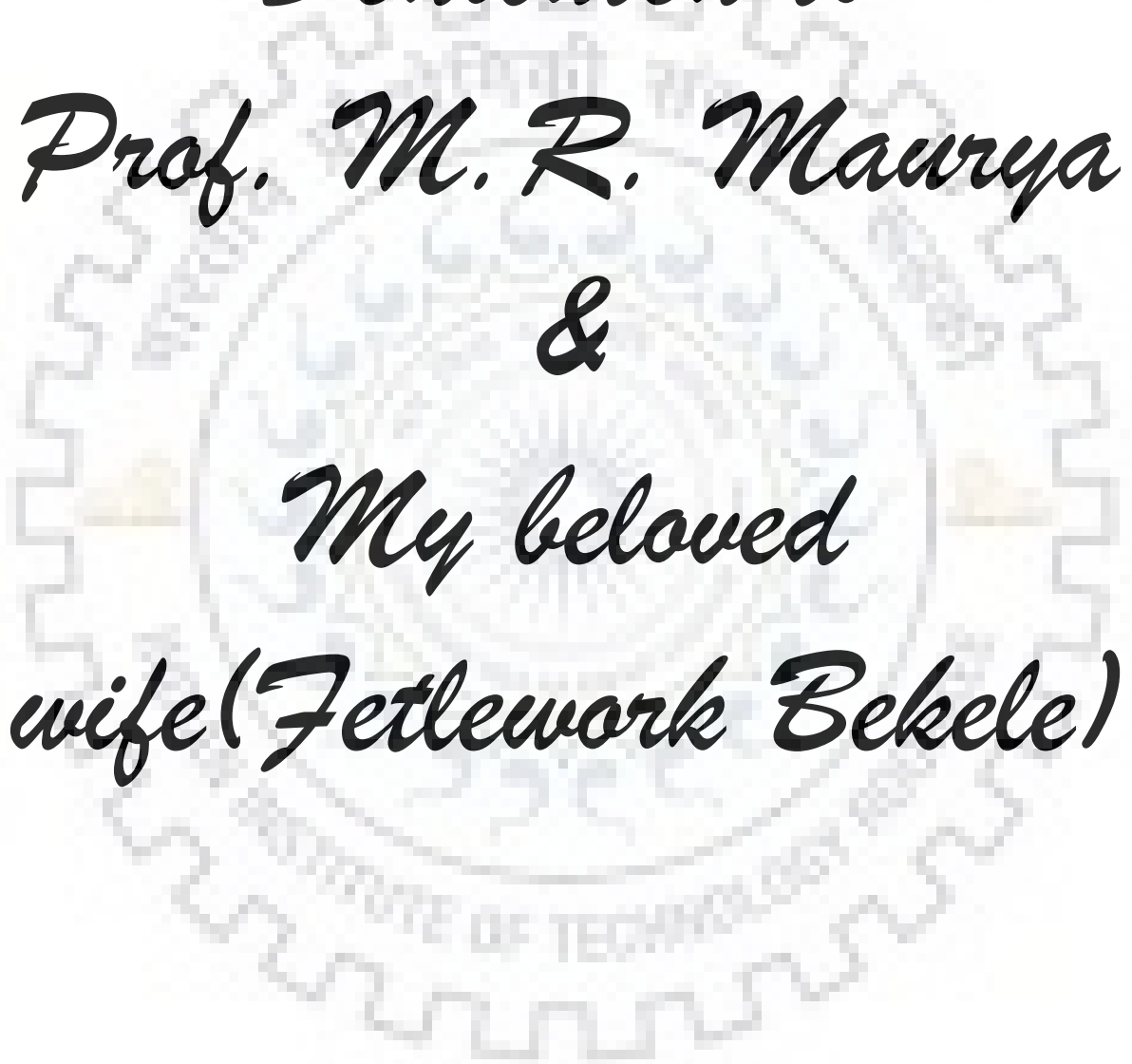
This is to certify that the student has made all the corrections in the thesis.

Signature of Supervisor (s)

Head of the Department

Date: _____

Dedicated to
Prof. M. R. Maurya
&
My beloved
wife (Fetlework Bekele)



ABSTRACT

Molybdenum metal belongs to the 6th group of Modern Periodic table, and has the symbol Mo with atomic number 42. It is a silvery white metal with a gray cast. It has sixth highest melting point in periodic table. The trace element molybdenum is one of the few second transition row metals which is known to involve in more than 50 molybdenum-containing enzymes till date and has well defined functions in biology. Most mononuclear molybdenum enzymes are unique in terms of their active site structure and consist of a Mo center bound to a novel pyranopterin cofactor via dithiolene moiety, except the nitrogenases where Mo is present along with iron in a sulfur linked cluster. The mononuclear molybdenum enzymes based on their active site structure has classified as: (i) molybdenum hydroxylases, (ii) eukaryotic oxotransferases and (iii) prokaryotic oxotransferases.

These Mo enzymes are involved in various metabolic processes of the host organism and the products of the catalytic cycles play vital roles in metabolism of the carbon, nitrogen and Sulphur. Molybdenum has been discovered as the essential element for animals and plants. Several physiological abnormalities are produced in human like cancer from its deficiency and excess supply. Molybdenum complexes exhibit anticancer, antibacterial, antifungal and antifertility activity. The presence of at least one Mo=O unit in the active sites of molybdo-enzymatic systems, they are referred as oxido-molybdenum enzymes and this inspired researchers to focus their research on the synthetic oxidomolybdenum complexes in homogeneous or heterogeneous systems in order to mimic the biological systems.

Among actinides, uranium is a silvery-white element having symbol U and atomic number 92. Uranium is a naturally occurring element which is found in low levels within all rock, soil, and water. The most common isotopes of naturally occurring uranium are U²³⁸ and U²³⁵. Most uses of uranium employ its unique nuclear properties like in nuclear power plants and nuclear weapons. The most important oxidation states exhibited

by uranium are uranium (IV) and uranium (VI), and exists in these states in the form of oxides, i.e. uranium (IV) dioxide (UO_2); and uranium (VI) trioxide (UO_3), respectively.

The coordination chemistry of uranium had been studied in nineties extensively but in the past one decade the coordination chemistry of uranium could not develop much like other transition metal ions possibly due to not much scope of the applications of coordination compounds of uranium. The most commonly used is no doubt the uranyl ion, $[\text{UO}_2]^{2+}$. The bonding in $[\text{UO}_2]^{2+}$ unit is very different, and is mainly due to the combination of d-p and f-p π interactions. The uranyl unit is highly stable to moisture and oxygen.

The extremely good catalytic activities rendered by molybdenum complexes and some recent catalytic results shown by uranium complexes encourages us to explore the chemistry and applications of molybdenum and uranium complexes built on aminobisphenol ligands. The coordination chemistry of aminobisphenol based ligands with different transition metals is well documented in the literature but their bio-catalytic/enzyme mimetic activity and catalytic activities are less explored. The structures and properties of the complexes vary greatly depending upon the precursors/conditions employed during synthesis; giving scope for exploring different geometries and coordination behavior around the metal center.

For convenience the work embodied in the thesis has been divided into following chapters:

First chapter is the introductory one and presents general remarks on synthesis, characterization and catalytic applications of molybdenum and uranium complexes of aminobis (phenol) based tetradentate ligands along with updated literature survey.

Chapter 2 presents the reaction of dibasic tetra dentate ONNO donor Mannich bases derived from ethylenediamine and 2,4-di-*tert*-butylphenol (H_2L^1) (**I**), 2,4-di-methylphenol (H_2L^2) (**II**), 2-*tert*-butyl-4-methylphenol (H_2L^3) (**III**), 2,4-di-chlorophenol (H_2L^4) (**IV**) and 2-naphthol (H_2L^5) (**V**) with $[\text{Mo}^{\text{VI}}\text{O}_2(\text{acac})_2]$ (Hacac = acetylacetonate) in a 1:1 molar ratio in refluxing MeOH. The obtained *cis*-dioxidomolybdenum (VI) complexes

are: $[\text{Mo}^{\text{VI}}\text{O}_2(\text{L}^1)]$ (**1**), $[\text{Mo}^{\text{VI}}\text{O}_2(\text{L}^2)]$ (**2**), $[\text{Mo}^{\text{VI}}\text{O}_2(\text{L}^3)]$ (**3**), $[\text{Mo}^{\text{VI}}\text{O}_2(\text{L}^4)]$ (**4**), and $[\text{Mo}^{\text{VI}}\text{O}_2(\text{L}^5)]$ (**5**), respectively. All complexes were characterized by elemental analysis, various spectroscopic (FT-IR, UV/Vis, ^1H and ^{13}C NMR) techniques and single-crystal X-ray analysis (of **1**, **2**, **3** and **5**). These complexes adopt a distorted six-coordinated octahedral geometry where ligands act as tetradentate, coordinating through the two $\text{O}_{\text{phenolate}}$ and two N_{amine} atoms in a *cis- α* type binding mode involving coordination of one of the N_{amine} atom in the apical position and one O_{oxido} terminal oxygen atom in the equatorial position. These complexes catalyze oxygen atom transfer between benzoin and dimethyl sulfoxide (DMSO) in acetonitrile at 80 °C. The formation of benzil could easily be monitored by HPLC. The electronic effect caused by the *para* substituent and the steric effect caused by the *ortho* substituent influence the formation of benzil and therefore conversion varied between 66 - 99% in 18 h of reaction time under optimized conditions; most active catalyst being $[\text{Mo}^{\text{VI}}\text{O}_2(\text{L}^5)]$. Almost similar trend has also been obtained with 4-chlorobenzoin. The pseudo first order rate constant for $[\text{Mo}^{\text{VI}}\text{O}_2(\text{L}^5)]$ was found to be 0.0998 h^{-1} . During catalytic reaction, the formation of the binuclear intermediate and its fast decay into the initial dioxidomolybdenum (VI) complex was established by time dependent UV/Vis studies.

The reaction of dibasic tetra dentate ONNO donor Mannich bases derived from ethylene diamine and 2,4-di-*tert*-butylphenol (H_2L^1) (**I**) and 2,4-di-methylphenol (H_2L^2) (**II**), 2-*tert*-butyl-4-methylphenol (H_2L^3) (**III**), and 2,4-di-chlorophenol (H_2L^4) (**IV**) with $\text{U}^{\text{VI}}\text{O}_2(\text{CH}_3\text{COO})_2 \cdot 2\text{H}_2\text{O}$ in a 1:1 molar ratio in refluxing MeOH gave the corresponding mononuclear *trans*-dioxidouranium(VI) complexes, $[\text{U}^{\text{VI}}\text{O}_2(\text{L}^1) \cdot \text{MeOH}]$ (**6**), $[\text{U}^{\text{VI}}\text{O}_2(\text{L}^2) \cdot \text{MeOH}]$ (**7**), $[\text{U}^{\text{VI}}\text{O}_2(\text{L}^3) \cdot \text{MeOH}]$ (**8**) and $[\text{U}^{\text{VI}}\text{O}_2(\text{L}^4) \cdot \text{MeOH}]$ (**9**), respectively. The synthesized complexes are stable in air, reddish-brown in color and soluble in most solvents. These complexes are characterized by elemental analysis, various spectroscopic (FT-IR, UV/Vis, ^1H and ^{13}C NMR) techniques and single-crystal X-ray analysis of **8** and **9**. The complexes adopt distorted pentagonal bipyramidal geometry around of metal centre. The ligand acts as tetra dentate, coordinated through two phenolato oxygen and two imino

nitrogen atoms; two oxido groups are *trans* to each other. These complexes are used as catalysts to study the oxidative bromination of thymol and styrene. The catalytic oxidative bromination of thymol resulted in the formation of three products namely, 2-bromothymol, 4-bromothymol and 2, 4-dibromothymol while oxidative bromination of styrene gave two products, 2-bromo-1-phenylethanol and 1-phenylethane-1, 2-diol. In order to find out the optimized reaction conditions for the fixed concentration (10 mmol) of substrate, effects of different amounts of catalyst, KBr, HClO₄, and oxidant (H₂O₂) have been investigated. Under the optimized reaction conditions, all the complexes have shown good catalytic potentials for the oxidative bromination of substrates, establishing the functional similarity to vanadium dependent haloperoxidases. All these details are presented in **Chapter 3**.

The stable dibasic tetra dentate ligand 1,4-bis-(2-hydroxy-3,5-dimethylbenzyl)piperazine (H₂pip-2,4-dmp, **VI**) prepared by reacting 2,4-dimethylphenol with piperazine in the presence of formaldehyde reacts with [Mo^{VI}O₂(acac)₂] and [U^{VI}O₂(CH₃COO)₂] in equimolar ratio to give neutral hexa-coordinated [Mo^{VI}O₂(pip-2,4-dmp)] (**10**) and hepta-coordinated [U^{VI}O₂(pip-2,4-dmp)(MeOH)] (**11**), respectively. **Chapter 4** presents details of these complexes. After characterizing these complexes by spectroscopic (IR, UV/Vis, ¹H and ¹³C NMR) data, elemental and thermal analyses (and single crystal X-ray diffraction study of uranium complex), they are used as catalysts to study the oxidative bromination of thymol. Such catalytic reactions are observed by many model vanadium complexes and are considered as a functional mimic of haloperoxidases. The catalytic oxidation resulted in the formation of three products namely, 2-bromothymol, 4-bromothymol and 2, 4-dibromothymol. The optimized reaction conditions are obtained considering concentration of substrate, KBr, HClO₄, and oxidant for the maximum yield of brominated products. Under the optimized reaction conditions, the product selectivity for both the prepared complexes is investigated. They are found to be competent homogeneous catalysts to afford the products in good yield.

Finally, summary and over all conclusions based on the achievements are presented.

Acknowledgements

“...the study of chemistry is profitable not only in as much as it promotes the material interest of mankind, but also because it furnishes us with insight into those wonders of creation, which immediately surround us and with which our existence, life and development, are most closely connected.”

Justus Von Liebig (1803 - 1873)

German Chemist

This thesis is the end of my journey in obtaining my Ph.D. I have not traveled in a vacuum in this scientific journey. This thesis has been kept on track and been seen through to completion with the support and encouragement of numerous people including my well-wishers, my friends, colleagues and various institutions. At the end of my thesis I would like to thank all those people who made this thesis possible. At the end of my thesis, it is a pleasant task to express my thanks to all those who contributed in many ways to the success of this study and made it an unforgettable experience for me.

At this moment of accomplishment, first of all I would like to express my sincere gratitude to my guide, Dr.M.R.Maurya (professor and Head, Department of Chemistry, IIT Roorkee) for his patience, motivation, enthusiasm, and immense knowledge. He always supported and guided me in my research work. I was very fortunate to have the chance to join his group in coordination chemistry laboratory & to work with him. I consider myself

extremely blessed to have worked under his scholarly guidance. I greatly benefited from his keen scientific insight and his ability to put complex ideas in to simple forms. I gained a lot from his vast chemistry knowledge & scientific curiosity. This work would not have been possible without his guidance, support and encouragement. Under his guidance I successfully overcame many difficulties and learned a lot.

A special thanks also goes to Mrs. Usha Maurya for providing me a homely environment with her love and care throughout my stay at IIT Roorkee.

I am thankful to Prof. Anil Kumar (former Head of the Department of Chemistry) for providing me with the basic facility. I would like to thank my SRC members Prof. U.P Singh, Dr. M. Sankar and Prof. R. prasad for their valuable suggestions and assistance from time to time.

I am also thankful to Prof. Fernando Avecilla, Departamnto de Química Fundamental, Facultad de Ciencias, Universidade da Coruña, Spain, for solving the Single Crystal X-ray analyses of my samples.

I would like to express sincerest thanks to my family who supported me throughout all the ups and downs of my life. I wish to thank my beloved wife, Fetlework Bekele Audo, for her love and affection, care, moral and material support and carrying out double responsibilities during my absence from home. She was my

inexhaustible sources of inspiration and energy and the pillar of my strength as well.

I want to thank all the academic, administrative and technicians' services for their collaboration.

Special thanks goes to my very unique friends Mr. Shailendra K. Maurya and Ms. Nidhi Sehrawat for their love, care, fun, cooperation and encouragement.

A very special thanks to my seniors and laboratory colleagues, Dr. Naveen Kumar, Dr. Neeraj Saini, Dr. Bhawna Uprety, Dr. Bithika Sarkar, and Dr. Lata Rana for their lively company and motivation for the completion of my scientific work. I would like to give my best wishes to my juniors Ms. Nancy Jangra, Ms. Reshu Tomar, Mr. Shailendra K. Maurya, Ms. Abhilasha Chauhan, Mr. Ved Prakash.

I would like to thank Dr. Surendra Saini for his motivation and help during my research work and his team members Dr. K. Kumar and Mr. Harish Kumar for their support.

I wish to thank my Ethiopian friends Mr. Abdulkadir Shube Hussen and Mrs. Muzey Bahta for their love, care, fun and friendship. I have spent best time with them. They gave me many happy and sweet memories.

I would like to acknowledge the Federal Democratic Republic of Ethiopia, Ministry of Education, for granting scholarship.

Finally, I would like to acknowledge all those whose names have not figured above, but have helped, supported and contributed to me in any form, directly or indirectly, during my this research work.

(Bekele Mengesha Dogie)



LIST OF FIGURES

- Figure 1.1.** Different mononuclear molybdenum enzymes based on their active site structures.
- Figure 1.2.** Dioxidomolybdenum(VI) complexes of chiral dibasic tetradentate Schiff base ligands their reduced analogues, linear and tripodal Mannich base ligands.
- Figure 1.3.** Two configurations: (a) C_2 -symmetric *cis- α* and (b) C_1 -asymmetric *cis- β* generally observed in chiral complexes.
- Figure 1.4.** Examples of molybdenum complexes having $\{MoO_2\}^{2-}$ core reported in literature.
- Figure 1.5.** Some common cores of higher nuclear molybdenum complexes.
- Figure 1.6.** Tridentate ligands resulting in dinuclear **36** and trinuclear **37** complexes.
- Figure 1.7.** Bidentate/tridentate ligands resulting in mononuclear **38** and dinuclear **39** complexes.
- Figure 1.8.** Synthesis and reactivity of dioxidomolybdenum(VI) complexes prepared from MoO_2Cl_2 .
- Figure 1.9.** Examples of dinuclear molybdenum complexes having varied cores.
- Figure 1.10.** Molybdenum complexes with unusual metal cores.
- Figure 1.11.** Dioxidouranium(VI) complexes of dibasic ONNO tetradentate N^1, N^4 -disalicyliden-*S*-alkyl-isothiosemicarbazone/ *S*-alkyl-thiosemicarbazone and related ligands.
- Figure 1.12.** Examples of dioxidouranium(VI) complexes.
- Figure 1.13.** Examples of di- and tri-nuclear dioxidouranium(VI) complexes.
- Figure 1.14.** Proposed overall catalytic cycle for the catalytic reduction of DMSO to DMS by DMSO reductases.
- Figure 1.15.** Aerobic oxidation of PMe_3 and PPh_3 to corresponding oxide (top) and oxygen atom transfer from dimethylsulfoxide to phosphines (below), catalyzed by *cis*-dioxidomolybdenum(VI) complexes.

- Figure 1.16.** Examples of olefins tested for their oxidation using molybdenum complexes as catalyst and their corresponding epoxides.
- Figure 1.17.** Examples of secondary alcohols that undergo oxidation using dioxidomolybdenum(VI) and oxidoperoxidomolybdenum(VI) complexes as catalysts.
- Figure 1.18.** Examples of bicyclic, cyclic and aromatic alcohols that undergo oxidation using dioxidomolybdenum(VI) complexes as catalysts. In some cases more than one product was obtained.
- Figure 1.19.** Examples of aliphatic and aromatic sulfides that undergo oxidation using dioxidomolybdenum(VI) complexes as catalysts.
- Figure 1.20.** Examples of substrates that undergo oxidative bromination using dioxidomolybdenum(VI) complexes as catalysts. Generally more than one product was identified in all cases.
- Figure 1.21.** Oxidation of benzoin to different products using dioxidomolybdenum(VI) complexes as catalysts.
- Figure 1.22.** Catalytically induced nucleophilic acyl substitution of acid anhydride.
- Figure 2.1.** ORTEP plot of complex $[\text{Mo}^{\text{VI}}\text{O}_2(\text{L}^1)]$ (**2.1**). All the non-hydrogen atoms are presented by their 50% probability ellipsoids.
- Figure 2.2.** ORTEP plot of complex $[\text{Mo}^{\text{VI}}\text{O}_2\text{L}^2]$ (**2.2**). All the non-hydrogen atoms are presented by their 50% probability ellipsoids.
- Figure 2.3.** ORTEP plot of complex $[\text{Mo}^{\text{VI}}\text{O}_2(\text{L}^3)]$ (**2.3**). All the non-hydrogen atoms are presented by their 50% probability ellipsoids.
- Figure 2.4.** ORTEP plot of complex $[\text{Mo}^{\text{VI}}\text{O}_2(\text{L}^5)]$ (**2.5**). All the non-hydrogen atoms are presented by their 50% probability ellipsoids.
- Figure 2.5.** X-ray fragment of $[\text{Mo}^{\text{VI}}\text{O}_2\text{L}^2]$ (**2.2**). C-H $\cdots\pi$ interactions in **2.2** are present in the crystal packing and they are drawn in dashed black lines.
- Figure 2.6.** View along b axis of the crystal packing of $[\text{Mo}^{\text{VI}}\text{O}_2(\text{L}^1)]$ (**2.1**). All the non-hydrogen atoms are presented by balls and sticks. Hydrogen atoms are omitted for clarity.
- Figure 2.7.** Crystal packing of $[\text{Mo}^{\text{VI}}\text{O}_2\text{L}^2]$ (**2.2**). All the non-hydrogen atoms are presented by balls and sticks. Hydrogen atoms are omitted for clarity.

- Figure 2.8.** Crystal packing of $[\text{Mo}^{\text{VI}}\text{O}_2(\text{L}^3)]$ (**2.3**). All the non-hydrogen atoms are presented by balls and sticks. Hydrogen atoms are omitted for clarity.
- Figure 2.9.** Crystal packing of $[\text{Mo}^{\text{VI}}\text{O}_2(\text{L}^5)]$ (**2.5**). All the non-hydrogen atoms are presented by balls and sticks. Hydrogen atoms are omitted for clarity.
- Figure 2.10.** UV/Vis spectra of complexes $[\text{Mo}^{\text{VI}}\text{O}_2\text{L}^{1-5}]$ (**2.1 - 2.5**).
- Figure 2.11.** ^1H NMR spectra of H_2L^2 and **2.2** in CDCl_3 .
- Figure 2.12.** ^1H NMR spectrum of H_2L^1 in CDCl_3 .
- Figure 2.13.** ^1H NMR spectrum of $[\text{MoO}_2\text{L}^1]$ in CDCl_3 .
- Figure 2.14.** ^1H NMR spectrum of H_2L^3 in CDCl_3 .
- Figure 2.15.** ^1H NMR spectrum of $[\text{Mo}^{\text{VI}}\text{O}_2\text{L}^3]$ in CDCl_3 .
- Figure 2.16.** ^1H NMR spectrum of H_2L^4 in DMSO-d_6 .
- Figure 2.17.** ^1H NMR spectrum of $[\text{Mo}^{\text{VI}}\text{O}_2\text{L}^4]$ in DMSO-d_6 .
- Figure 2.18.** ^1H NMR spectrum of H_2L^5 in DMSO-d_6 .
- Figure 2.19.** ^1H NMR spectrum of $[\text{Mo}^{\text{VI}}\text{O}_2\text{L}^5]$ in CDCl_3 .
- Figure 2.20.** ^{13}C NMR spectra [chemical shifts (δ) in ppm] of H_2L^1 and **2.1** in CDCl_3 .
- Figure 2.21.** The progress of the reaction as monitored by HPLC analysis of the reaction mixture at different time intervals using $[\text{Mo}^{\text{VI}}\text{O}_2(\text{L}^5)]$ (**2.5**) as the catalyst. Mobile phase: MeCN : H_2O : TFA 60 : 40 : 0.02 (for details, see text).
- Figure 2.22.** Results for oxygen atom transfer reaction between DMSO and benzoin catalyzed by *cis*- $[\text{MoO}_2]^{2+}$ complexes (for details, see text).
- Figure 2.23.** Hammet plot for OAT reaction between DMSO and benzoin catalyzed by *cis*- $[\text{MoO}_2]^{2+}$ complexes.
- Figure 2.24.** Results for oxygen atom transfer reaction between DMSO and 4-chlorobenzoin catalyzed by *cis*- $[\text{MoO}_2]^{2+}$ complexes (for details, see text).
- Figure 2.25.** Variation of [Benzoin] with time for the *cis*- $[\text{Mo}^{\text{VI}}\text{O}_2(\text{L}^5)]$ (**2.5**) catalysed oxygen atom transfer reaction in the presence of DMSO. Reaction

conditions: [Benzoin]₀ (5 mmol), DMSO (1.00 mL), catalyst (3.00 mg) and MeCN (10 mL).

- Figure 2.26.** Plot of $\ln k_1$ vs $\ln[\text{catalyst}]$ for oxido transfer reaction between benzoin and DMSO catalysed by $[\text{Mo}^{\text{VI}}\text{O}_2(\text{L}^5)]$ (**2.5**) at 80 °C for 18 h reaction time.
- Figure 2.27.** Time-dependent spectral changes observed in the OAT reaction between **2.4**, benzoin and DMSO in acetonitrile after 8 h of reaction time. The spectra were recorded every 10 s from 80 °C to room temperature.
- Figure 3.1.** ORTEP for the compound $[\text{U}^{\text{VI}}\text{O}_2(\text{L}^3)(\text{MeOH})]$ (**3.3**). All the non-hydrogen atoms are presented by their 50% probability ellipsoids. Hydrogen atoms are omitted for clarity.
- Figure 3.2.** ORTEP for the compound $[\text{U}^{\text{VI}}\text{O}_2(\text{L}^4)(\text{EtOH})]$ (**3.4**). All the non-hydrogen atoms are presented by their 50% probability ellipsoids. Hydrogen atoms are omitted for clarity.
- Figure 3.3.** Crystal packing in the compound $[\text{U}^{\text{VI}}\text{O}_2(\text{L}^3)(\text{MeOH})]$ (**3.3**). Drawing was done in ball and sticks.
- Figure 3.4.** Crystal packing in the compound $[\text{U}^{\text{VI}}\text{O}_2(\text{L}^4)(\text{EtOH})]$ (**3.4**). Drawing was done in ball and sticks.
- Figure 3.5.** UV-Visible spectra of **I – IV** recorded in MeCN.
- Figure 3.6.** UV-Visible spectra of dioxidouranium(VI) complexes (**3.1 – 3.4**) recorded in MeCN. (a) Recorded in the region 250-550 nm and (b) Expanded region of 300-600 nm with more concentrated solution.
- Figure 3.7.** ^{13}C NMR spectrum of $[\text{U}^{\text{VI}}\text{O}_2(\text{L}^4)(\text{EtOH})]$ (**3.4**). Spectrum below 50 ppm is not shown as this region mostly have solvent and water signals.
- Figure 3.8.** Effect of variation of amount of catalyst on the oxidative bromination of thymol. Reaction conditions: thymol (1.5g, 10 mmol), 30% aqueous H_2O_2 (10 mmol, 1.13 g), KBr (10 mmol, 1.19 g), and HClO_4 (10 mmol, 1.43 g) at room temperature.
- Figure 3.9.** Effect of variation of amount of oxidant on the oxidative bromination of thymol. Reaction conditions: thymol (1.5g, 10 mmol), catalyst $[\text{U}^{\text{VI}}\text{O}_2(\text{L}^2)(\text{MeOH})]$ (**3.2**) (0.002 g, 3.2×10^{-3} mmol), KBr (10 mmol, 1.19 g), and HClO_4 (10 mmol, 1.43 g) at room temperature.
- Figure 3.10.** Effect of varying amount of additive (KBr) on the oxidative bromination of thymol. Reaction conditions: thymol (1.5g, 10 mmol), catalyst

$[\text{U}^{\text{VI}}\text{O}_2(\text{L}^2)(\text{MeOH})]$ (**3.2**) (0.002 g, 3.2×10^{-3} mmol), 30% aqueous H_2O_2 (30 mmol, 3.39 g), and HClO_4 (10 mmol, 1.43 g) at room temperature.

- Figure 3.11.** Effect of varying amount of HClO_4 on oxidative bromination of thymol. Reaction conditions: thymol (1.5g, 10 mmol), catalyst $[\text{U}^{\text{VI}}\text{O}_2(\text{L}^2)(\text{MeOH})]$ (**3.2**) (0.002 g, 3.2×10^{-3} mmol), 30% aqueous H_2O_2 (30 mmol, 3.39 g), and KBr (30 mmol, 3.57 g), at room temperature.
- Figure 3.12.** Plot representing conversion of thymol in the presence of different $[\text{UO}_2]^{2+}$ complexes and without catalyst.
- Figure 3.13.** Effect of variation of amount of catalyst on the oxidative bromination of styrene. Reaction conditions: styrene (1.04 g, 10 mmol), 30% aqueous H_2O_2 (10 mmol, 1.13 g), KBr (10 mmol, 1.19 g), and HClO_4 (10 mmol, 1.43 g) at room temperature.
- Figure 3.14.** Effect of variation of amount of oxidant on the oxidative bromination of styrene. Reaction conditions: styrene (1.04g, 10 mmol), catalyst $[\text{U}^{\text{VI}}\text{O}_2(\text{L}^2)(\text{MeOH})]$ (**3.2**) (0.001g, 1.6×10^{-3} mmol), KBr (10 mmol, 1.19 g), and HClO_4 (10 mmol, 1.43 g) at room temperature.
- Figure 3.15.** Effect of varying amount of additive (KBr) on the oxidative bromination of styrene. Reaction conditions: styrene (1.04 g, 10 mmol), catalyst $[\text{U}^{\text{VI}}\text{O}_2(\text{L}^2)(\text{MeOH})]$ (**3.2**) (0.001 g, 1.6×10^{-3} mmol), 30% aqueous H_2O_2 (20 mmol, 2.26 g), and HClO_4 (10 mmol, 1.43 g) at room temperature.
- Figure 3.16.** Effect of varying amount of HClO_4 on oxidative bromination of styrene. Reaction conditions: styrene (1.04g, 10 mmol), catalyst $[\text{U}^{\text{VI}}\text{O}_2(\text{L}^2)(\text{MeOH})]$ (**3.2**) (0.001g, 1.6×10^{-3} mmol), 30% aqueous H_2O_2 (20 mmol, 2.26 g), and KBr (30 mmol, at room temperature.
- Figure 3.17.** Plot representing conversion of styrene in the presence of different $[\text{UO}_2]^{2+}$ complexes.
- Figure 3.18.** Plots representing the Spectral changes during titration of $[\text{U}^{\text{VI}}\text{O}_2(\text{L}^1)(\text{MeOH})]$ (**3.1**) with H_2O_2 . Spectra were obtained after successive addition of one drop portion 30% H_2O_2 (0.108 g, 0.95 mmol) dissolved in 5 mL of MeCN to 25 mL of 8.75×10^{-2} M solution of **3.1** in MeCN .
- Figure 3.19.** Plots representing the Spectral changes during titration of $[\text{U}^{\text{VI}}\text{O}_2(\text{L}^3)(\text{MeOH})]$ (**3.3**) with H_2O_2 . Spectra were obtained after successive addition of one drop portion 30% H_2O_2 (0.108 g, 0.95 mmol)

dissolved in 5 mL of MeCN to 25 mL of 7.7×10^{-2} M solution of **3.3** in MeCN.

Figure 3.20. Plots representing the Spectral changes during titration of $[\text{U}^{\text{VI}}\text{O}_2(\text{L}^4)(\text{MeOH})]$ (**3.4**) with H_2O_2 . Spectra were obtained after successive addition of one drop portion 30% H_2O_2 (0.108 g, 0.95 mmol) dissolved in 5 mL of MeCN to 25 mL of 6.48×10^{-2} M solution of **3.4** in MeCN.

Figure 3.21. Plots representing the spectral changes during titration of $[\text{U}^{\text{VI}}\text{O}_2(\text{L}^2)(\text{MeOH})]$ (**3.2**) with H_2O_2 . Spectra were obtained after successive addition of one drop portions of 30% H_2O_2 (0.108 g, 0.95 mmol) dissolved in 5 mL of MeCN to 25 mL of 9.97×10^{-2} M solution of **3.2** in MeCN.

Figure 4.1. TGA, DTA and DTG profiles of $[\text{U}^{\text{VI}}\text{O}_2(\text{pip-2,4-dmp})(\text{MeOH})]$ (**4.2**) under air atmosphere.

Figure 4.2. ORTEP for the compound $[\text{U}^{\text{VI}}\text{O}_2(\text{pip-2,4-dmp})(\text{DMSO})]$ (**4.2a**). All the non-hydrogen atoms are presented by their 50% probability ellipsoids. Hydrogen atoms are omitted for clarity.

Figure 4.3. Crystal packing of the compound $[\text{U}^{\text{VI}}\text{O}_2(\text{pip-2,4-dmp})(\text{DMSO})]$ (**4.2a**). Drawing was done in balls and sticks using SHELXL package. Hydrogen atoms are omitted for clarity.

Figure 4.4. UV-Visible spectra of $\text{H}_2\text{pip-2,4 dmp}$ and complexes, $[\text{Mo}^{\text{VI}}\text{O}_2(\text{pip-2,4 dmp})(\text{MeOH})]$ (**4.1**) and $[\text{U}^{\text{VI}}\text{O}_2(\text{pip-2,4 dmp})(\text{MeOH})]$ (**4.2**) recorded in MeCN.

Figure 4.5. ^1H NMR spectrum of ligand, $\text{H}_2\text{pip-2,4-dmp}$ (**4.1**).

Figure 4.6. ^1H NMR spectrum of $[\text{Mo}^{\text{VI}}\text{O}_2(\text{pip-2,4-dmp})]$ (**4.1**).

Figure 4.7. ^1H NMR spectrum of $[\text{U}^{\text{VI}}\text{O}_2(\text{pip-2,4-dmp})(\text{MeOH})]$ (**4.2**).

Figure 4.8. ^{13}C NMR spectra of $\text{H}_2\text{pip-2,4-dmp}$ (**4.1**) and $[\text{U}^{\text{VI}}\text{O}_2(\text{pip-2,4-dmp})(\text{MeOH})]$ (**4.2**).

Figure 4.9. Conversion of 10 mmol of thymol with varying amounts of $[\text{Mo}^{\text{VI}}\text{O}_2(\text{pip-2,4- dmp})]$ (**4.1**). Other reaction conditions (in mmol), substrate : H_2O_2 : KBr : HClO_4 ratios of 10 : 10 : 10 : 10.

Figure 4.10. Effect of oxidant on the oxidative bromination of 10 mmol of thymol using $[\text{Mo}^{\text{VI}}\text{O}_2(\text{pip-2,4-dmp})]$ (**4.1**) as catalyst. Other reaction conditions (in

mmol), substrate: catalyst : KBr : HClO₄ ratios of 10 : 4.16×10^{-3} : 10 : 10.

Figure 4.11. Effect of variation of KBr on the oxidative bromination of thymol using [Mo^{VI}O₂(pip-2,4-dmp)] (**4.1**) complex as catalyst. Other reaction conditions (in mmol), substrate : oxidant : catalyst : HClO₄ ratios of 10 : 10 : 4.16×10^{-3} : 10.

Figure 4.12. Effect of variation of HClO₄ on the oxidative bromination of thymol using [Mo^{VI}O₂(pip-2,4-dmp)] (**4.1**) complex as catalyst. Other reaction conditions (in mmol), substrate : oxidant : catalyst : KBr ratios of 10 : 10 : 4.16×10^{-3} : 10 : 10.

Figure 4.13. Conversion of thymol with varying amounts of [U^{VI}O₂(pip-2,4-dmp)(MeOH)] (**4.2**) as catalyst. Other reactions, Other reaction conditions (in mmol), substrate : H₂O₂ : KBr : HClO₄ ratios of 10 : 10 : 10 : 10.

Figure 4.14. Effect of oxidant on the oxidative bromination of thymol using [U^{VI}O₂(pip- 2,4- dmp)(MeOH)] (**4.2**) as a catalyst. Other reaction conditions (in mmol), substrate : catalyst : KBr : HClO₄ ratios of 10 : 4.8×10^{-3} : 10 : 10.

Figure 4.15. Effect of variation of KBr on the oxidative bromination of thymol using [U^{VI}O₂(pip-2,4-dmp)(MeOH)] (**4.2**) as catalyst. Other reaction conditions (in mmol), substrate: catalyst : KBr : HClO₄ ratios of 10 : 4.8×10^{-3} : 10 : 10.

Figure 4.16. Effect of variation of HClO₄ on the oxidative bromination of thymol using [U^{VI}O₂(pip-2,4-dmp)(MeOH)] (**4.2**) complex as catalyst. Other reaction conditions (in mmol), substrate : oxidant : catalyst : KBr ratios of 10 : 4.8×10^{-3} : 10 : 10.

Figure 4.17. Plots representing the spectral changes observed during the titration of [U^{VI}O₂(pip-2,4 dmp)(MeOH)] (**4.2**) with H₂O₂. Spectra were obtained after successive addition of one drop portion of 30% H₂O₂ (0.108 g, 0.95 mmol) dissolved in 5 mL of MeCN to 25 mL of 4.8×10^{-3} M solution of **4.2** in MeCN.

LIST OF TABLES

- Table 2.1.** Crystal data and structure refinement for $[\text{Mo}^{\text{VI}}\text{O}_2(\text{L}^1)]$ (2.1), $[\text{Mo}^{\text{VI}}\text{O}_2(\text{L}^2)]$ (2.2), $[\text{Mo}^{\text{VI}}\text{O}_2(\text{L}^3)]$ (2.3) and $[\text{Mo}^{\text{VI}}\text{O}_2(\text{L}^5)]$ (2.5). CCDC: 1573125-1573128.
- Table 2.2.** Bond lengths [\AA] and angles [$^\circ$] for $[\text{Mo}^{\text{VI}}\text{O}_2(\text{L}^1)]$ (2.1), $[\text{Mo}^{\text{VI}}\text{O}_2(\text{L}^2)]$ (2.2), $[\text{Mo}^{\text{VI}}\text{O}_2(\text{L}^3)]$ (2.3) and $[\text{Mo}^{\text{VI}}\text{O}_2(\text{L}^5)]$ (2.5).
- Table 2.3.** Hydrogen bonds for $[\text{Mo}^{\text{VI}}\text{O}_2(\text{L}^1)]$ (2.1), $[\text{Mo}^{\text{VI}}\text{O}_2(\text{L}^2)]$ (2.2) and $[\text{Mo}^{\text{VI}}\text{O}_2(\text{L}^3)]$ (2.3).
- Table 2.4.** Selected IR data (in cm^{-1}) for the ligands and complexes with tentative assignments.
- Table 2.5.** UV/Vis spectral data of ligands and complexes.
- Table 2.6.** ^{13}C NMR spectral data of ligands and complexes.
- Table 2.7.** Dioxidomolybdenum(VI) complexes catalyzed oxygen atom transfer between benzoin and DMSO in acetonitrile at 80°C in 18 h of reaction time; conversion, TOF and selectivity data.
- Table 2.8.** Dioxidomolybdenum(VI) complexes catalyzed oxygen atom transfer between 4-chlorobenzoin and DMSO in acetonitrile at 80°C in 18 h of reaction time; conversion, TOF and selectivity data.
- Table 3.1.** Crystal Data and Structure Refinement for $[\text{U}^{\text{VI}}\text{O}_2(\text{L}^3)(\text{MeOH})]$ (3.3) and $[\text{U}^{\text{VI}}\text{O}_2(\text{L}_4)(\text{EtOH})]$ (3.4).
- Table 3.2.** Bond lengths [\AA] and angles [$^\circ$] for the compounds for $[\text{U}^{\text{VI}}\text{O}_2(\text{L}^3)(\text{MeOH})]$ (3.3) and $[\text{U}^{\text{VI}}\text{O}_2(\text{L}_4)(\text{EtOH})]$ (3.4).
- Table 3.3.** Hydrogen bonds in the $[\text{U}^{\text{VI}}\text{O}_2(\text{L}^3)(\text{MeOH})]$ (3.3) and $[\text{U}^{\text{VI}}\text{O}_2(\text{L}_4)(\text{EtOH})]$ (3.4).
- Table 3.4.** Selected IR data (in cm^{-1}) for the ligands and complexes with tentative assignments.
- Table 3.5.** UV/Vis spectral data of ligands and complexes.
- Table 3.6.** ^{13}C NMR spectral data of ligands and complexes.
- Table 3.7.** Conversion of thymol (1.5 g, 0.010 mol) using $[\text{U}^{\text{VI}}\text{O}_2(\text{eda-2,4-dmp})(\text{MeOH})]$ (3.2) as a catalyst, turn over frequency, and selectivity of

different products for 2h of reaction time under different reaction conditions.

- Table 3.8.** Conversion, turn over frequency and selectivity parameters for various catalysts for the oxidative bromination of thymol.
- Table 3.9.** Solvent effect on the oxidative bromination of thymol and selectivity of products catalysed by complex **3.2**.
- Table 3.10.** Conversion of styrene (1.04 g, 10 mmol), using complex **3.2** as a catalyst, turn over frequency, and product selectivity for 2 h of reaction time under different reaction conditions.
- Table 3.11.** Conversion, turn over frequency and selectivity parameters for various catalysts for the oxidative bromination of styrene.
- Table 3.12.** Solvent effect on the selectivity of products catalysed by complex **3.2**.
- Table 4.1.** Crystal Data and Structure Refinement for $[\text{U}^{\text{VI}}\text{O}_2(\text{pip-2,4-dmp})(\text{DMSO})]$ (**4.2a**).
- Table 4.2.** Bond lengths [\AA] and angles [$^\circ$] for the compounds $[\text{U}^{\text{VI}}\text{O}_2(\text{pip-2,4-dmp})(\text{DMSO})]$ (**4.2a**)
- Table 4.3.** IR spectral data (cm^{-1}) of ligand and complexes.
- Table 4.4.** UV-visible spectral data of ligand and complexes.
- Table 4.5.** ^1H NMR (δ in ppm) of ligand and metal complexes.
- Table 4.6.** ^{13}C NMR data (δ in ppm) of ligand and metal complexes.
- Table 4.7.** Conversion of 10 mmol (1.50 g) of thymol using $[\text{Mo}^{\text{VI}}\text{O}_2(\text{pip-2,4-dmp})]$ (**4.1**) complex as a catalyst precursor for 2h of reaction time under different reaction conditions.
- Table 4.8.** Conversion of 10 mmol (1.5 g) thymol using $[\text{U}^{\text{VI}}\text{O}_2(\text{pip-2,4-dmp})(\text{MeOH})]$ (**4.2**) as a catalyst for 2 h of reaction time under different reaction conditions.

LIST OF PUBLICATIONS

Papers published/ accepted for publication

1. Mannar R. Maurya, **Bekele Mengesha**, Bhawna Uprety, Nancy Jangra, Reshu Tomar and Fernando Avecilla, "Oxygen Atom Transfer Between DMSO and Benzoin Catalyzed by *cis*-Dioxidomolybdenum(VI) Complexes of Tetradentate Mannich Bases", *New J. Chem.*, 42 (2018) 6225 - 6235.
2. Mannar R. Maurya, **Bekele Mengesha**, Shailendra K. Maurya and Fernando Avecilla, "Dioxidouranium(VI) complexes of ONNO tetradentate Mannich bases as catalyst for the oxidative bromination of thymol and styrene in presence of H₂O₂-KBr-HClO₄", *Inorg. Chim. Acta*, (In press).
3. Mannar R. Maurya, **Bekele Mengesha**, Shailendra K. Maurya, Nidhi Sehrawat and Fernando Avecilla, "Dioxomolybdenum(VI) and dioxouranium(VI) complexes as functional mimic of haloperoxidases catalytic activity in presence of H₂O₂-KBr-HClO₄", *Inorg. Chim. Acta*, 486 (2019) 757-765.

Papers Presented in Symposia / Conferences

1. Mannar R. Maurya, **Bekele Mengesha**, Bhawna Uprety, Nancy Jangra, Reshu Tomar and Fernando Avecilla, "Oxygen Atom Transfer Between DMSO and Benzoin Catalyzed by *cis*-Dioxidomolybdenum(VI) Complexes of Tetradentate Mannich Bases", *New J. Chem.*, 42 (2018) 6225-6235.(Poster).

CONTENTS

	Page No.
CANDIDATE'S DECLARATION	
ABSTRACT	I
ACKNOWLEDGEMENTS	IV
LIST OF FIGURES.....	VII
LIST OF TABLES.....	XIV
LIST OF PUBLICATIONS.....	XVI
CONTENTS.....	XVII
CHAPTER 1	
<i>General introduction and literature survey</i>	
1.1 Historical	1
1.2 Coordination complexes of molybdenum and uranium and their catalytic activities.....	2
1.3 Catalytic activities of molybdenum and uranium complexes.....	14
1.4 Objectives of the present thesis	23
CHAPTER 2	
<i>Oxygen atom transfer between DMSO and Benzoin catalysed by cis- dioxido molybdenum (VI) complexes of tetradentate Mannich bases</i>	
2.1. Introduction.....	27
2.2. Experimental section.....	28
2.2.1. Materials and general methods.....	28
2.2.2. Preparations of ligands.....	29
2.2.3. Preparations of complexes.....	30
2.2.4. X-Ray crystal structure determination.....	31
2.3. Results and discussion.....	33
2.3.1. Solid state characterizations.....	33

2.3.2. IR spectral studies.....	40
2.3.3. UV-Visible spectral studies.....	40
2.3.4. ¹ H NMR spectral studies.....	42
2.3.5. ¹³ C NMR spectral studies.....	46
2.3.6. Oxygen atom transfer between benzoin and DMSO.....	48
2.4. Conclusions.....	55

CHAPTER 3

Dioxidouranium(VI) complexes of ONNO tetradentate Mannich bases as catalyst for the oxidative bromination of thymol and styrene in presence of H₂O₂-KBr-HClO₄

3.1. Introduction.....	58
3.2. Experimental section.....	59
3.2.1. Materials and general methods.....	59
3.2.2. Preparation of complexes [U ^{VI} O ₂ L ¹⁻⁴ (MeOH)] (3.1 – 3.4).....	59
3.2.3. X-Ray crystal structure determination.....	60
3.2.4. Catalytic activity study.....	62
3.2.4.1. Oxidative bromination of thymol.....	62
3.2.4.2. Oxidative bromination of styrene.....	62
3.3. Results and discussion	62
3.3.1. Solid state characterization.....	63
3.3.2. Spectral studies.....	66
3.3.2.1. FT-IR Spectral Study.....	66
3.3.2.2. UV-Visible Spectral Study	67
3.3.2.3. ¹ H NMR Spectral Study	69
3.3.2.4. ¹³ C NMR Spectral Study	69
3.3.3. Catalytic activity study	71
3.3.3.1. Oxidative bromination of thymol	71
3.3.3.2. Oxidative bromination of Styrene.....	77
3.3.4. Reactivity	83
3.4. Conclusions	86

CHAPTER 4***Dioxidomolybdenum(VI) and dioxidouranium(VI) complexes as functional mimic of haloperoxidases catalytic activity in presence of H₂O₂–KBr–HClO₄***

4.1. Introduction	88
4.2. Experimental.....	88
4.2.1. Materials.....	88
4.2.2. General procedures and techniques	89
4.2.3. Synthesis of [Mo ^{VI} O ₂ (pip-2,4-dmp)] (4.1)	89
4.2.4. Synthesis of [U ^{VI} O ₂ (pip-2,4-dmp)(MeOH)] (4.2)	89
4.2.5. X-Ray crystal structure determination.....	90
4.2.6. Catalytic activity study: Oxidative bromination of thymol	91
4.3. Results and discussion.....	91
4.3.1. Thermogravimetric analysis study	92
4.3.2. Description of structure of [U ^{VI} O ₂ (pip-2,4-dmp)(DMSO)] (4.2a)	93
4.3.3. IR spectral study	95
4.3.4. UV-Vis spectral study	96
4.3.5. ¹ H NMR spectral study	97
4.3.6. ¹³ C NMR spectral study	100
4.3.7. Catalytic activity study: Oxidative bromination of thymol.....	102
4.3.8. Reactivity of uranium complex with H ₂ O ₂ and possible reaction mechanism	109
4.4. Conclusion.....	110
Summary and conclusions	112
References.....	116

1.1. Historical

Molybdenum metal belongs to the 6th group of Modern Periodic table, and has the symbol Mo with atomic number 42. It is a silvery white metal with a gray cast. It has sixth highest melting point in periodic table. The trace element molybdenum is one of the few second transition row metals which is known to involve in more than 50 molybdenum-containing enzymes till date and has well defined functions in biology [1, 2, 3]. Most mononuclear molybdenum enzymes are unique in terms of their active site structure and consist of a Mo center bound to a novel pyranopterin cofactor via dithiolene moiety, except the nitrogenases where Mo is present along with iron in a sulfur linked cluster [1, 4-7]. Hille has classified the mononuclear molybdenum enzymes based on their active site structure as: (i) molybdenum hydroxylases, (ii) eukaryotic oxotransferases and (iii) prokaryotic oxotransferases; Figure 1.1 [6].

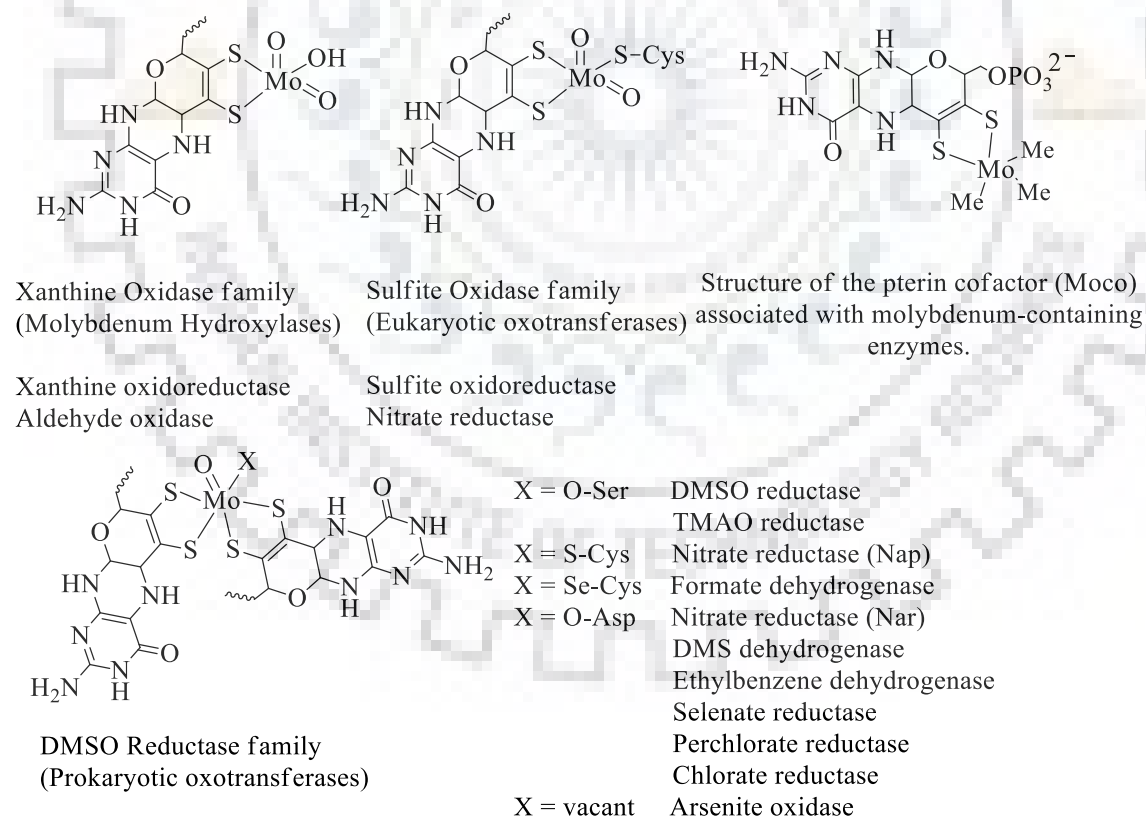


Fig. 1.1. Different mononuclear molybdenum enzymes based on their active site structures.

These Mo enzymes are involved in various metabolic processes of the host organism and the products of the catalytic cycles play vital roles in metabolism of the carbon, nitrogen and Sulphur [8, 9]. Molybdenum has been discovered as the essential element for animals and plants. Several physiological abnormalities are produced in human like cancer from its deficiency and excess supply [10]. Molybdenum complexes exhibit anticancer [11-13], antibacterial [14], antifungal [13, 15, 16] and antifertility [16] activities. Due to the presence of at least one Mo=O unit in the active sites of molybdo-enzymatic system, they are referred as oxido-molybdenum enzymes and this inspired researchers to focus their research on the synthetic oxido-molybdenum complexes in homogeneous or heterogeneous systems in order to mimic the biological systems [17, 18].

Among actinides, uranium is a silvery-white element having symbol U and atomic number 92. Uranium is a naturally occurring element which is found in low levels within all rock, soil, and water. The most common isotopes of naturally occurring uranium are U^{238} and U^{235} . Most uses of uranium employ its unique nuclear properties like in nuclear power plants and nuclear weapons. The most important oxidation states exhibited by uranium are uranium (IV) and uranium (VI), and exists in these states in the form of oxides, i.e. uranium (IV) dioxide (UO_2) and uranium (VI) trioxide (UO_3), respectively.

The coordination chemistry of uranium had been studied in nineties extensively [19] but in the past one decade the coordination chemistry of uranium could not develop much like other transition metal ions possibly due to not much scope of the applications of coordination compounds of uranium. The most common moiety in uranium (VI) complexes is the dioxidouranium(VI) ion, $[UO_2]^{2+}$. The bonding in $[UO_2]^{2+}$ unit is very different, and is mainly due to the combination of d-p and f-p π interactions. The uranyl unit is highly stable to moisture and oxygen.

1.2. Coordination complexes of molybdenum and uranium and their catalytic activities

As molybdenum is found in the biological systems, the coordination chemistry of molybdenum with particular emphasis on Mo=O bond containing complexes, has triggered considerable interest. Recently, catalytic applications of these complexes have also prompted the attention of researchers to develop coordination chemistry of molybdenum and check their potential catalytic activities. In addition, the functional models for enzymes [20–22] have also contributed considerably in the development of molybdenum chemistry. The coordination chemistry of uranium, particularly dioxidouranium (VI) complexes, has been the attraction of researchers to understand mainly the basic coordination chemistry as such complexes have very much similarities with the complexes of dioxidomolybdenum(VI) and dioxidotungsten (VI).

Commonly used precursors for the preparation of molybdenum complexes are $[\text{Mo}^{\text{VI}}\text{O}_2(\text{acac})_2]$, $[\text{Mo}^{\text{VI}}\text{O}_2\text{Cl}_2]$, $[\text{Mo}^{\text{VI}}\text{O}_2\text{C}_1_2(\text{DMF})_2]$, $[\text{Mo}^{\text{VI}}\text{O}_2\text{C}_1_2(\text{DMSO})_2]$, $[\text{Mo}^{\text{VI}}\text{O}_2\text{C}_1_2(\text{OPPh}_3)_2]$ etc. while acetate and nitrate salts of uranium have been used extensively in the development of coordination complexes of uranium. The dioxidomolybdenum(VI) complexes of chiral dibasic tetradentate Schiff base ligands, their reduced analogues, linear and tripodal Mannich base ligands have been prepared by the reaction of $[\text{Mo}^{\text{VI}}\text{O}_2(\text{acac})_2]$ or other metal precursors in solvents. The molecular structures of most complexes have been confirmed by single-crystal X-ray diffraction analysis in addition to spectroscopic characterization [23–41]. Fig. 1.2 presents list of some of such complexes.

For chiral complexes (examples like **1** – **6** and **13**) two configurations: (a) C_2 -symmetric *cis*- α and (b) C_1 -asymmetric *cis*- β (Fig. 1.3) are possible but based on spectroscopic (^1H and ^{13}C NMR) studies a C_1 -asymmetric *cis*- β -configuration has been suggested for **1–4** while complexes **5**, **6** and **13** were suggested to have diastereomer of C_2 -symmetric *cis*- α configuration [25, 27, 28].

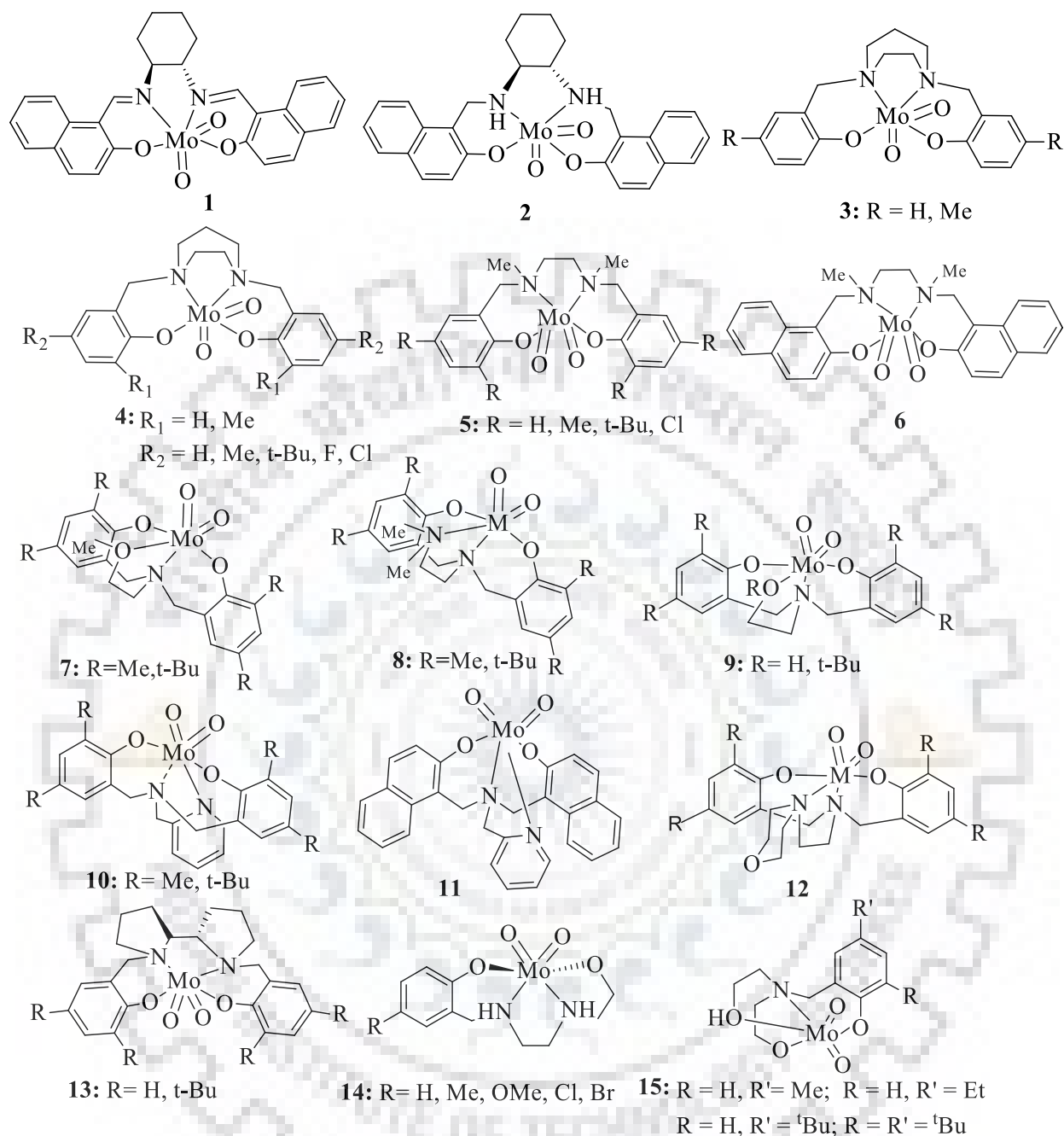


Fig. 1.2. Dioxidomolybdenum(VI) complexes of chiral dibasic tetra dentate Schiff base ligands their reduced analogues, linear and tripodal Mannich base ligands

(a) C_2 -symmetric *cis- α* (b) C_1 -asymmetric *cis- β*

Fig. 1.3. Two configurations: (a) C_2 -symmetric *cis- α* and (b) C_1 -asymmetric *cis- β* generally observed in chiral complexes.

Complexes **16** – **35** presented in Fig. 1.4 are based on some bidentate and tridentate Schiff base, reduced Schiff base and Mannich base ligands. The chloride ion coordinated Mo complexes (e.g. **16** and **19**) were prepared from $[\text{Mo}^{\text{VI}}\text{O}_2\text{Cl}_2]$ while others were isolated from mostly from $[\text{Mo}^{\text{VI}}\text{O}_2(\text{acac})_2]$ or other precursors [43–57].

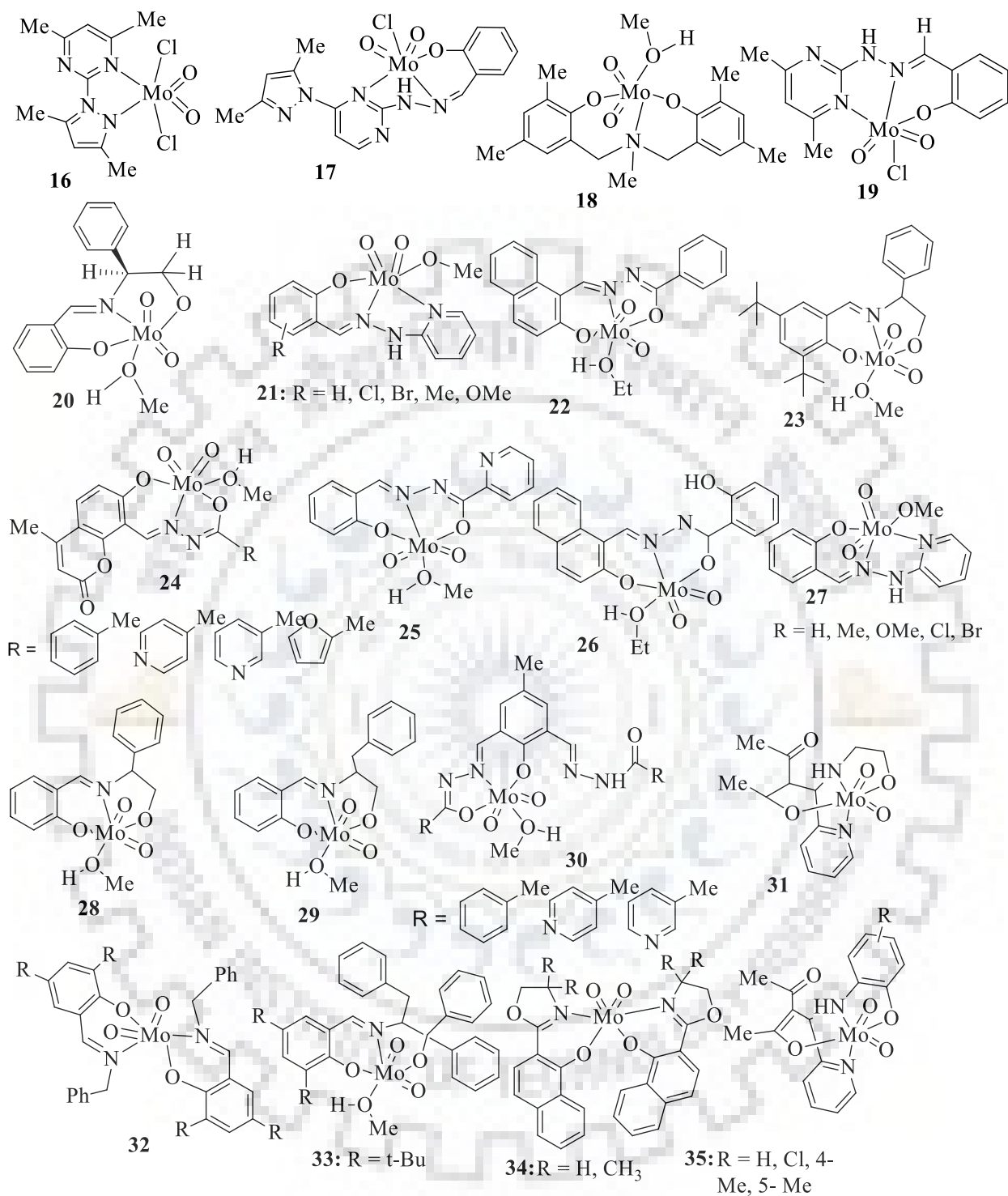


Fig. 1.4. Examples of molybdenum complexes having $\{\text{MoO}_2\}^{2-}$ core reported in literature [43–57].

Higher nuclear molybdenum complexes have also appeared in literature. Some common cores of higher nuclear molybdenum complexes are presented in Fig. 1.5.

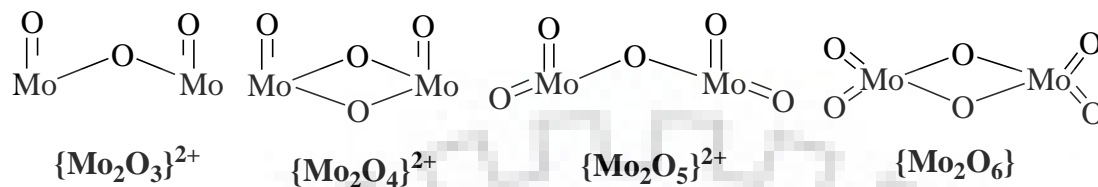


Fig. 1.5. Some common cores of higher nuclear molybdenum complexes.

Only recently group of Nordlander have prepared very interesting dinuclear and trinuclear complexes **36** and **37** (Fig. 1.6), respectively, with tridentate ligands using $[\text{Mo}^{\text{VI}}\text{O}_2(\text{acac})_2]$ as precursor in MeCN. These complexes have Mo–O–Mo bridging but the bridging bonds break down and complexes change to the corresponding mononuclear complexes in MeOH [58]. Interestingly, using very similar ligands (i) Schiff bases having –OMe, –NMe₂ or Et group in place of alcoholic –OH, and (ii) reduced Schiff bases having –OMe or –NMe₂ group in place of alcoholic –OH have also been prepared (complexes **38** and **39**) but in monomeric complexes **38**, ligands behave as monobasic bidentate while in dinuclear **39**, they behave as monobasic tridentate (Fig. 1.7) [29, 60]. Complexes **38** were prepared from $[\text{MoO}_2(\eta^2\text{-tBu}_2\text{pz})_2]$ while complexes **39** were prepared from $[\text{Mo}^{\text{VI}}\text{O}_2(\text{acac})_2]$.

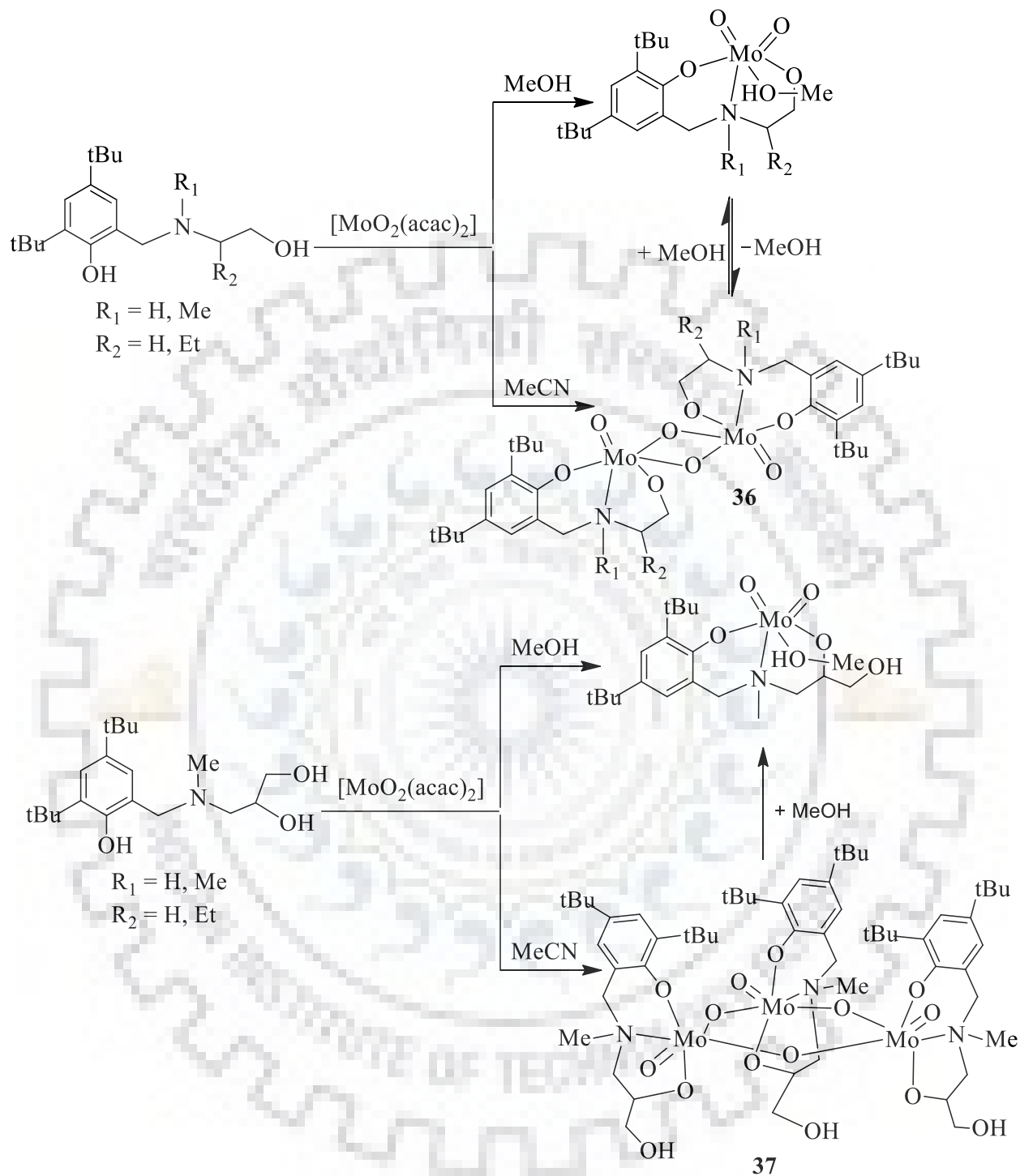


Fig. 1.6. Tridentate ligands resulting in dinuclear **36** and trinuclear **37** complexes.

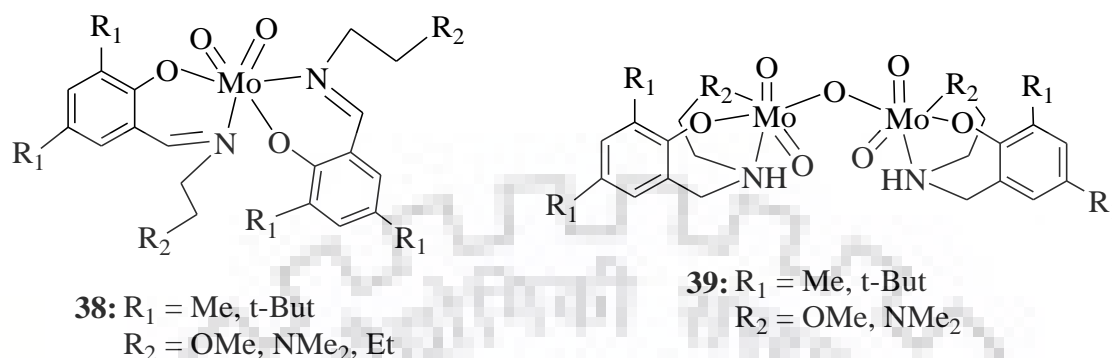


Fig. 1.7. Bidentate/tridentate ligands resulting in mononuclear **38** and dinuclear **39** complexes.

Dioxidomolybdenum(VI) complexes **40–42** prepared using MoO_2Cl_2 and the corresponding ONO aroylhydrazone in methanol show very interesting behavior in solvent, in presence of base in solvent and in mechano-chemical approach. In dry MeOH, methanol is coordinated to sixth coordination position but water takes the sixth position on exposure to moisture or upon suspending them in water. In the presence of a stoichiometric amount of Et_3N , complexes **40** and **41** change to **43** and **44**, while **42** changes to polymeric **45** (Fig. 1.8). Similar results were also obtained by grinding these complexes with Et_3N in presence of small amount of MeOH. UV radiation (254 nm) of **40–42** in dry methanol also gave corresponding complexes i.e. **43–45** [61]

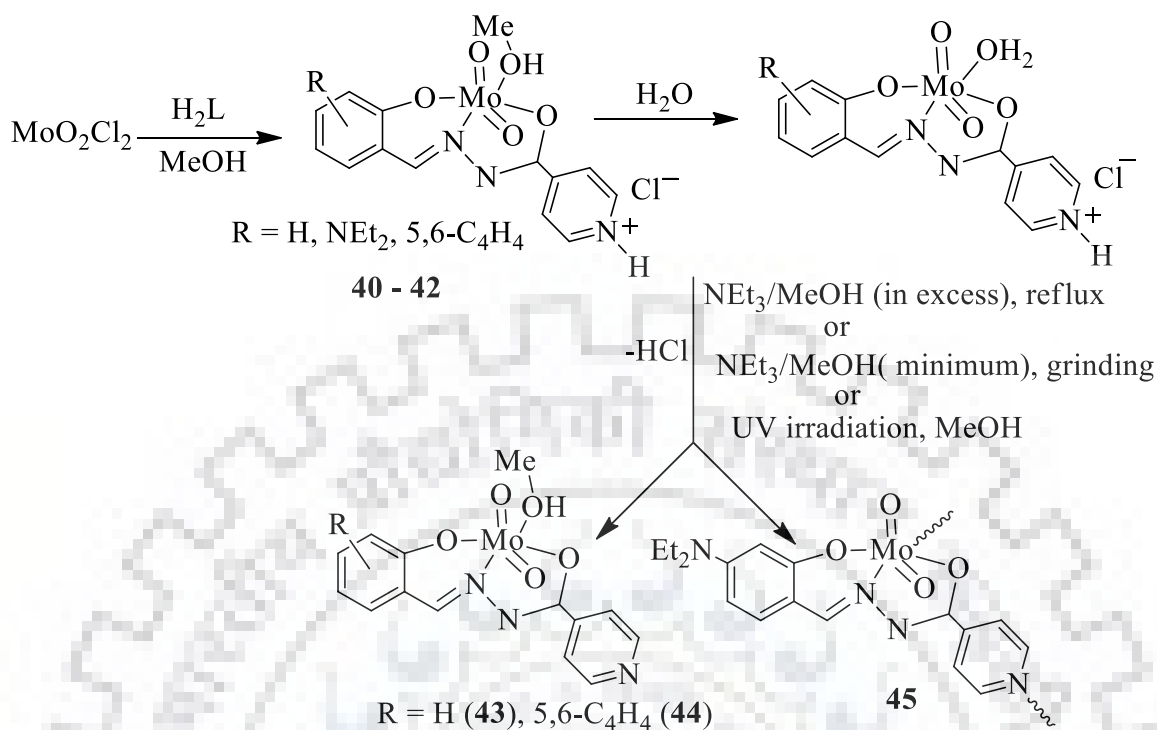


Fig. 1.8. Synthesis and reactivity of dioxidomolybdenum(VI) complexes prepared from MoO_2Cl_2 .

Fig. 1.9 presents some examples of dinuclear molybdenum complexes using different metal precursors [62–66]. Complexes are mostly prepared by usual methods. Increasing chain length of diamine of the tetra dentate ligands derived from pyridoxal and diamine, dinuclear complexes (in place of monuclear) have been isolated where ligands behave as bis(ON bidentate) [67].

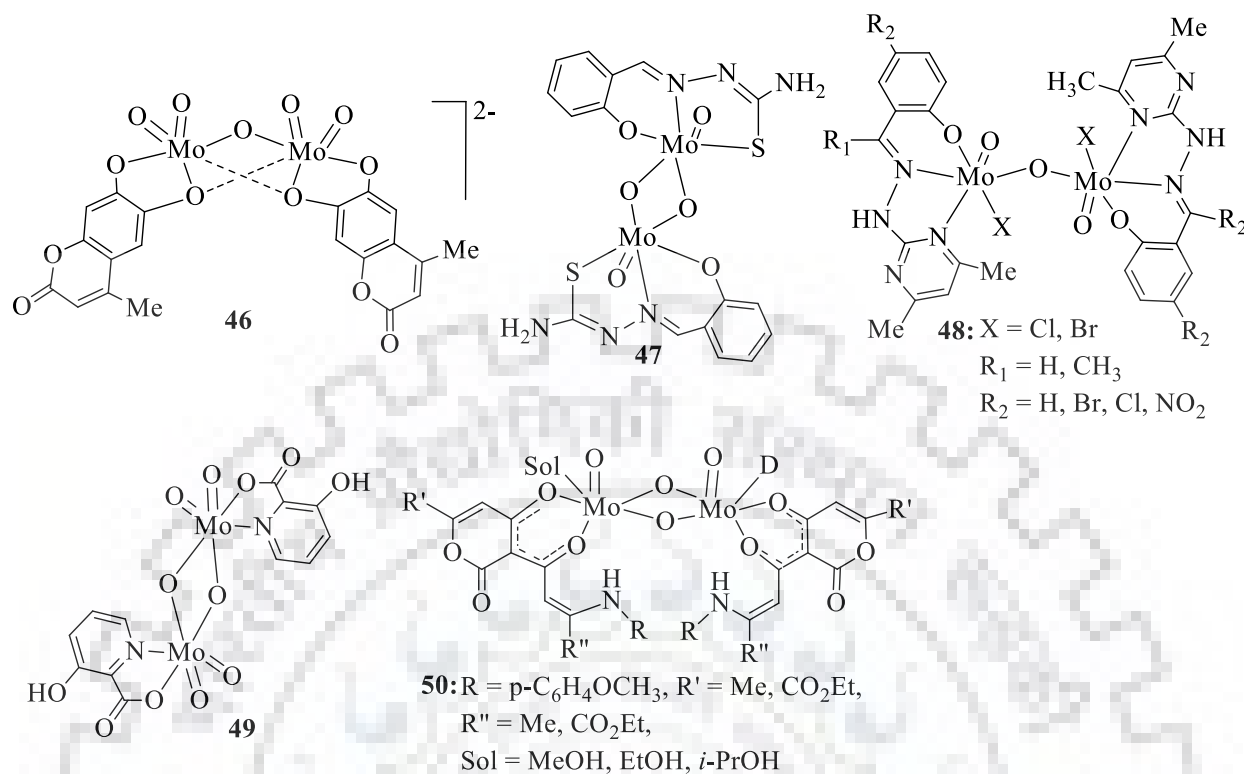


Fig. 1.9. Examples of dinuclear molybdenum complexes having varied cores.

Some other high nuclear molybdenum complexes are also known but they do not have systematic cores e.g. complexes **51** and **52** (Fig. 1.10) [68-70].

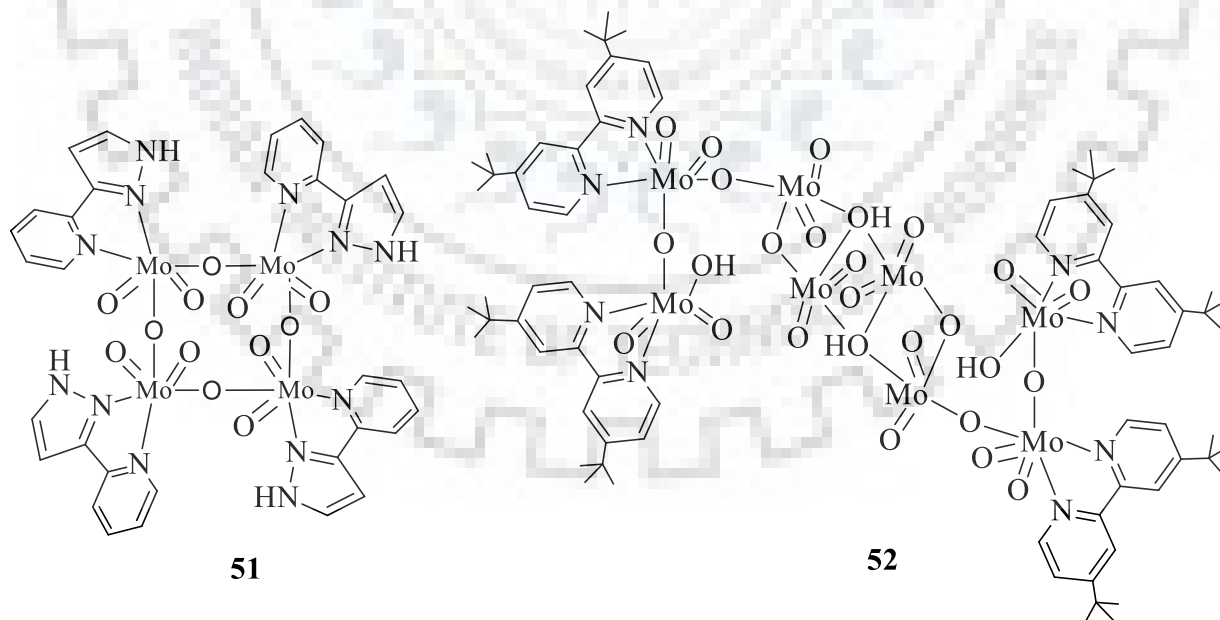
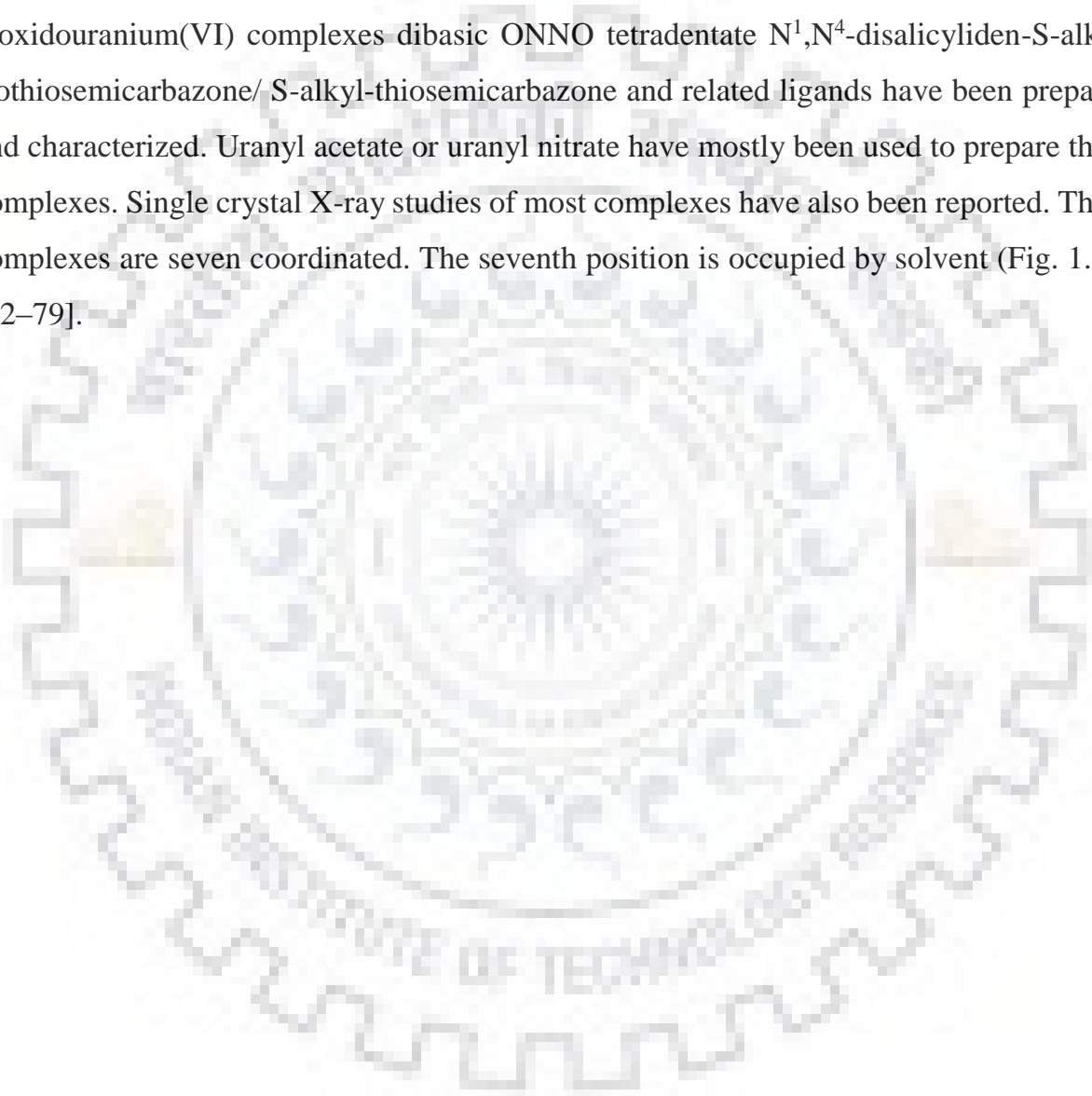


Fig. 1.10. Molybdenum complexes with unusual metal cores.

During nineties coordination chemistry of uranium were reported considerably [19] but later not much attention was paid. In 2006, Sessler et al. have reviewed vanadium chemistry of polydentate ligands and have reported mostly mononuclear as well as some complexes of higher nuclearity [71]. However, in recent past coordination chemistry of uranium started appearing again and much progress have been made. Recently, dioxidouranium(VI) complexes dibasic ONNO tetradentate N^1, N^4 -disalicyliden-S-alkyl-isothiosemicarbazone/ S-alkyl-thiosemicarbazone and related ligands have been prepared and characterized. Uranyl acetate or uranyl nitrate have mostly been used to prepare these complexes. Single crystal X-ray studies of most complexes have also been reported. These complexes are seven coordinated. The seventh position is occupied by solvent (Fig. 1.11) [72–79].



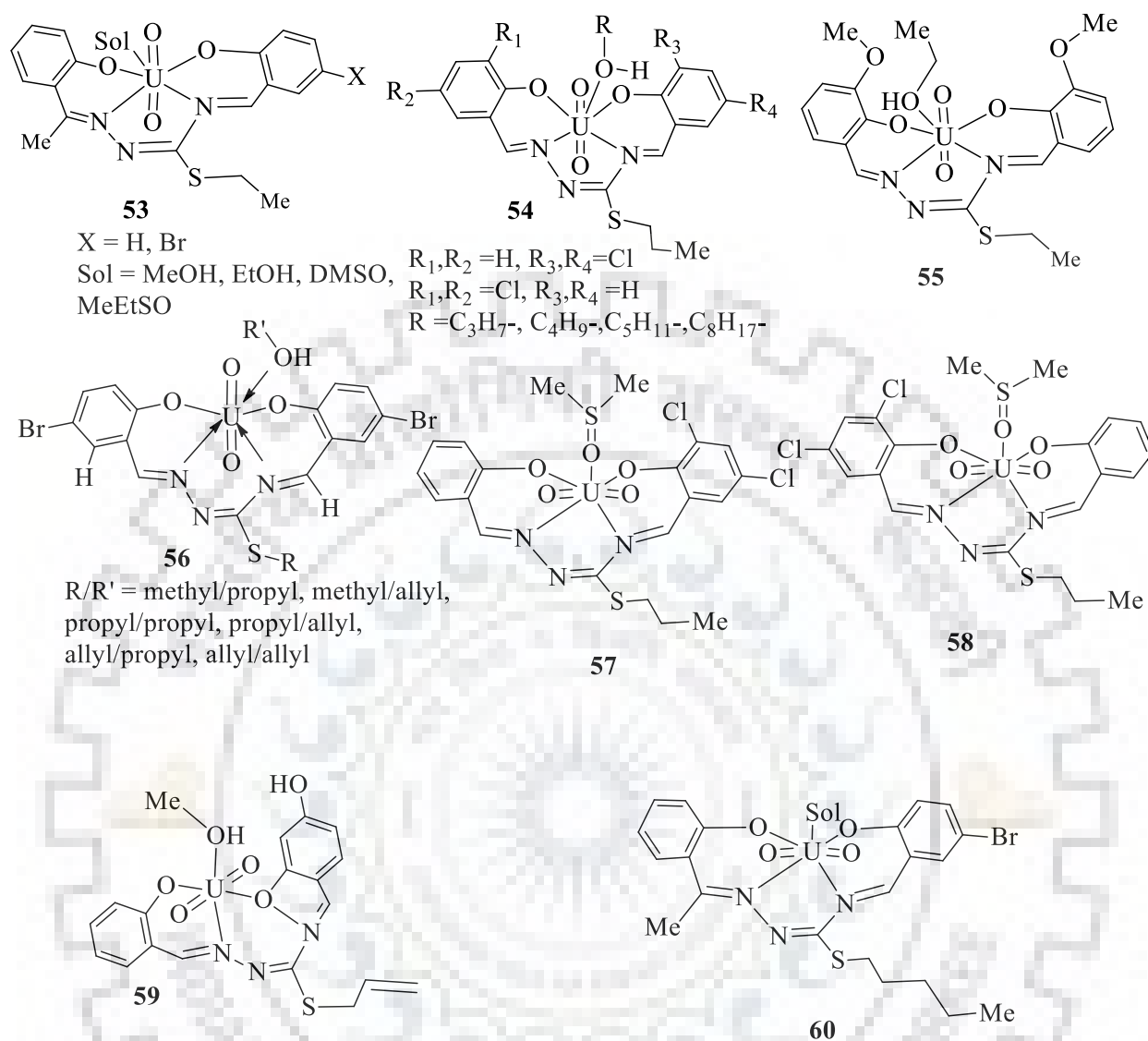


Fig. 1.11. Dioxidouranium(VI) complexes of dibasic ONNO tetra dentate N^1, N^4 -disalicyliden-S-alkyl-isothiosemicarbazone/ S-alkyl-thiosemicarbazone and related ligands

Some other complexes of bi-, tri- and tetra dentate ligands are presented in Fig. 1.12 [81–84]. Synthetic procedures of most complexes are similar except the use of starting metal precursor, which differ in some complexes. Examples of di- and tri-nuclear complexes are given in Fig. 1.13 [84, 85]

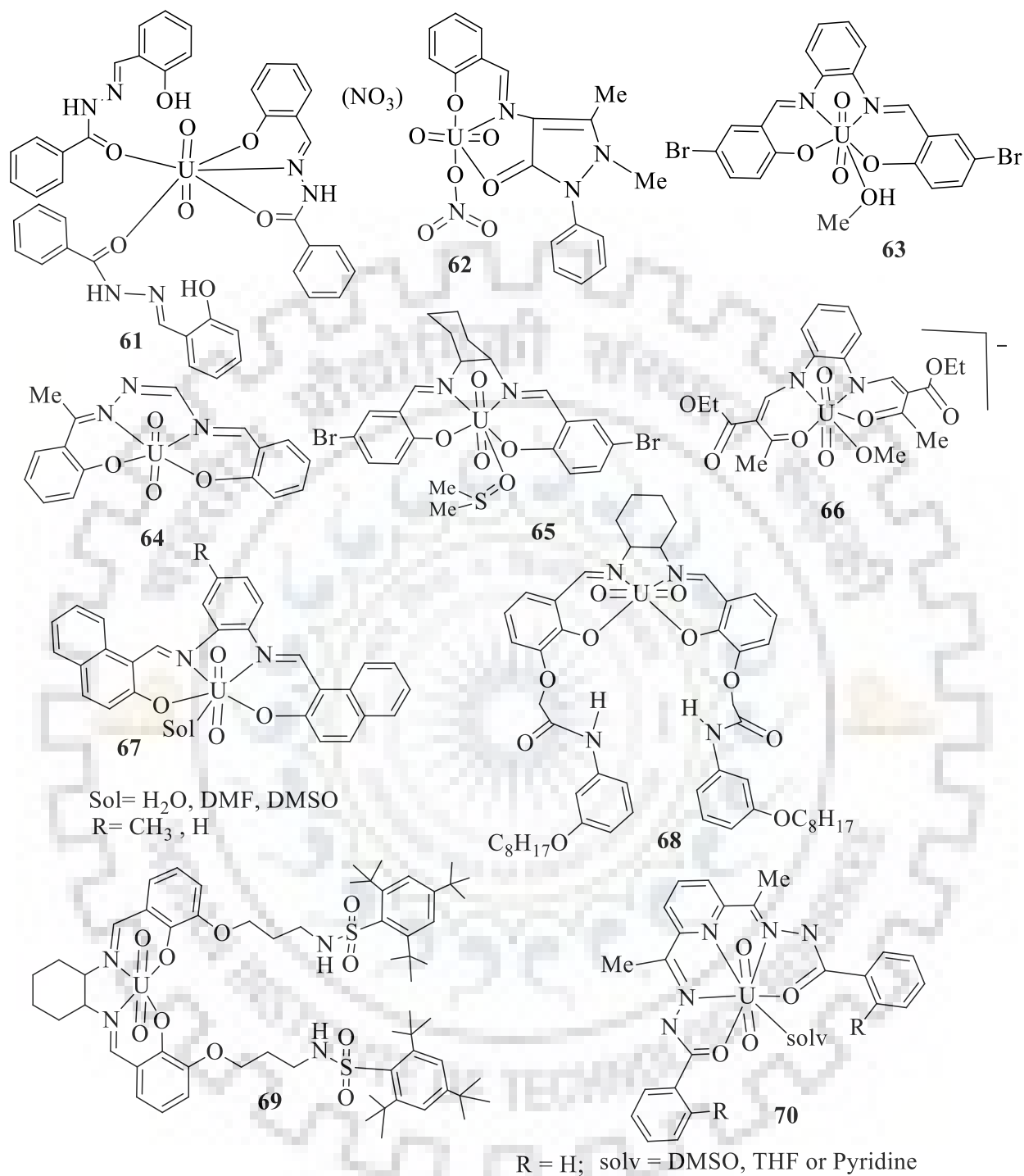


Fig. 1.12. Examples of dioxidouranium(VI) complexes.

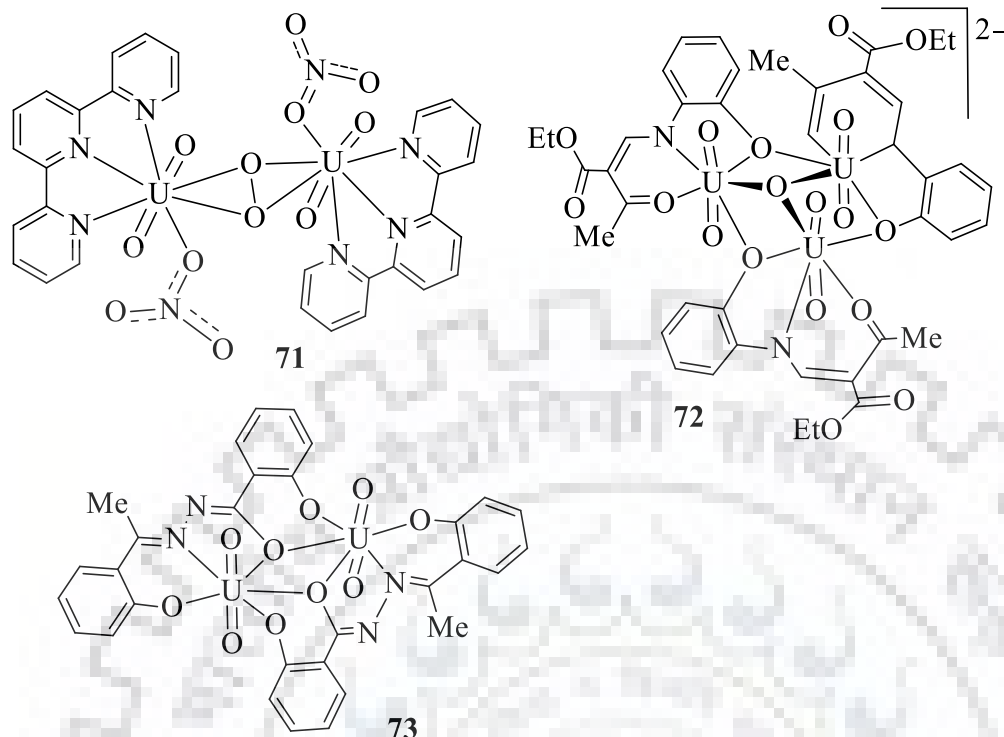


Fig. 1.13. Examples of di- and tri-nuclear dioxidouranium(VI) complexes.

1.3. Catalytic activities of molybdenum and uranium complexes

During oxygen atom transfer in molybdenum containing enzymes the molybdenum center shuffles between Mo (VI)/Mo (IV) during the catalytic cycles.



One of the best known examples is the catalytic reduction of DMSO to DMS by DMSO reductases. The overall catalytic cycle is depicted in Figure 1.14 [86]. Several synthetic models of DMSO reductases based on *cis*-[MoO₂]²⁺ core have been proposed and evaluated for their oxygen atom transfer properties and related mechanistic pathways [27, 30, 32, 87–94].

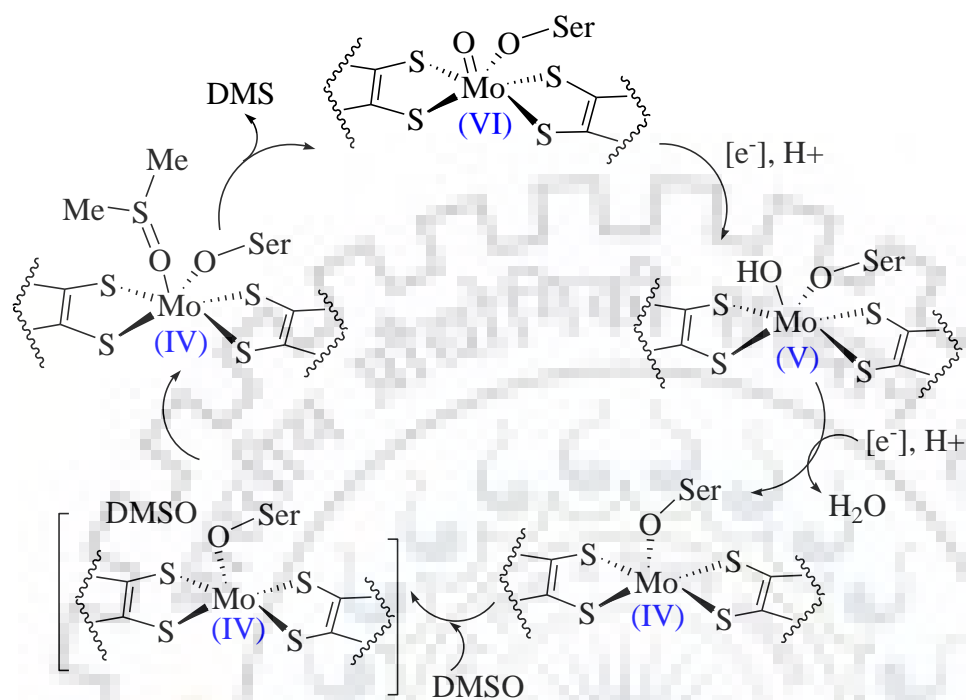


Fig. 1.14. Proposed overall catalytic cycle for the catalytic reduction of DMSO to DMS by DMSO reductases.

Mösch-Zanetti and coworkers have used dioxidomolybdenum(VI) complexes of phenolate ligands for the oxygen atom transfer reactions of PMe_3 and PPh_3 where the yield of formed corresponding oxide was measured by ^1H NMR spectra [95]. Similarly, cis-dioxidomolybdenum(VI) complexes show oxygen atom transfer from dimethylsulfoxide to triphenylphosphine. The effect electron withdrawing and electron releasing groups on salicylaldehyde was also considered while studying this catalytic reaction (Fig. 1.15) [89].

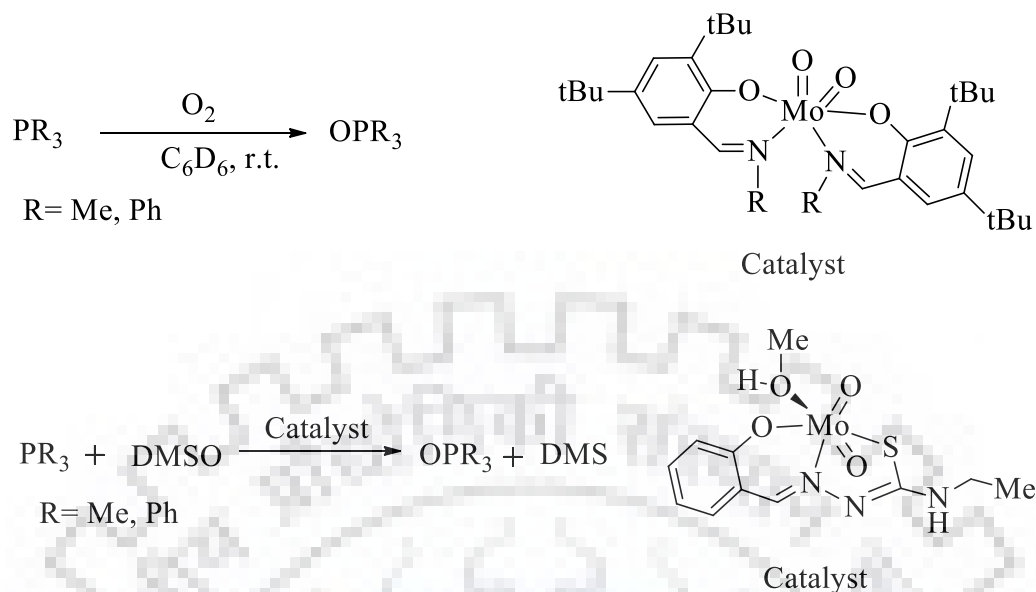


Fig. 1.15. Aerobic oxidation of PMe_3 and PPh_3 to corresponding oxide (top) and oxygen atom transfer from dimethylsulfoxide to phosphines (below), catalyzed by cis-dioxidomolybdenum(VI) complexes.

Recently, dioxidomolybdenum(VI) complexes of tripodal tetradentate ligands have been used for the catalytic oxygen atom transfer between benzoin and DMSO in acetonitrile. The kinetic studies reveal first order rate in benzoin as well as in catalyst, and the rate constant for the second order oxygen atom transfer reaction was found to be $0.0162 \text{ M}^{-1}\text{h}^{-1}$. The formation of dinuclear intermediate $[\text{LMo}^{\text{V}}(\mu\text{-O})\text{Mo}^{\text{V}}\text{L}]$ was established by MALDI-TOF mass analysis and UV-Visible spectroscopy [29].

Olefins (terminal and internal alkenes) such as cyclohexene, cyclooctene, cyclohexenone, styrene, *trans*-stilbene, 1-hexene, 1-octene etc. are some common substrates which have been tested for the catalytic oxidation using dioxidomolybdenum (VI) complexes (Fig. 1.16) [23, 24, 25, 28, 31, 32, 34, 35, 42, 50, 51, 60].

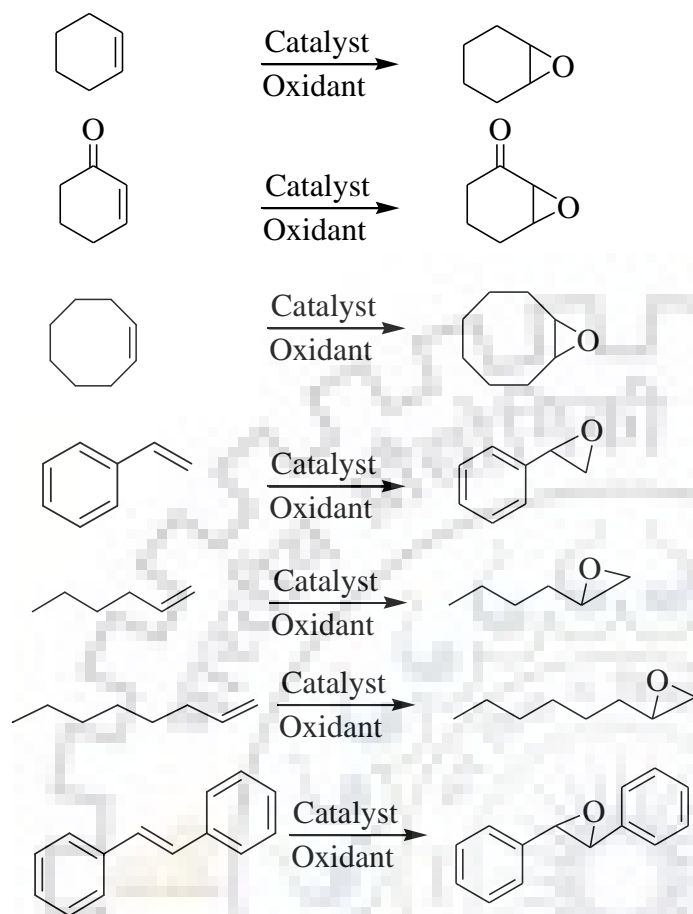
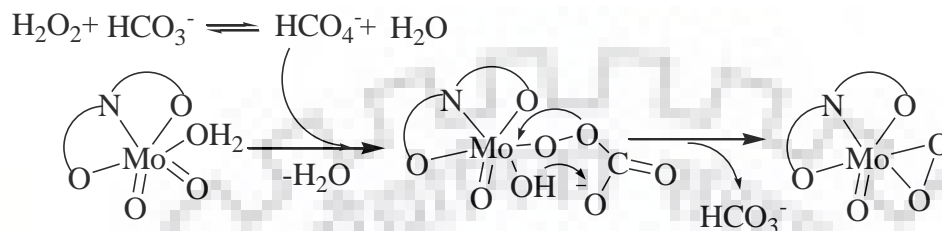


Fig. 1.16. Examples of olefins tested for their oxidation using molybdenum complexes as catalyst and their corresponding epoxides.

Generally, molecular oxygen (in limited cases), *tert*-butyl hydroperoxide (TBHP) and H_2O_2 are frequently used as oxidant in different solvents. However, it has been observed that these oxidants alone give poor conversion along with more than one products but epoxide is generally taken into account because of their potential applications. Recently, promoter like NaHCO_3 has been used along with H_2O_2 which improved the catalytic efficiency of molybdenum complexes along with their selectivity towards epoxides [96–98]. In the presence of NaHCO_3 , dioxidomolybdenum(VI) complexes reacts with H_2O_2 and form oxidoperoxidomolybdenum(VI) intermediate species. This intermediate moiety is responsible for transfer of oxygen to the substrate during catalytic epoxidation. The promoter NaHCO_3 enhances the formation of

oxidoperoxidomolybdenum(VI) intermediate as compared to H_2O_2 alone through other possible intermediate (Scheme 1.1) which ultimately affect the catalytic conversion of substrate(s) and the selectivity of reaction product [99–101].



Scheme 1.1. Proposed mechanism for the formation of oxidoperoxidomolybdenum(VI) complex by the reaction of complex with H_2O_2 in the presence of NaHCO_3 (ONO is dibasic tridentate ligand).

Maurya et al. have reported oxidation of secondary alcohols (1-phenyl ethanol, 2-propanol and 2-butanol) catalyzed by dioxidomolybdenum(VI) and oxidoperoxidomolybdenum(VI) complexes. Both conventional as well Microwave methods have been applied and reactions were carried out in presence and absence of N-based additive and results are compared [102]. All secondary alcohols selectively gave high yield of ketone under the optimized reaction conditions (Fig. 1.17). Addition of N-based additive assists both catalytic systems in reducing time and simultaneously increasing the conversion.

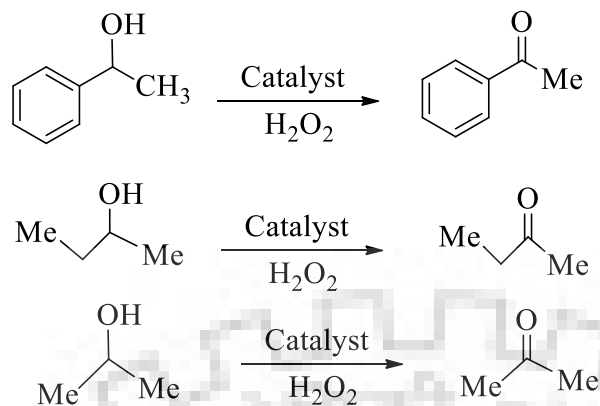


Fig. 1.17. Examples of secondary alcohols that undergo oxidation using dioxidomolybdenum(VI) and oxidoperoxidomolybdenum(VI) complexes as catalysts.

Oxidation of bicyclic alcohols (isoborneol and fenchyl alcohol), cyclic (cyclohexanol) and aromatic alcohols (benzyl alcohol and cumic alcohol) have also been carried out in the presence of molybdenum complexes and a range of N-base additives. Molybdenum complexes are good catalysts for the oxidation of these alcohols in the presence of 30% aqueous H₂O₂. Again, the N-base additives play important role in abstracting hydrogen from H₂O₂ and generate the oxidoperoxidomolybdenum(VI) species which easily facilitate the transfer of oxygen to the substrate resulting in good yield of oxidized products (Fig. 1.18) [103, 104].

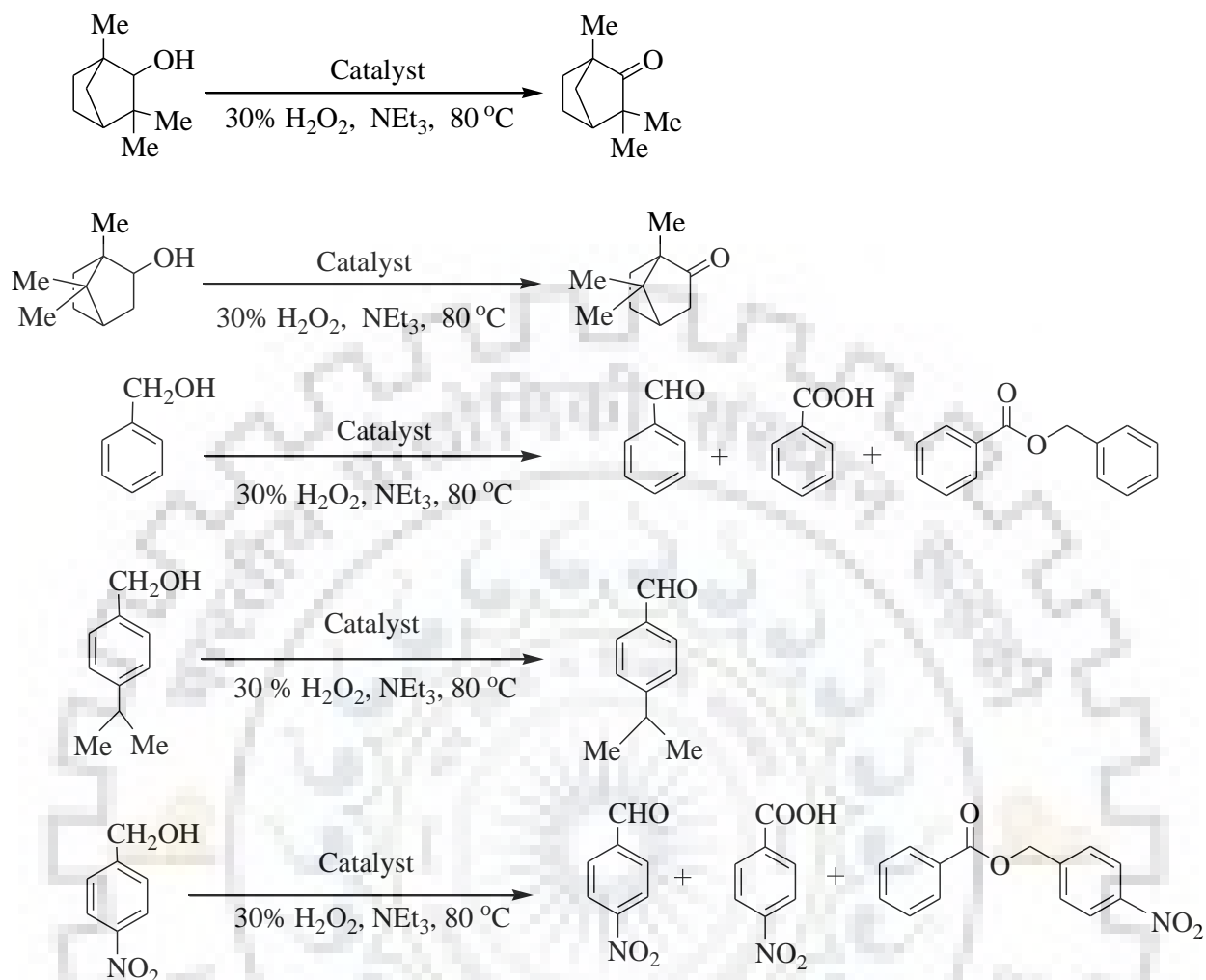


Fig. 1.18. Examples of bicyclic, cyclic and aromatic alcohols that undergo oxidation using dioxidomolybdenum(VI) complexes as catalysts. In some cases more than one product was obtained.

Molybdenum complexes also serve as good catalysts for the oxidation of sulfides. Several groups have studied these reactions in detail. Organic sulfides (chiral or achiral, aliphatic and aromatic) give corresponding two products sulfoxide and sulfone (Fig. 1.19) [105–107]. A comprehensive review on this subject has appeared recently from the group of Chand [108].

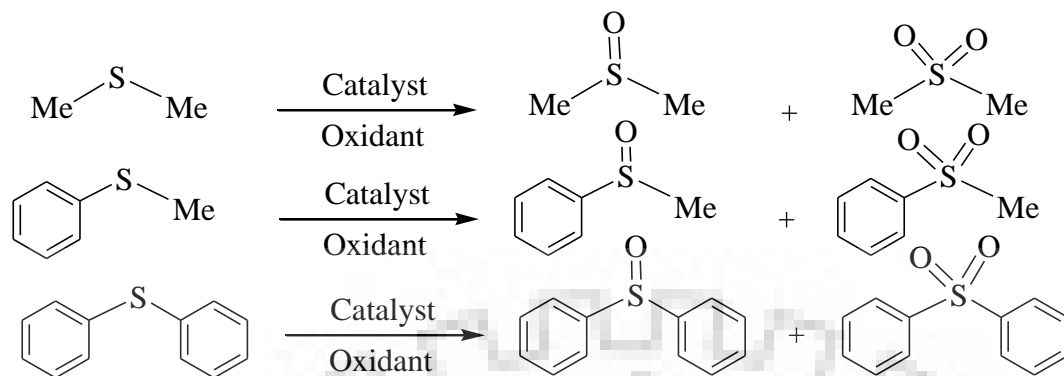


Fig. 1.19. Examples of aliphatic and aromatic sulfides that undergo oxidation using dioxidomolybdenum(VI) complexes as catalysts.

Oxidative bromination of organic substrates, a reaction normally promoted by vanadium haloperoxidase enzymes [109, 110] has also been studied considering dioxidomolybdenum(VI) complexes [111, 112]. Salicylaldehyde, styrene and thymol etc. (Fig. 1.20) are some substrates that have been oxidized using dioxidomolybdenum(VI) complexes as catalyst and H_2O_2 as oxidant in the presence of KBr and HClO_4 .

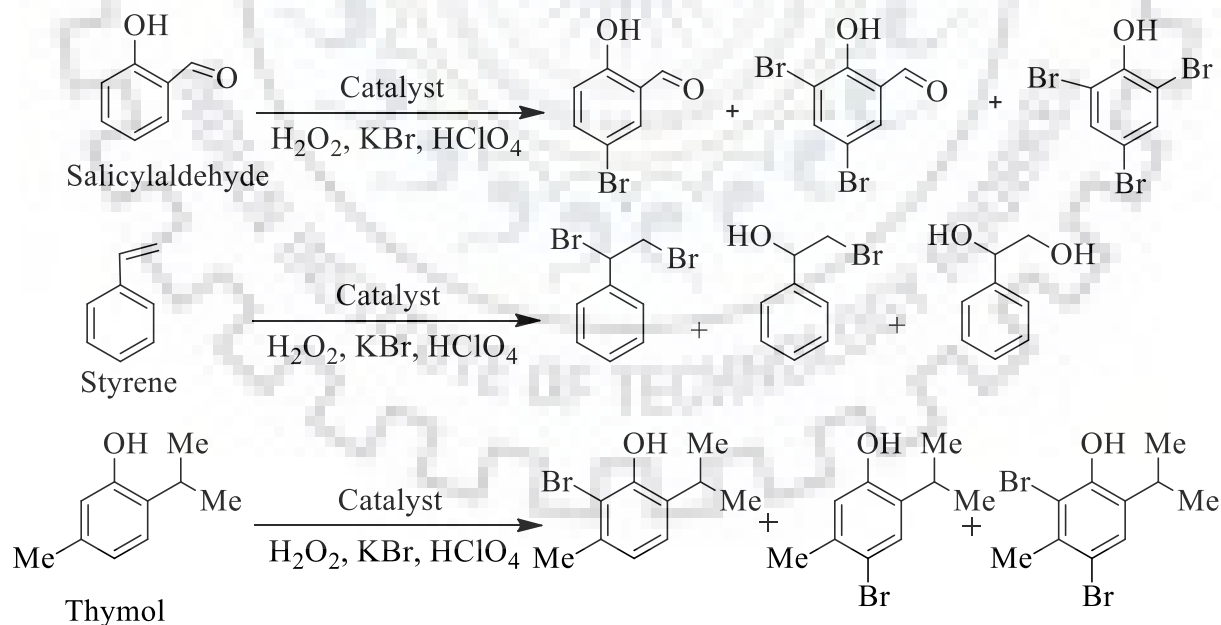
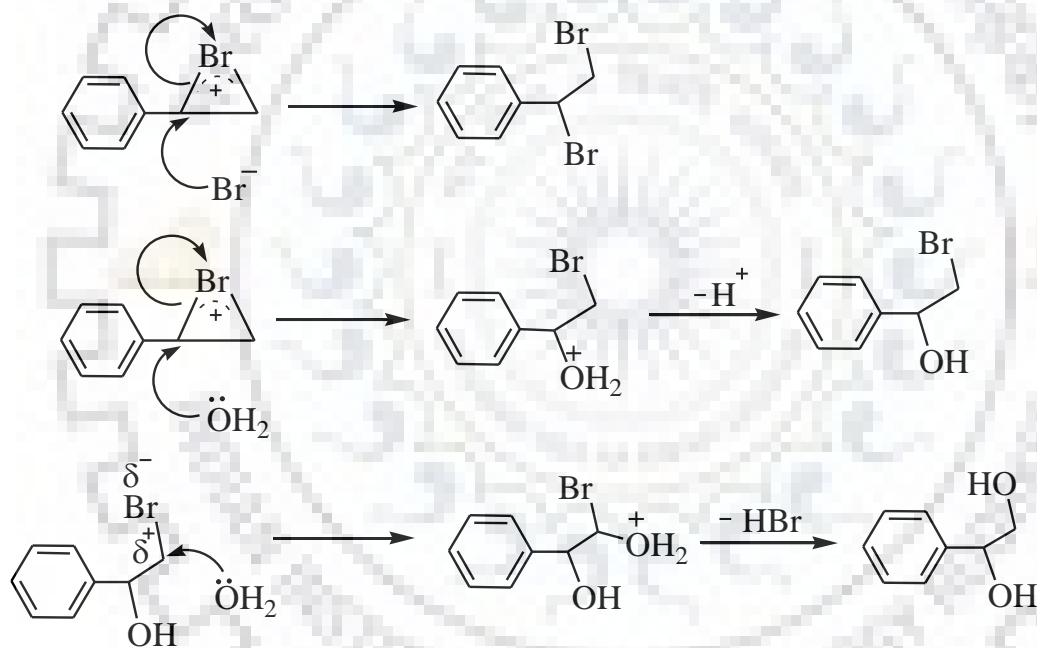


Fig. 1.20. Examples of substrates that undergo oxidative bromination using

dioxidomolybdenum(VI) complexes as catalysts. Generally more than one product was identified in all cases.

The catalytically generated HOBr and/or Br^+ , Br_2 , Br^{3-} , by the reaction of molybdenum complexes with KBr in the presence of H_2O_2 and HClO_4 , react with styrene to give bromonium ion as an intermediate. The nucleophile Br^- as well as H_2O both may attack on the α -carbon of the intermediate to give 1,2-dibromo-1-phenylethane and 2-bromo-1-phenylethane-1-ol, respectively (Scheme 1.2). The nucleophile H_2O may further attack on the α -carbon of 2-bromo-1-phenylethane-1-ol to give 1-phenylethane-1,2-diol (Scheme 1.2) [112].



Scheme 1.2. Mechanism of action of HOBr on styrene.

Oxidation of benzoin to benzoic acid, benzaldehyde, dimethylacetal, methyl benzoate and benzyl has also been carried out using molybdenum complexes as catalyst. As many as four products have been identified (Fig. 1.21) in the reaction conditions in the presence of 30% H_2O_2 as an oxidant in methanol [97].

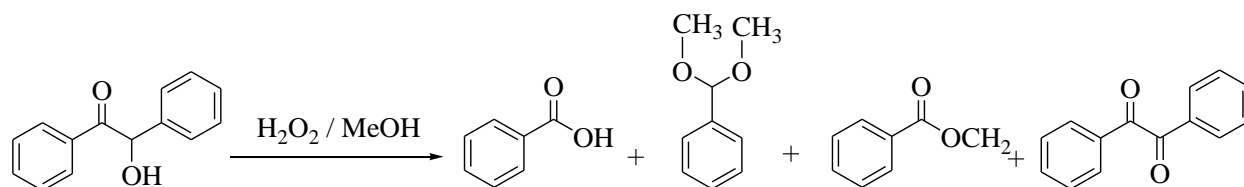


Fig. 1.21. Oxidation of benzoin to different products using dioxidomolybdenum(VI) complexes as catalysts.

We did not come across any review article on uranium which deals with their catalytic activity, though one good review appeared on uranium complexes of polydentate ligands in 2006 [71]. After that good number of publications appeared in literature on uranium complexes (see previous section) but catalytic activities of these complexes have narrowly been explored. Since most dioxidouranium(VI) complexes with tri- and tetradentate ligands are generally associated with one solvent or neutral donor ligand which is flexible in nature and may play an important role in catalytic reactions like shown by dioxidomolybdenum(VI) complexes (vide infra). In fact, one recent paper on dioxidouranium(VI) complexes reports on the catalytic oxidation of alkenes using H_2O_2 and *tert*-butyl hydroperoxide as oxidants [113].

$[\text{U}^{\text{VI}}\text{O}_2(\text{salophen})] \cdot \text{EtOH}$ ($\text{H}_2\text{salophen}$ = *N,N'*-disalicylidene-orthophenylenediamine) (ethanol)dioxouranium(VI) and $[\text{U}^{\text{VI}}\text{O}_2(\text{dbm})] \cdot 2\text{EtOH}$ (Hdbm = dibenzoylmethane) have been used as catalysts in the nucleophilic acyl substitution of acid anhydrides. Reaction could start only above 50°C and yielded $>90\%$ conversion in 7 and 4 h, respectively. The obtained products EtOAc and AcOH only (Fig. 1.22), demonstrates the high selectivity of these systems [114].

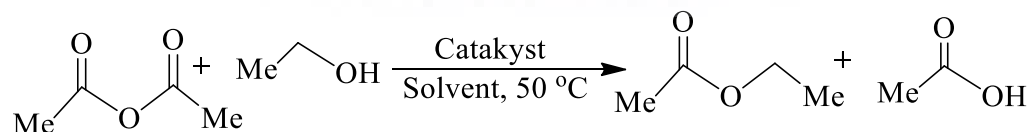


Fig. 1.22. Catalytically induced nucleophilic acyl substitution of acid anhydride.

Not related to dioxidouranium(VI), uranium(III) complex of bulky polydentate arene-anchored tris(phenoxide) ligand (6,6',6''-((2,4,6-trimethylbenzene-1,3,5-triyl)tris(methylene))tris(2-(adamantan-1-yl)-4-methylphenolate), serves as electrocatalyst for the conversion of H₂O into H₂ in tetrahydrofuran (THF), with a turnover frequency of 10⁶ h⁻¹ at potential of 1.3 V [115]. The crucial role of the arene moiety has been explored to provide important insight for the design of improved electrocatalysts [116].

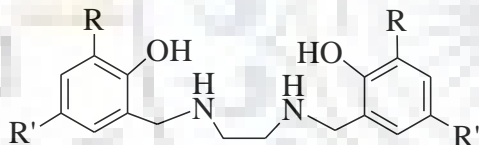


1.4. Objectives of the present thesis

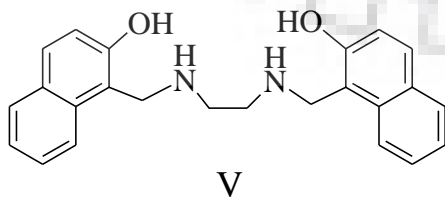
While going through the chemistry of dioxidomolybdenum(VI) and dioxidouranium(VI) complexes discussed above and based on other literature on these complexes (which could not be included here), it is clear that both types of complexes have potential in catalyzing the organic transformations which might open a new path to develop catalytic system for various industrial and pharmaceutical processes. Therefore, it's worth to prepare complexes of these metal ions and investigate their catalytic potentials.

In the present investigation, we have synthesized dioxidomolybdenum (VI) and dioxidouranium(VI) complexes with the following ligands:

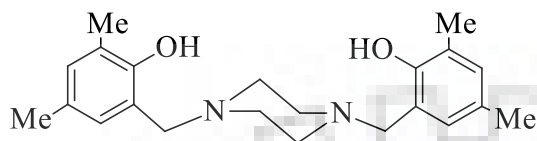
1. Five dibasic tetra dentate ONNO donor Mannich base based ligands derived from the condensation between ethylene diamine, 40% formaldehyde and 2,4-disubstituted phenols or 2-naphthol (1 : 2 : 2 molar ratio) in refluxing MeOH.



R	R'	Ligand
<i>tert</i> -butyl	<i>tert</i> -butyl	I
Methyl	Methyl	II
<i>tert</i> -butyl	Methyl	III
Chloro	Chloro	IV



2. A dibasic tetra dentate ONNO donor Mannich base based ligand derived from the condensation between piperazine, 40% formaldehyde and 2,4-dimethyl phenol (1 : 2 : 2 molar ratio) in refluxing MeOH.

**VI**

All ligands and their dioxidomolybdenum(VI) and dioxidouranium(VI) complexes have successfully been characterized by various spectroscopic techniques such as FT-IR, UV-Vis, ^1H and ^{13}C NMR and element analysis. In addition, above complexes have also been characterized by thermogravimetric analysis and some of them by single crystal X-ray diffraction studies. These complexes have been investigated for their catalytic potentials for the following reactions:

- Oxygen atom transfer between DMSO and benzoin
- Oxidative bromination of thymol
- Oxidative bromination of styrene

For the oxidative bromination reactions different biphasic solvent systems and their effect on the selectivity of different products have also been investigated. A suitable reaction condition has been obtained for the maximum reaction products in all catalytic reactions.

2.1. Introduction

The most prominent role of second row transition element, molybdenum, in chemistry and biology is that of an important bio-catalyst, since a wide variety of chemical transformations in biology are catalyzed by molybdenum enzymes [117, 118]. Molybdenum enzymes have long enjoyed the status of being vital eukaryotic enzymes catalyzing reactions involved in carbon, nitrogen and sulfur bio geochemical cycles in the atmosphere [8, 94, 119, 120]. Apart from nitrogenases (in which the metal is incorporated into a unique [MoFe₇S₉] cluster) all molybdenum enzymes are quite uniform in their active site structure and can be divided into three large and non-overlapping families, as exemplified by the enzymes xanthine oxidase, sulfite oxidase and DMSO reductase [5,87]. In all of these families, the molybdenum cofactor (commonly abbreviated as Moco), consists of a molybdenum ion coordinated to either one or two bidentate pterindithiolene ligands ([2-amino-4(1*H*)-pteridinone]) [5]. The enzymes from the DMSO reductase family (the most diverse of all) have only been found in bacteria and archea whilst enzymes from the other two families are found in all forms of life [3,121].

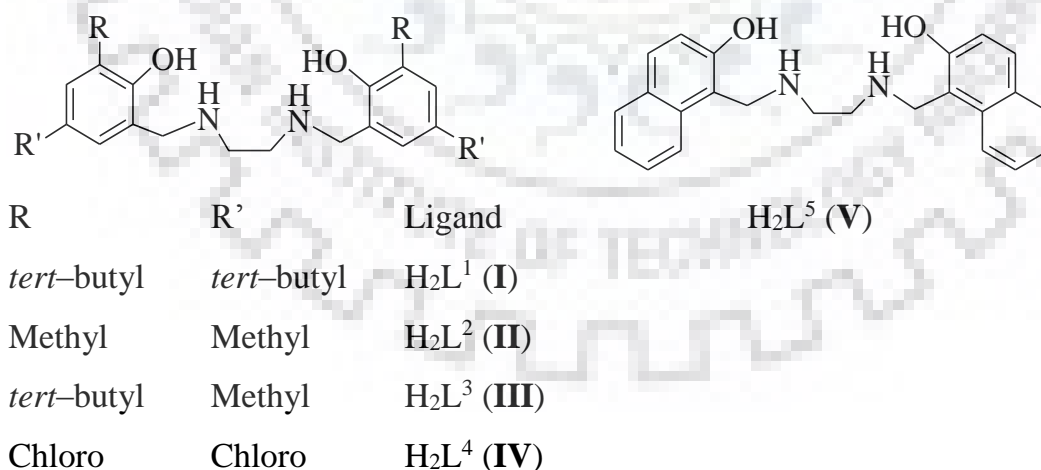
The DMSO reductase family is the largest family of molybdopterin enzymes, and is widely studied for its reactivity and mechanism. They oxidize or reduce suitable substrates (for e.g. DMSO to DMS), and thus catalyze oxygen atom transfer (OAT) reactions according to equation 1 [94]. The process is accompanied by two electron reduction, and usually the oxygen removed from the substrate (SO) coordinates the metal in the oxidized state. Thus, the presence of Mo=O moiety become an essential functional requirement for model studies for this class of enzymes [3, 90, 123].



One of the most explored enzymes of DMSO reductase family is the name enzyme, DMSO reductases. It catalyses the reduction of DMSO to DMS, and the molybdenum center shuttles between Mo(VI) and Mo(IV) oxidation states during the catalytic cycle. A number of structurally diverse dioxidomolybdneum(VI) complexes have been developed

and evaluated for their oxygen atom transfer abilities for biomimetic modelling as well as industry relevant processes [55, 89, 93,124]. Most of these model studies are based on oxygen atom transfer involving tertiary phosphines and/or DMSO. Tertiary phosphines are not the biological substrate for DMSO reductases, however, they are often a substrate of choice for OAT modelling studies, since their properties can be desirably tuned and the reactions can be easily monitored by ^{31}P NMR studies [57, 88, 89,125-129].

In our recent reports, we have evaluated the OAT ability of *cis*-dioxidomolybdenum(VI) complexes built on aminobisphenoltripodal ligands [29], between DMSO and benzoin in acetonitrile at 80 °C in 24 h of reaction time. Similar reactions have also been reported by Sillanpää *et al.* and Ng *et al.* in DMSO at ambient temperature [30, 91, 130]. A detailed mechanistic study had revealed an overall steric control in our reactions [29]. We have further extended the study to a new series of *cis*-[MoO₂]²⁺ complexes derived from Mannich bases of ethylene diamine and 2, 4-disubstituted phenols (Scheme 2.1). The present systems employed for catalytic OAT reactions were made sterically less hindered by using dipodal ligands, as against tripodal ligands reported earlier by us. We have achieved almost 99 % conversion in only 18 h of reaction time. We have also derived the second order rate equation using the most active catalyst, [MoO₂L⁵].



Scheme 2.1. Structure of ligands used in this study.

2.2. Experimental Section

2.2.1. Materials and general methods

Ammonium molybdate, acetylacetone (SRL, India), 2,4-di-*tert*-butylphenol, 2,4-di-methylphenol, 2-*tert*-butyl-4-methylphenol, 2,4-di-chlorophenol, ethylenediammine (Himedia, India), benzoin (S.D. fine chemicals, India), formaldehyde and DMSO (Rankem, India) were used as obtained. Other chemicals and solvents were of AR grade. The precursor complex $[\text{Mo}^{\text{VI}}\text{O}_2(\text{acac})_2]$ was prepared following a literature method [131].

All measurements were made after drying the metal complexes at 100 °C. Elemental analyses of the complexes were carried out on an Elementar model Vario-EI-III after drying the samples at 100 °C. IR spectra were recorded as KBr pellets on a Nicolet 1100 FT-IR spectrometer. Electronic spectra of the complexes were recorded in acetonitrile on a Shimadzu 1601 UV-Vis spectrophotometer. ^1H and ^{13}C NMR spectra were recorded in $\text{CDCl}_3/\text{DMSO-d}_6$ on a JEOL ECX 400 MHz spectrometer. GC-MS was run on a Perkin-Elmer Clarus 500 instrument. HPLC was performed on a Shimadzu LC-2010A HT instrument using 250×4.6 mm C-18 column in low pressure gradient mode with a flow rate of 0.5 mL min^{-1} and injection volume of 40 μL . The mobile phase used was MeCN : H_2O : trifluoroacetic acid, 60 : 40 : 0.02.

2.2.2. Preparation of ligands

H_2L^1 (I). A solution of ethylenediammine (0.300 g, 5 mmol), 39% formaldehyde (0.770 g, 10 mmol,) and 2,4-di-*tert*-butylphenol (2.063 g, 10 mmol) in MeOH (20 mL) was refluxed for ca. 18 h. During this period, a white solid slowly separated; the solid was collected by filtration, washed well with cold MeOH and then dried under vacuum. Yield: 1.90 g (76%). Found: C 76.69; H, 10.35; N, 5.70%. Calcd for $\text{C}_{32}\text{H}_{52}\text{N}_2\text{O}_2$ (496.0 g mol^{-1}): C, 77.37; H, 10.55; N, 5.64%. ^1H NMR (400 MHz, CDCl_3): δ 10.73 (br, 2H, OH), 7.25 (s, 2H), 6.85 (s, 2H) (aromatic), 3.92 (s, 4H, $-\text{CH}_2-$), 3.54 (s, 2H, $-\text{NH}$), 3.03 (s, 4H, -

CH₂CH₂-), 1.44 (s, 18H), 1.30 (s, 18H, -CH₃). ¹³C NMR (400 MHz, CDCl₃): δ 150.83, 142.17, 136.68, 121.87, 118.89, 82.23, 51.35, 49.69, 34.89, 34.27, 31.58, 29.61.

Ligands H₂L² (II), H₂L³ (III), H₂L⁴ (IV) and H₂L⁵ (V) were prepared by the procedure outlined for H₂L¹ (I) using 10 mmol each of 2,4-di-methylphenol, 2-*tert*-butyl-4-methylphenol, 2,4-di-chlorophenol and 2-naphtol, respectively, in place of 2,4-di-*tert*-butylphenol.

Data for H₂L² (II). Yield: 1.22 g (74%). Found: C, 73.46; H, 8.42; N, 8.81%. Calcd for C₂₀H₂₈N₂O₂ (328.0 g mol⁻¹): C, 73.14; H, 8.59; N, 8.53%. ¹H NMR (400 MHz, CDCl₃): δ 10.42 (br, 2H, OH), 6.89 (s, 2H), 6.66 (s, 2H) (aromatic), 3.85 (s, 4H, -CH₂-), 3.54 (s, 2H, -NH), 2.97 (s, 4H, -CH₂CH₂-), 2.22 (s, 12H, -CH₃). ¹³C NMR (400 MHz, CDCl₃): δ 153.13, 131.24, 127.86, 126.29, 124.88, 120.61, 58.36, 51.77, 20.46, 15.86.

Data for H₂L³ (III). Yield: 1.04 g (50%). Found: C, 52.17; H, 5.54; N, 6.00%. Calcd for C₂₆H₄₀N₂O₂ (412.0 g mol⁻¹): C, 75.68; H, 9.77; N, 6.79%. ¹H NMR (400 MHz, CDCl₃): δ 10.58 (br, 2H, OH), 6.98 (s, 2H), 6.66 (s, 2H) (aromatic), 3.85 (s, 4H, -CH₂-), 3.44 (s, 2H, -NH), 2.99 (s, 4H, -CH₂CH₂-), 2.22 (s, 6H), 1.41 (s, 18H) (CH₃). ¹³C NMR (400 MHz, CDCl₃): δ 154.21, 136.07, 127.47, 126.83, 121.78, 100.03, 58.05, 50.89, 34.48, 29.89, 20.64.

Data for H₂L⁴ (IV). Yield: 1.28 g (62%). Found: C, 48.44; H, 4.06; N, 6.92%. Calcd for C₁₆H₁₆N₂O₂Cl₄ (410.12 g mol⁻¹): C, 46.86; H, 3.93; N, 6.83%. ¹H NMR (400 MHz, CDCl₃): δ 7.34 (s, 2H), 7.07 (s, 2H) (aromatic), 3.97 (s, 4H, -CH₂-), 4.96 (s, 2H, -NH), 2.79 (s, 4H, -CH₂CH₂-). ¹³C NMR (400 MHz, DMSO-d₆): δ 154.26, 127.92, 127.33, 126.84, 121.33, 121.18, 50.71, 46.48.

Data for H₂L⁵ (V). Yield: 1.02 g (55%). Found: C, 73.86; H, 6.61; N, 7.73%. Calcd for C₂₄H₂₄N₂O₂ (372.46 g mol⁻¹): C, 77.39; H, 6.49; N, 7.52%. ¹H NMR (400 MHz, d₆-

[DMSO]): δ 6.12 (d, 2H), 7.12 (d, 2H), 7.26 (dd, 2H), 7.68 (dd, 2H), 7.71 (d, 2H), 7.98 (d, 2H), (aromatic), 4.74 (s, 4H -CH₂-), 5.00 (s, 2H, -NH), 4.07 (s, 4H -CH₂CH₂-).

2.2.3. Preparations of complexes

[MoO₂L¹] (2.1). To a suspension of H₂L¹ (0.496 g, 1.0 mmol) in MeOH (10 mL) was added a filtered solution of metal precursor [Mo^{VI}O₂(acac)₂] (0.326 g, 1.0 mmol) in MeOH (10 mL) with magnetic stirring where a clear orange solution was obtained within a few minutes. The resulting reaction mixture was then heated under reflux for 4 h on a water bath. After cooling to room temperature, the precipitated orange solid was collected by filtration, washed with cold MeOH and dried under vacuum. Yield 0.461 g (74%). Found: C, 61.36; H, 8.24; N, 4.58%. Calcd for C₃₂H₅₀N₂O₄Mo (622.0 g mol⁻¹): C, 61.72; H, 8.09; N, 4.50%. ¹H NMR (400 MHz, CDCl₃): δ 7.26 (s, 2H), 6.86 (s, 2H) (aromatic), 5.17-5.18 (d, 1H), 5.20-5.21 (d, 1H), 3.93-3.94 (d, 1H), 3.97-3.98 (d, 1H) (-CH₂-), 2.94 (s, 2H, -NH), 2.68-2.73 (t, 2H), 2.84-2.87 (t, 2H) (-CH₂CH₂-), 1.43 (s, 18H), 1.28 (s, 18H) (-CH₃). ¹³C NMR (400 MHz, CDCl₃): δ 154.23, 140.84, 135.83, 123.43, 123.20, 120.97, 59.34, 51.87, 35.01, 34.28, 31.80, 29.75.

Complexes 2.2–2.5 were prepared similarly using [Mo^{VI}O₂(acac)₂] (0.326 g, 1.0 mmol) and respective ligands (1.0 mmol).

Data for [MoO₂L²] (2.2). Yield 0.363 g (80%). Found: C, 75.17; H, 9.54; N 6.90%. Calcd for C₂₀H₂₆N₂O₄Mo (454.0 g mol⁻¹): C, 52.86; H, 5.77; N 6.17%. ¹H NMR (400 MHz, CDCl₃): δ 6.68 (s, 2H), 6.89 (s, 2H) (aromatic), 5.21-5.24 (d, 2H), 3.94-3.96 (d, 2H) (-CH₂-), 2.70 (s, 2H, -NH), 3.05 (s, 2H), 2.91 (s, 2H) (-CH₂CH₂-), 2.23 (s, 6H), 2.19 (s, 6H) (CH₃). ¹³C NMR (400 MHz, CDCl₃): δ 156.36, 137.86, 130.45, 129.47, 119.56, 99.81, 53.45, 45.49, 20.52, 17.03.

Data for [MoO₂L³] (2.3). Yield 0.480 g (89 %). Found: C, 57.47; H, 7.23; N, 5.41%. Calcd for C₂₆H₃₈N₂O₄Mo (538.0 g mol⁻¹): C, 57.98; H, 7.11; N, 5.20%. ¹H NMR (400 MHz, CDCl₃): δ 6.89 (s, 2H), 6.68 (s, 2H) (aromatic), 5.21 (d, 1H), 5.24 (d, 2H), 3.95 (d,

1H), 3.97 (d, 1H) (-CH₂-), 2.91 (s, 2H, -NH), 3.05-3.08 (t, 2H), 2.70-2.73 (t, 2H) (-CH₂CH₂-), 2.27 (s, 6H), 1.58 (s, 18H) (CH₃). ¹³C NMR (400 MHz, CDCl₃): δ 156.71, 138.5, 129.18, 126.71, 127.77, 121.23, 53.20, 45.71, 34.58, 29.36, 20.60.

Data for [MoO₂L⁴] (2.4). Yield 0.487 g (91%). Found: C, 35.59; H, 2.54; N, 5.29%. Calcd for C₁₆H₁₄Cl₄N₂O₄Mo (536.0 g mol⁻¹): C, 35.85; H, 2.63; N 5.23%. ¹H NMR (400 MHz, DMSO): δ 7.20 (s, 2H), 7.40 (s, 2H) (aromatic), 4.72 (dd, 2H), 3.95 (dd, 2H) (-CH₂-), 5.40 (s, 2H, -NH), 2.17 (t, 2H), 2.80-2.76 (t, 2H) (-CH₂CH₂-). ¹³C NMR (400 MHz, DMSO-d₆): δ 154.43, 128.17, 127.53, 125.42, 123.36, 123.04, 52.31, 45.72.

Data for [MoO₂L⁵] (2.5). Yield 0.417 g (83%). Found: C, 58.23; H, 4.54; N, 5.47%. Calcd for C₂₄H₂₂N₂O₄Mo (498.0 g mol⁻¹): C, 57.84; H, 4.45; N 5.62%. ¹H NMR (400 MHz, CDCl₃): δ 7.00 (d, 2H), 7.40 (d, 2H), 7.62 (dd, 2H), 7.75 (dd, 2H), 7.86 (d, 2H), 7.98 (d, 2H), (aromatic), 3.09 (dd, 2H), 4.40 (dd, 2H) (-CH₂-), 5.00 (s, 2H, -NH), 1.27 (t, 2H), 1.75 (t, 2H) (-CH₂CH₂-).

2.2.4. X-Ray crystal structure determination

Three-dimensional X-ray data were collected on a Bruker Kappa Apex CCD diffractometer at low temperature for **2.2** and at room temperature for **2.1**, **2.3** and **2.5**, by the ϕ - ω scan method. Reflections were measured from a hemisphere of data collected from frames, each of them covering 0.3° in ω . A total of 78032 for **2.1**, 47390 for **2.2**, 64461 for **2.3** and 36101 for **2.5** reflections measured were corrected for Lorentz and polarization effects and for absorption by multi-scan methods based on symmetry-equivalent and repeated reflections. A total of 5937 for **2.1**, 4529 for **2.2**, 3886 for **2.3** and 3813 for **2.5**, independent reflections exceeded the significance level ($|F|/\sigma|F|$) > 4.0, respectively. After data collection, in each case an empirical absorption correction (SADABS) [132] was applied, and the structures were solved by direct methods and refined by full matrix least-squares on F^2 data using SHELX suite of programs [133]. In **2.1**, hydrogen atoms were included in calculated position and refined in the riding mode, except for N(1) and N(2),

which were located in difference Fourier map and fixed to the nitrogen atoms. In **2.2** and **2.3**, hydrogen atoms were located in difference Fourier map and left to refine freely, except for C(2), C(10), C(11), C(19) and C(20) in **2.2**, and C(8), C(9), C(10), C(11), C(23), C(24), C(25) and C(26) in **2.3**, which were included in calculated position and refined in the riding mode, respectively. In **2.5**, hydrogen atoms were included in calculated position and refined in the riding mode, except for C(8), N(1) and N(2), which were located in difference Fourier map and left to refine freely. Refinements were done with allowance for thermal anisotropy of all non-hydrogen atoms. A final difference Fourier map showed no residual density outside, except for compound **2.1**, due to a disordered water molecules which were not refined: 1.369 and -0.524 e.Å⁻³ for **2.1**, 0.411 and -0.318 for **2.2** and 0.605 and -0.588 e.Å⁻³ for **2.3** and 0.569 and -0.735 for **2.5**. A weighting scheme $w = 1/[\sigma^2(F_o^2) + (0.108000 P)^2 + 2.394000 P]$ for **2.1**, $w = 1/[\sigma^2(F_o^2) + (0.024300 P)^2 + 1.332900 P]$ for **2.2**, , $w = 1/[\sigma^2(F_o^2) + (0.054500 P)^2 + 0.00000 P]$ for **2.3** and $w = 1/[\sigma^2(F_o^2) + (0.066700 P)^2 + 0.00000 P]$ for **5**, where $P = (|F_o|^2 + 2|F_c|^2)/3$, were used in the latter stages of refinement. An important disorder on *t*-butyl groups appear in the crystal of **2.1**. This disorder has been refined and two atomic sites have been observed and refined with the anisotropic atomic displacement parameters for two *t*-butyl groups. More specifically this disorder was refined using 243 restraints (ISOR, SADI, SIMU and DELU restraints were used). The site occupancy factors were 0.43339 for C(15A), C(16A) and C(17A) and 0.45583 for C26(A), C(27A) and C(28A). Further details of the crystal structure determination are given in Table 2.

Table 2.1. Crystal data and structure refinement for complexes, **2.1**, **2.2**, **2.3** and **2.5**.

	2.1	2.2
Formula	C ₃₂ H ₅₀ Mo N ₂ O ₄	C ₂₀ H ₂₆ Mo N ₂ O ₄
Formula weight	622.68	454.37
T, K	293(2)	99(2)
Wavelength, Å	0.71073	0.71073
Crystal system	Trigonal	Monoclinic
Space group	P $\bar{3}$	P2 ₁ /c
a/Å	19.0694(6)	12.1153(11)
b/Å		10.9427(10)
c/Å	17.1332(6)	15.7160(14)
α /°	90	90
β /°	90	112.296(4)
γ /°	120	90
V/Å ³	5395.6(3)	1927.8(3)
Z	6	4
F ₀₀₀	1980	936
D _{calc} /g cm ⁻³	1.150	1.566
μ /mm ⁻¹	0.397	0.709
θ (°)	1.19 to 28.28	1.82 to 28.32
R _{int}	0.0453	0.0216
Crystal size/ mm ³	0.30 × 0.23 × 0.07	0.50 × 0.40 × 0.35
Goodness-of-fit on F ²	1.031	1.077
R ₁ [I > 2 σ (I)] ^a	0.0521	0.0196
wR ₂ (all data) ^b	0.1827	0.0524
Largest differences peak and hole (eÅ ⁻³)	1.369 and -0.524	0.411 and -0.318

$${}^a R_1 = \frac{\sum ||F_o| - |F_c||}{\sum |F_o|} \quad {}^b wR_2 = \left\{ \frac{\sum [w(|F_o|^2 - |F_c|^2)|^2]}{\sum [w(F_o^2)]} \right\}^{1/2}$$

Table 2.1. continued.....

	2.3	2.5
Formula	C ₂₆ H ₃₈ Mo N ₂ O ₄	C ₂₄ H ₂₂ Mo N ₂ O ₄
Formula weight	538.52	498.38
T, K	293(2)	296(2)
Wavelength, Å	0.71073	0.71073
Crystal system	Orthorhombic	Monoclinic
Space group	Pcab	P2 ₁ /c
a/Å	12.9405(4)	15.164(2)
b/Å	14.0380(4)	12.8563(18)
c/Å	28.3268(10)	10.6927(14)
α/°	90	90
β/°	90	90.963(7)
γ/°	90	90
V/Å ³	5145.8(3)	2084.2(5)
Z	8	4
F ₀₀₀	2256	1016
D _{calc} /g cm ⁻³	1.390	1.588
μ/mm ⁻¹	0.543	0.664
θ (°)	1.44 to 28.40	1.34 to 28.37
R _{int}	0.0973	0.0644
Crystal size/ mm ³	0.31 × 0.19 × 0.15	0.25 × 0.13 × 0.05
Goodness-of-fit on F ²	0.937	1.093
R ₁ [I > 2σ(I)] ^a	0.0367	0.0352
wR ₂ (all data) ^b	0.1059	0.1228
Largest differences peak and hole (eÅ ⁻³)	0.605 and -0.588	0.569 and -0.735

$${}^a R_1 = \frac{\sum ||F_o| - |F_c||}{\sum |F_o|} \quad {}^b wR_2 = \left\{ \frac{\sum [w(|F_o|^2 - |F_c|^2)]^2}{\sum [w(F_o^2)]} \right\}^{1/2}$$

2.3. Results and Discussion

A controlled Mannich condensation between ethylene diamine, formaldehyde and 2, 4-disubstituted phenols or 2-naphthol (1: 2: 2 molar ratio) in MeOH yields the corresponding secondary amine Mannich base ligands, H_2L^{1-5} in moderate to excellent yields. The reaction of the dibasic tetra dentate Mannich base ligands, H_2L^{1-5} in 1:1 molar ratio with $[Mo^{VI}O_2(acac)_2]$ in MeOH, results in the formation of the corresponding dioxidomolybdenum (VI) complexes, $[Mo^{VI}O_2(L^{1-5})]$ (**2.1–2.5**) in good yields. All complexes are yellow/orange air stable solids, soluble in common organic solvents such as MeOH, $CHCl_3$, MeCN, DMSO, DMF etc.

2.3.1. Solid state characterizations

The coordination style of the ligands and the resulting geometry around the metal centre was confirmed by SC-XRD studies. ORTEP diagrams for the compounds $[Mo^{VI}O_2(L^1)]$ (**2.1**), $[Mo^{VI}O_2L^2]$ (**2.2**), $[Mo^{VI}O_2(L^3)]$ (**2.3**) and $[Mo^{VI}O_2(L^5)]$ (**2.5**) are presented in Figs. 1, 2, 3, and 4, respectively. Selected bond distances and angles are given in Table 2.2.

The structure of the complexes **2.1**, **2.2**, **2.3** and **2.5** adopt a distorted six-coordinated octahedral geometry with two O_{oxido} terminal oxygen atoms and the ligands act as tetra dentate, coordinating through the two $O_{phenolate}$ and two N_{amine} atoms in a *cis- α* type binding mode involving coordination of one of the N_{amine} atom in the apical position and one O_{oxido} terminal oxygen atom in the equatorial position [134]. The axial sites are occupied by the oxido atoms, O(1), and by the nitrogen atoms, N(1), of the ligand. The equatorial plane is formed for the three atoms of the ligand [N(2), O(3) and O(4)] and one of the terminal oxygen atoms, O(2), and it is distorted with respect to the planarity, [mean deviation from the plane for N(2), O(2), O(3), O(4), 0.0041(2) Å in **2.1**, 0.0208(6) Å in **2.2**, 0.0298(11) Å in **2.3** and 0.0088(13) Å in **2.5**]. The molybdenum atoms are displaced toward the apical oxido ligand, O(1), from the equatorial plane defined by N(2), O(2), O(3) and O(4), 0.3025(3) Å in **2.1**, 0.3185(2) Å in **2.2**, 0.2712(12) Å in **2.3** and 0.2751(2) Å in **2.5**. The Mo- O_{oxido} bond lengths [Mo(1)-O(1) and Mo(1)-O(2) (see Table 2)] and bond

angles [O=Mo=O angle are: 108.08(11)° in **2.1**, 108.93(6)° in **2.2**, 106.67(11)° in **2.3** and 107.51(14)° in **2.5**] are within the ranges for the bond distances typically observed in these type of compounds [135].

π - π Interactions were not observed in the crystal packing of the four complexes. Intermolecular hydrogen bonds were observed in compounds **2.1**, **2.2** and **2.3** (see Table 2.3). Complex **2.2** forms self-assembled dimers in the solid state packing (Fig. 2.5), which are stabilized by C-H \cdots π non covalent interactions in an antiparallel architecture. The distance between hydrogen atoms of the ethyl groups and centroids of the phenyl rings are 2.578 Å [136]. Interestingly, crystal packing of three complexes are entirely different while they belong to very similar ligand system (Figs. 2.6-2.9).

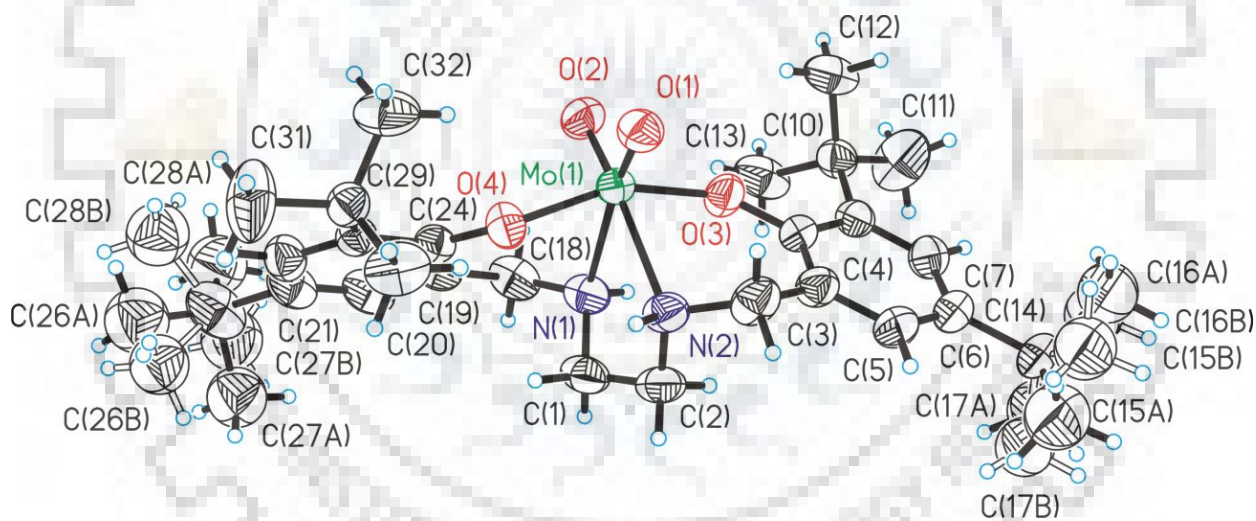


Fig. 2.1. ORTEP plot of complex [Mo^{VI}O₂ (L¹)] (**2.1**). All the non-hydrogen atoms are presented by their 50% probability ellipsoids.

Table 2.2. Bond lengths [Å] and angles [°] for [Mo^{VI}O₂ (L¹)] (**2.1**), [Mo^{VI}O₂L²] (**2.2**), [Mo^{VI}O₂ (L³)] (**2.3**) and [Mo^{VI}O₂ (L⁵)] (**2.5**).

Bond lengths	2.1	2.2	2.3	2.5
Mo(1)-O(1)	1.710(2)	1.7055(10)	1.707(2)	1.708(2)
Mo(1)-O(2)	1.707(2)	1.7248(10)	1.701(2)	1.717(2)
Mo(1)-O(3)	1.939(2)	1.9460(10)	1.9364(18)	1.934(2)
Mo(1)-O(4)	1.936(2)	1.9546(9)	1.954(2)	1.965(2)
Mo(1)-N(1)	2.351(3)	2.3501(11)	2.345(2)	2.314(3)
Mo(1)-N(2)	2.356(3)	2.3077(11)	2.357(3)	2.316(3)
Angles	2.1	2.2	2.3	2.5
O(1)-Mo(1)-O(2)	108.23(12)	108.83(5)	106.67(11)	107.40(13)
O(1)-Mo(1)-O(4)	96.42(11)	96.13(4)	98.98(9)	97.21(10)
O(2)-Mo(1)-O(4)	97.42(11)	98.34(4)	95.58(8)	91.96(10)
O(1)-Mo(1)-O(3)	99.67(12)	98.76(5)	93.18(9)	96.02(11)
O(2)-Mo(1)-O(3)	93.78(11)	96.92(4)	99.61(8)	102.04(11)
O(4)-Mo(1)-O(3)	156.43(10)	153.94(4)	156.94(8)	156.88(10)
O(1)-Mo(1)-N(1)	160.52(11)	164.15(4)	163.31(10)	162.22(11)
O(2)-Mo(1)-N(1)	90.69(12)	86.63(4)	89.50(10)	90.37(12)
O(4)-Mo(1)-N(1)	75.99(10)	77.70(4)	83.15(8)	82.16(10)
O(3)-Mo(1)-N(1)	83.23(11)	82.26(4)	79.76(8)	79.47(10)
O(1)-Mo(1)-N(2)	89.33(11)	90.98(5)	90.94(10)	89.18(11)
O(2)-Mo(1)-N(2)	161.92(11)	160.13(4)	162.35(10)	160.48(12)
O(4)-Mo(1)-N(2)	84.47(10)	80.45(4)	80.18(8)	75.55(10)
O(3)-Mo(1)-N(2)	78.64(10)	78.04(4)	80.11(8)	85.77(10)
N(1)-Mo(1)-N(2)	72.25(11)	73.69(4)	73.03(9)	73.31(10)

Table 2.3. Hydrogen bonds for $[\text{Mo}^{\text{VI}}\text{O}_2(\text{L}^1)]$ (**2.1**), $[\text{Mo}^{\text{VI}}\text{O}_2\text{L}^2]$ (**2.2**) and $[\text{Mo}^{\text{VI}}\text{O}_2(\text{L}^3)]$ (**2.3**).

Compound	D-H...A	d(D-H)	d(H...A)	d(D...A)	$\angle(\text{DHA})$
2.1	N(2)-H(2N)...O(1)#1	0.95	2.31	3.067(4)	137.0
2.2	N(2)-H(2N)...O(2)#2	0.85(2)	2.06(2)	2.8663(14)	157.5(18)
2.3	N(1)-H(1N)...O(1)#3	0.96(3)	2.59(3)	3.194(3)	121(2)

Symmetry transformations used to generate equivalent atoms: #1 $x-y, x, -z+1$ #2 $-x+1, y-1/2, -z+1/2$ #3 $x, y-1/2, -z+1/2$

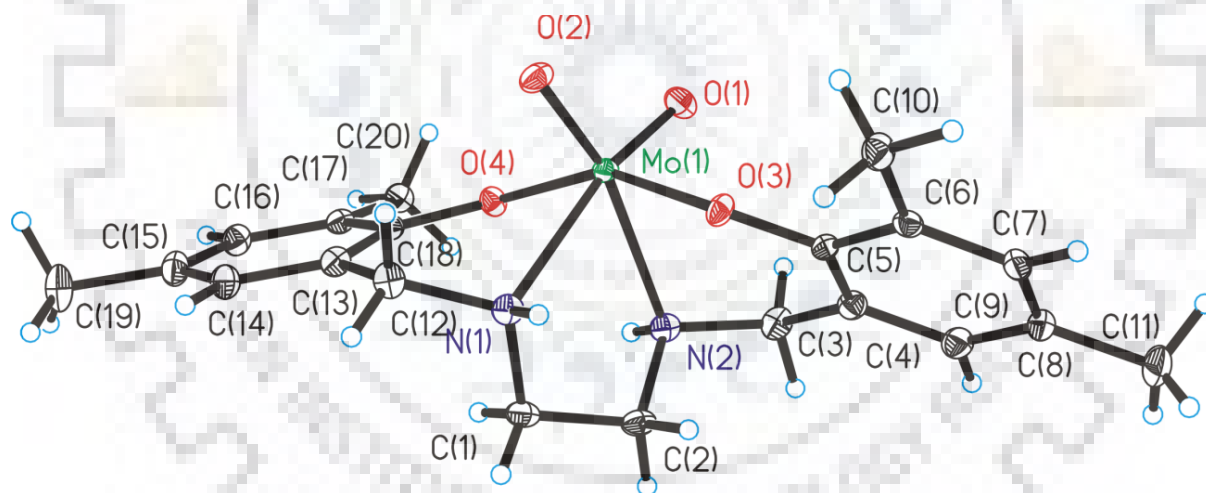


Fig. 2.2. ORTEP plot of complex $[\text{Mo}^{\text{VI}}\text{O}_2\text{L}^2]$ (**2.2**). All the non-hydrogen atoms are presented by their 50% probability ellipsoids.

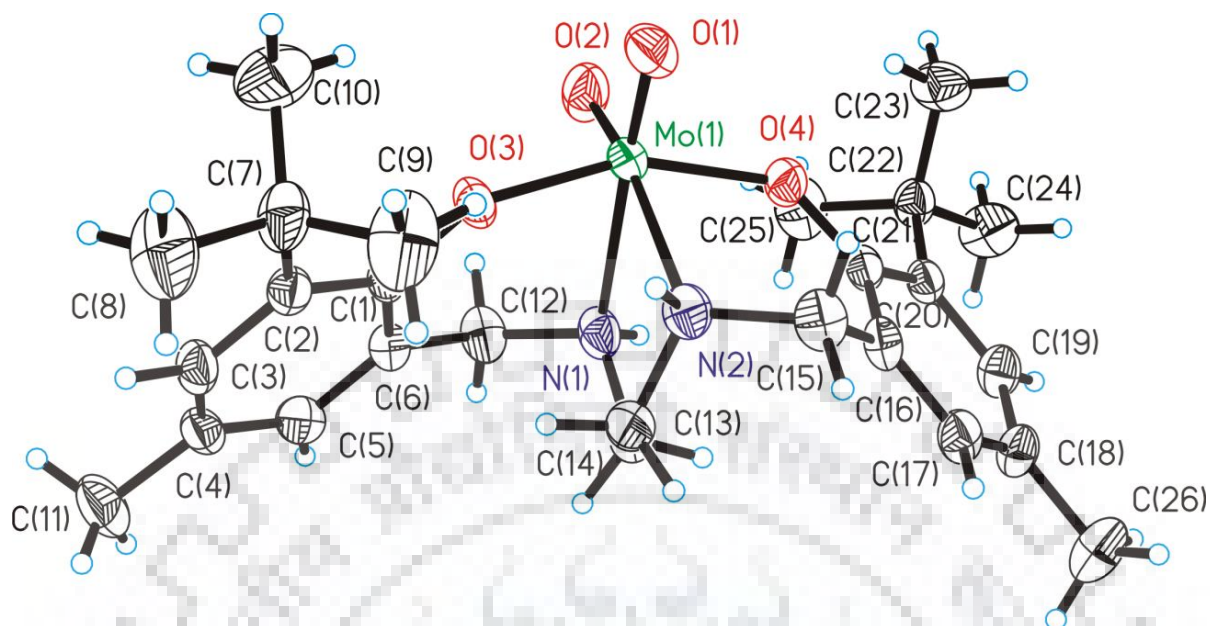


Fig. 2.3. ORTEP plot of complex $[\text{Mo}^{\text{VI}}\text{O}_2 (\text{L}^3)]$ (2.3). All the non-hydrogen atoms are presented by their 50% probability ellipsoids.

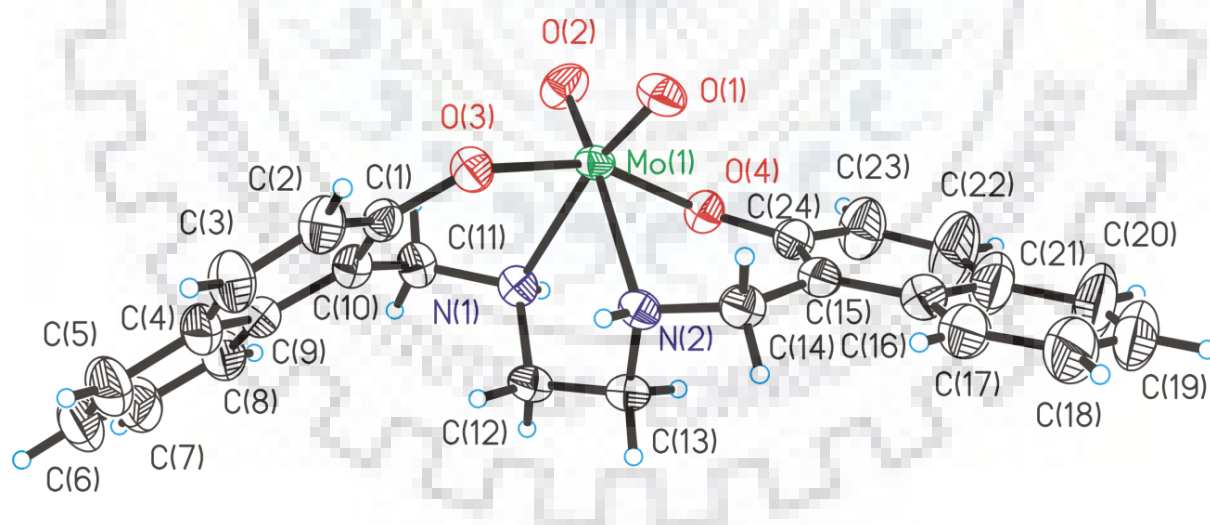


Fig. 2.4. ORTEP plot of complex $[\text{Mo}^{\text{VI}}\text{O}_2 (\text{L}^5)]$ (2.5). All the non-hydrogen atoms are presented by their 50% probability ellipsoids.

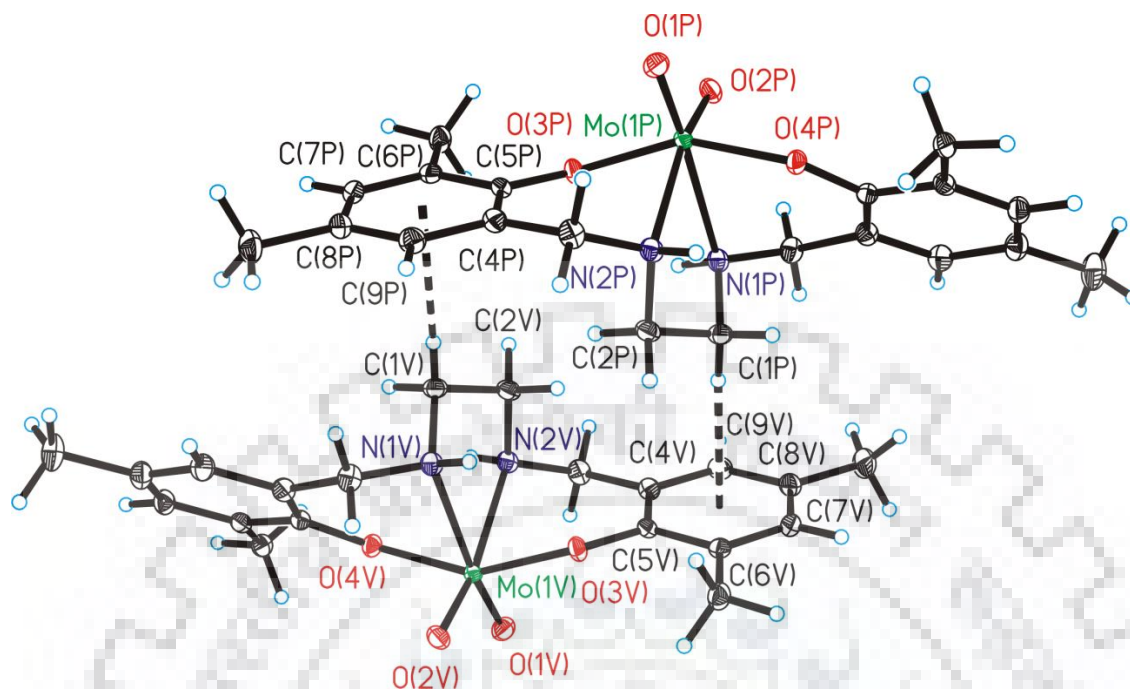


Fig. 2.5. X-ray fragment of $[\text{Mo}^{\text{VI}}\text{O}_2\text{L}^2]$ (**2.2**). C-H $\cdots\pi$ interactions in **2.2** are present in the crystal packing and they are drawn in dashed black lines.

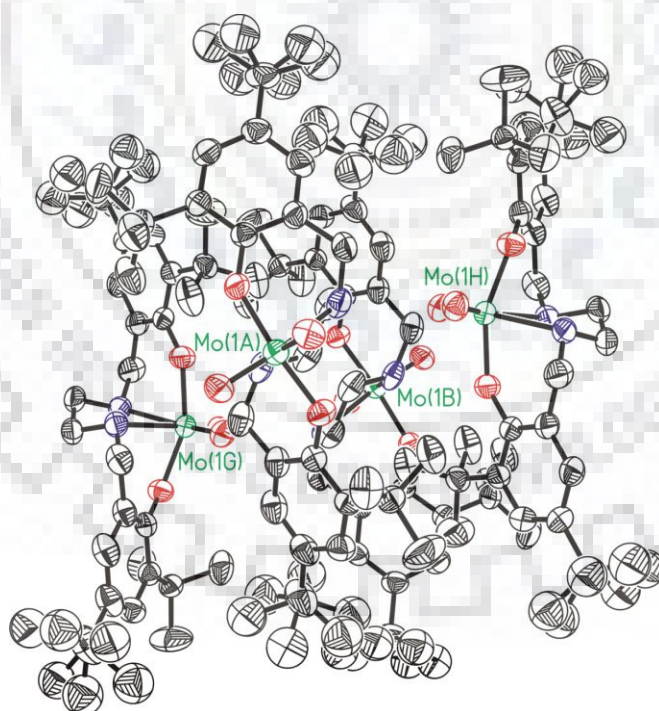


Fig. 2.6. View along b axis of the crystal packing of $[\text{Mo}^{\text{VI}}\text{O}_2(\text{L}^1)]$ (**2.1**). All the non-hydrogen atoms are presented by balls and sticks. Hydrogen atoms are omitted for clarity.

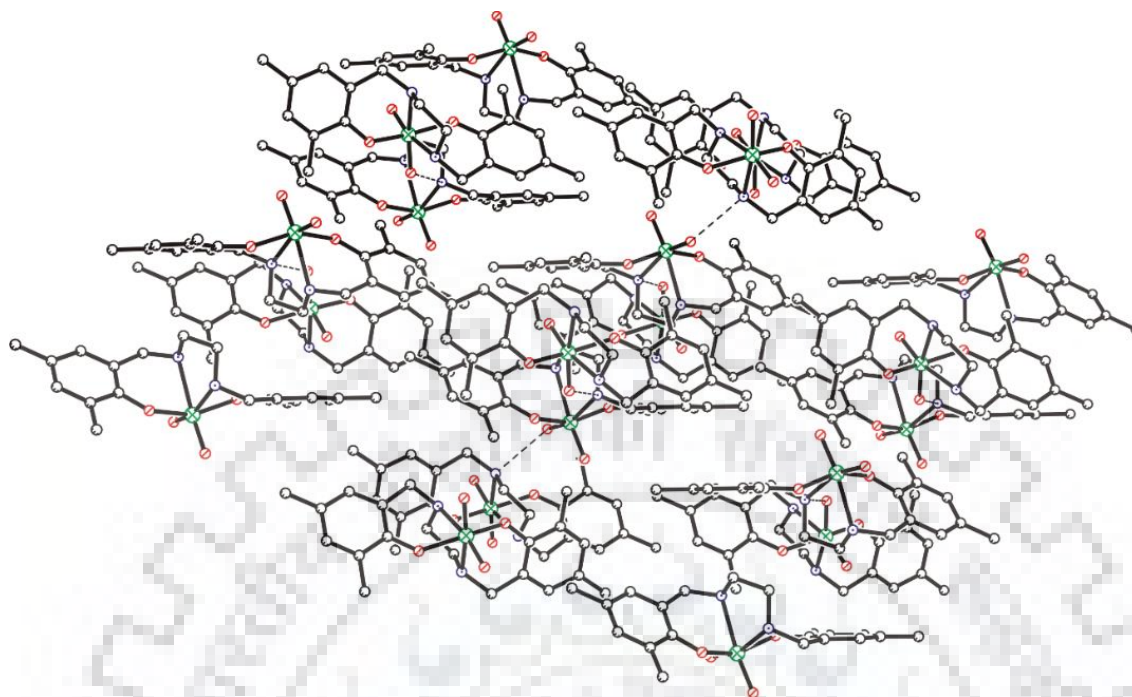


Fig. 2.7. Crystal packing of [Mo^{VI}O₂L²] (2.2). All the non-hydrogen atoms are presented by balls and sticks. Hydrogen atoms are omitted for clarity.

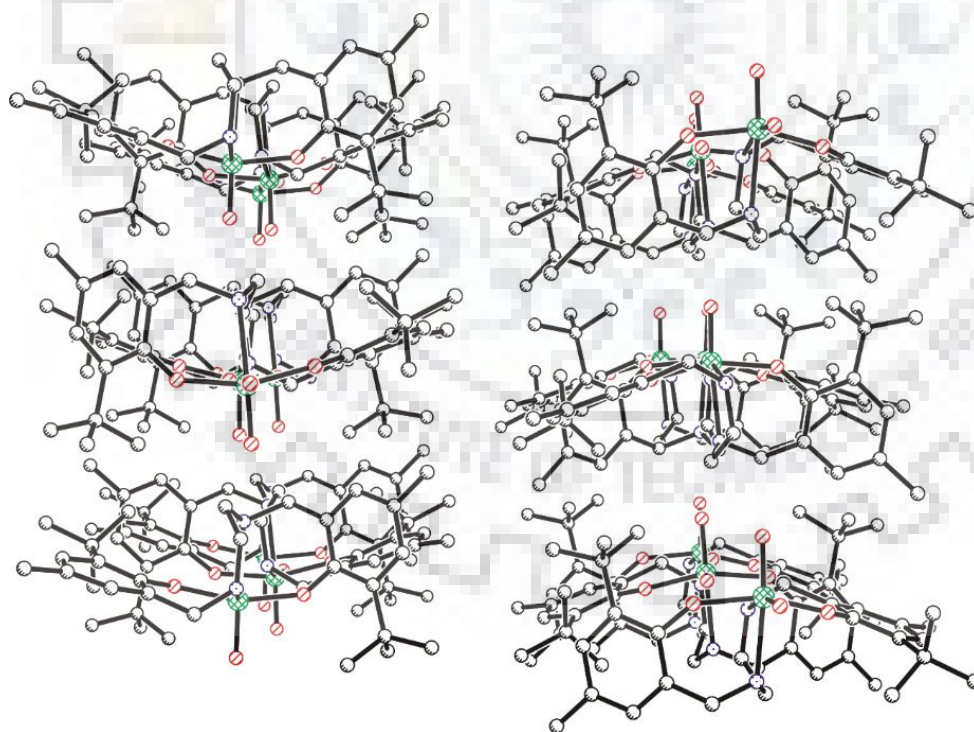


Fig. 2.8. Crystal packing of [Mo^{VI}O₂(L³)] (2.3). All the non-hydrogen atoms are presented by balls and sticks. Hydrogen atoms are omitted for clarity.

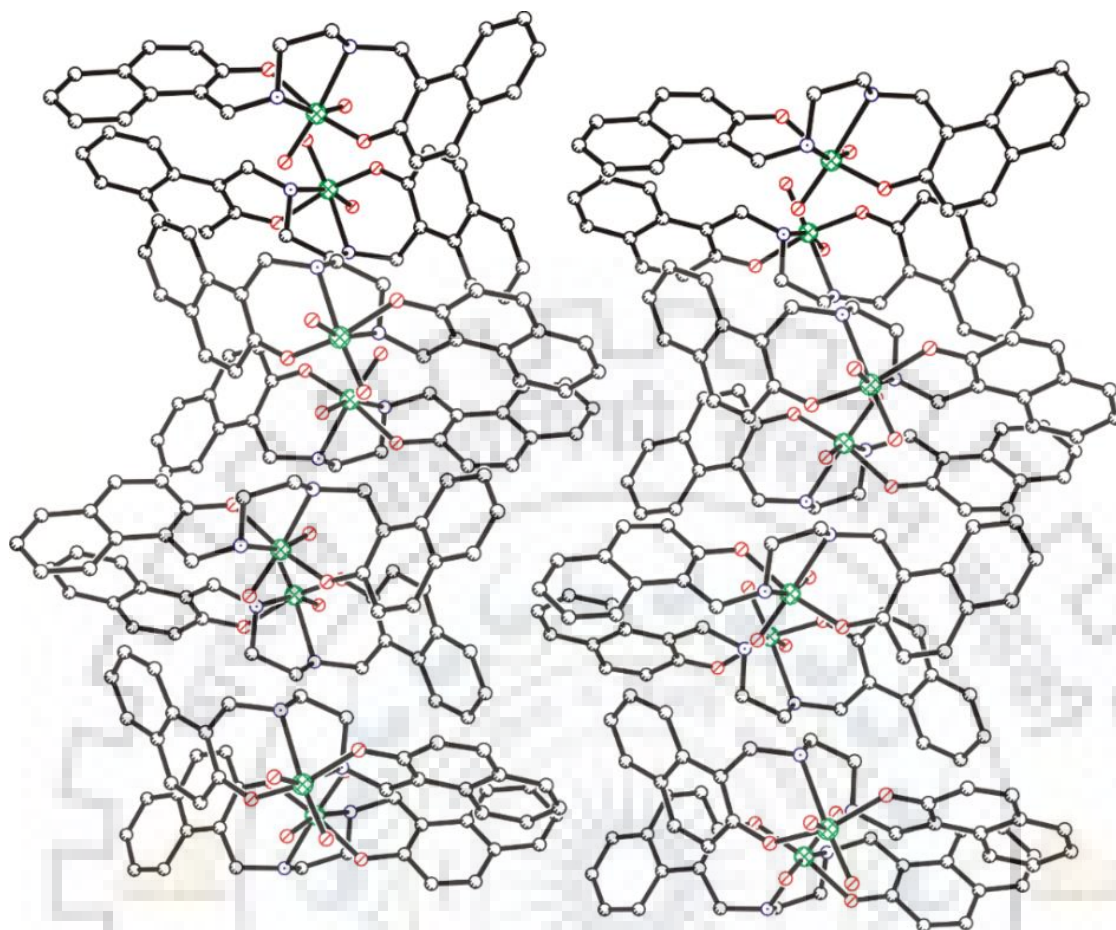


Fig. 2.9. Crystal packing of $[\text{Mo}^{\text{VI}}\text{O}_2(\text{L}^5)]$ (**2.5**). All the non-hydrogen atoms are presented by balls and sticks. Hydrogen atoms are omitted for clarity.

2.3.2. IR Spectral studies

The coordination modes of the ligands towards metal centre was further confirmed by spectroscopic analyses of all the ligands and the metal complexes. The IR spectra of all complexes exhibits two characteristics IR bands around 883-902 and 902-955 cm^{-1} (Table 2.4), due to the respective symmetric and asymmetric stretching of *cis*-[MoO₂] core [137]. Additionally, the broad peak around *ca.* 3400 cm^{-1} present in the spectra of all the ligands due to phenolic -OH is absent in the corresponding complexes indicating the coordination of phenolic oxygen following deprotonation. Coordination of nitrogen functionalities could not be ascertained unequivocally by IR spectral study because the spectra of the ligands as well as complexes both exhibit $\nu(\text{NH})$ bands around 3050-3100 cm^{-1} . However, this

coordination is well supported by single crystal X-ray study (vide supra). Other characteristic bands present in the spectra of the ligands as well as the complexes include the stretching frequencies around 2800–3000 cm^{-1} due to different alkyl substitution at the phenolic rings.

Table 2.4. Selected IR data (in cm^{-1}) for the ligands and complexes with tentative assignments.

Entry	Compounds	$\nu(\text{OH})$	$\nu(\text{N-H})$	$\nu_{\text{asym}}(\text{O}=\text{Mo}=\text{O})$	$\nu_{\text{sym}}(\text{O}=\text{Mo}=\text{O})$
1	H_2L^1 (I)	3270(b)	3000	-	-
2	$[\text{Mo}^{\text{VI}}\text{O}_2\text{L}^1]$ (2.1)		2960, 3260	927	883
3	H_2L^2 (II)	3440(b)	3130(b)		
4	$[\text{Mo}^{\text{VI}}\text{O}_2\text{L}^2]$ (2.2)		3182, 3295	927	884
5	H_2L^3 (III)	3425(b)	3050	-	-
6	$[\text{Mo}^{\text{VI}}\text{O}_2\text{L}^3]$ (2.3)		3300	904	884
7	H_2L^4 (IV)	3440(b)	2990, 3128(b)		
8	$[\text{Mo}^{\text{VI}}\text{O}_2\text{L}^4]$ (2.4)		3220	914	899
9	H_2L^5 (V)	3450(b)	3055	-	-
10	$[\text{Mo}^{\text{VI}}\text{O}_2\text{L}^5]$ (2.5)		3055, 3245	955	902

2.3.3. UV-Visible spectral studies

Table 2.5 presents UV/Vis spectral data of ligands and their *cis*- $[\text{MoO}_2]^{2+}$ complexes recorded in MeCN and Fig. 2.10 presents spectra of complexes. The UV-Vis spectra of the ligands display two spectral bands around 224–280 and 286–336 nm which can be attributed to $\pi \rightarrow \pi^*$ and $n \rightarrow \pi^*$ transitions, respectively (See Table 2.5 for exact values). These transitions undergo a hypsochromic shift in the metal complexes, and thus the corresponding UV-Vis spectra of the complexes display only the $n \rightarrow \pi^*$ band around 260–336 nm. This is possibly due to rearrangement of the ligand structure after coordination with metal ion. Additionally, all complexes also display an intense but broad band in the 330–380 nm due to ligand to metal charge transfer transition.

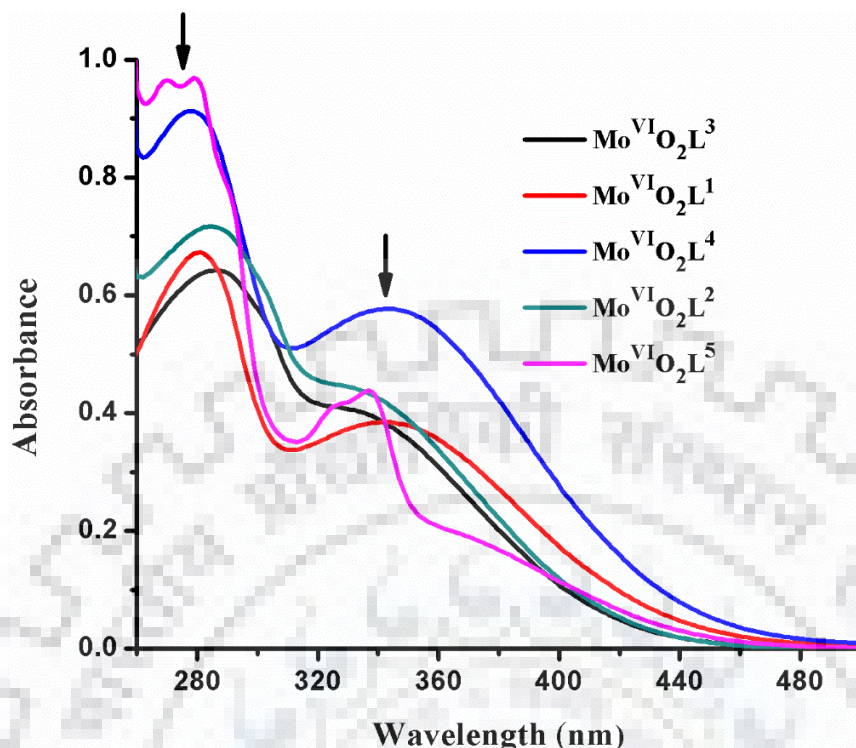


Fig. 2.10. UV/Vis spectra of complexes $[\text{Mo}^{\text{VI}}\text{O}_2\text{L}^{1-5}]$ (2.1 - 2.5).

Table 2. 5. UV/Vis spectral data of ligands and complexes.

Compound	λ [nm] (ϵ , litre mole ⁻¹ cm ⁻¹)
H_2L^1 (I)	234 (2.48×10^3), 294 (1.22×10^3)
$[\text{Mo}^{\text{VI}}\text{O}_2\text{L}^1]$ (2.1)	280 (4.2×10^3), 345 (2.39×10^3)
H_2L^2 (II)	224 (1.46×10^3), 286 (4.73×10^3)
$[\text{Mo}^{\text{VI}}\text{O}_2\text{L}^2]$ (2.2)	284 (3.25×10^3), 324 (2.04×10^3)
H_2L^3 (III)	226 (1.75×10^3), 286 (1.02×10^3)
$[\text{Mo}^{\text{VI}}\text{O}_2\text{L}^3]$ (2.3)	285 (3.46×10^3), 330 (2.19×10^3)
H_2L^4 (IV)	237 (1.43×10^3), 295 (6.66×10^2)
$[\text{Mo}^{\text{VI}}\text{O}_2\text{L}^4]$ (2.4)	277 (4.90×10^3), 342 (3.09×10^3)
H_2L^5 (V)	280 (2.23×10^3), 336 (1.24×10^3)
$[\text{Mo}^{\text{VI}}\text{O}_2\text{L}^5]$ (2.5)	260 (4.82×10^3), 336 (2.17×10^3), 380 (6×10^3)

2.3.4. ^1H NMR spectral studies

The coordinating modes of ligands to the metal complexes were further ascertained by recording their ^1H NMR spectra in CDCl_3 . Experimental section presents spectral data, Fig. 2.11 provides the representative spectra (ligand **II** and complex **2.2**) and Figs. 2.12 – 2.19 provide ^1H NMR spectra of other ligands and complexes for the series. All ligands' spectra show a signal at $\delta = 10.25\text{--}10.73$ ppm due to two phenolic --OH protons which are equivalent in nature. The disappearance of this signal in the spectra of complexes indicates the coordination of the phenolic oxygen after their deprotonation. A relatively broad signal appearing at $\delta = 3.45\text{--}3.64$ ppm due to --NH protons in ligands shows slight shift in their position in the corresponding complexes, indicating their coordination to the metal center and the resulting change in electron density. Signals due to methylene groups, connecting to --NH and aromatic ring, appears as small singlet at $\delta = 3.77\text{--}3.92$ ppm except ligand H_2L^5 which exhibits two singlets at $\delta = 4.80$ (s, 2H) and 4.3 (s, 2H) ppm. This signal become diastereotopic following coordination and splits into two doublets (in **2.2**, **2.4** and **2.5**) with two protons each or four doublets (in **2.1** and **2.3**) with one proton each and appear at relatively higher δ values. This trend is more common in tripodal ligand containing complexes [138 - 141]. Similarly, the ethylene protons attached to two dipodal --NH appears as singlet at $\delta = 2.57\text{--}3.03$ ppm in ligands and this splits into two triplets and appears at slightly lower positions. Signals due to aromatic protons, methyl and *tert*-butyl groups in ligands as well as in complexes appear in the expected region with slight variations.

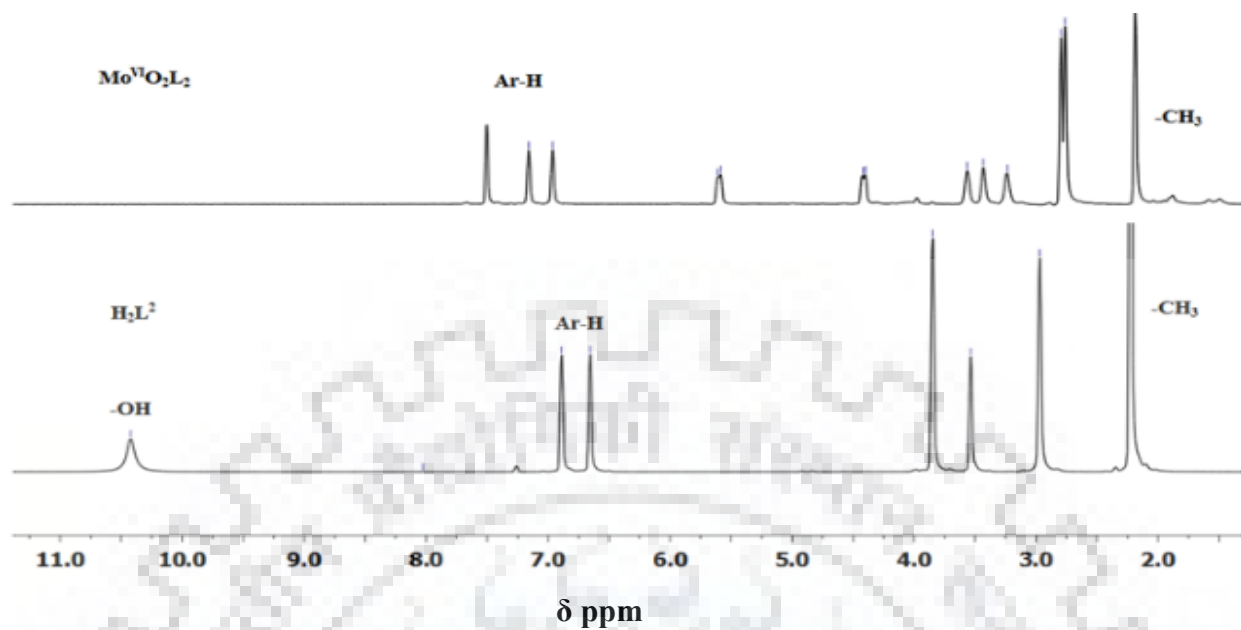


Fig. 2.11. ^1H NMR spectra of H_2L^2 and **2.2** in CDCl_3 .

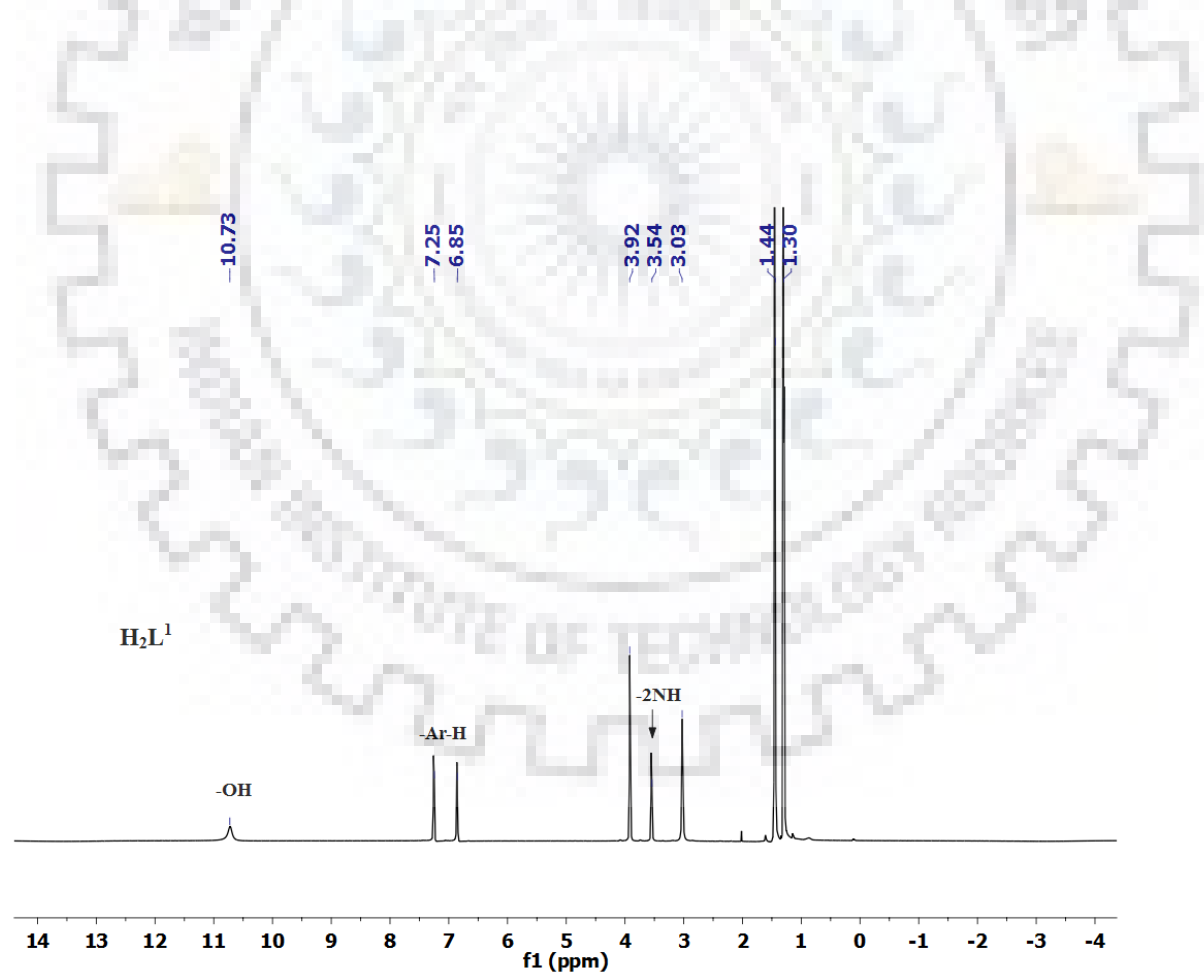


Fig. 2.12. ^1H NMR spectrum of H_2L^1 in CDCl_3

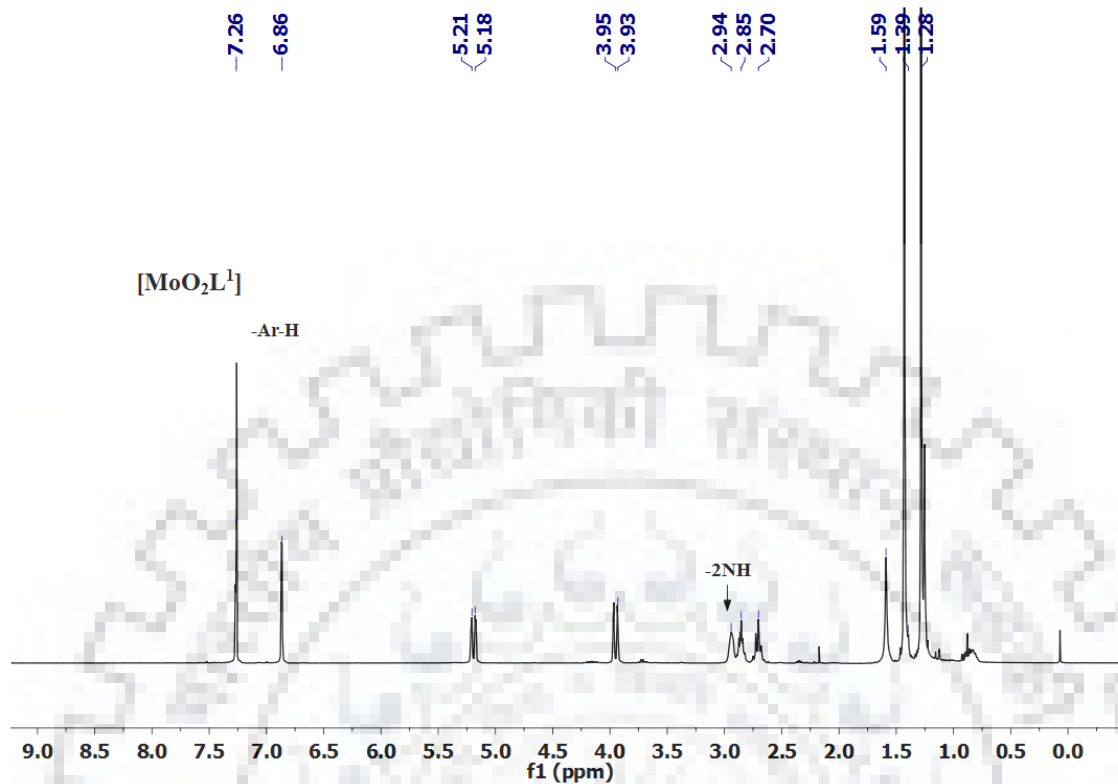


Fig. 2.13. ^1H NMR spectrum of $[\text{Mo}^{\text{VI}}\text{O}_2\text{L}^1]$ in CDCl_3

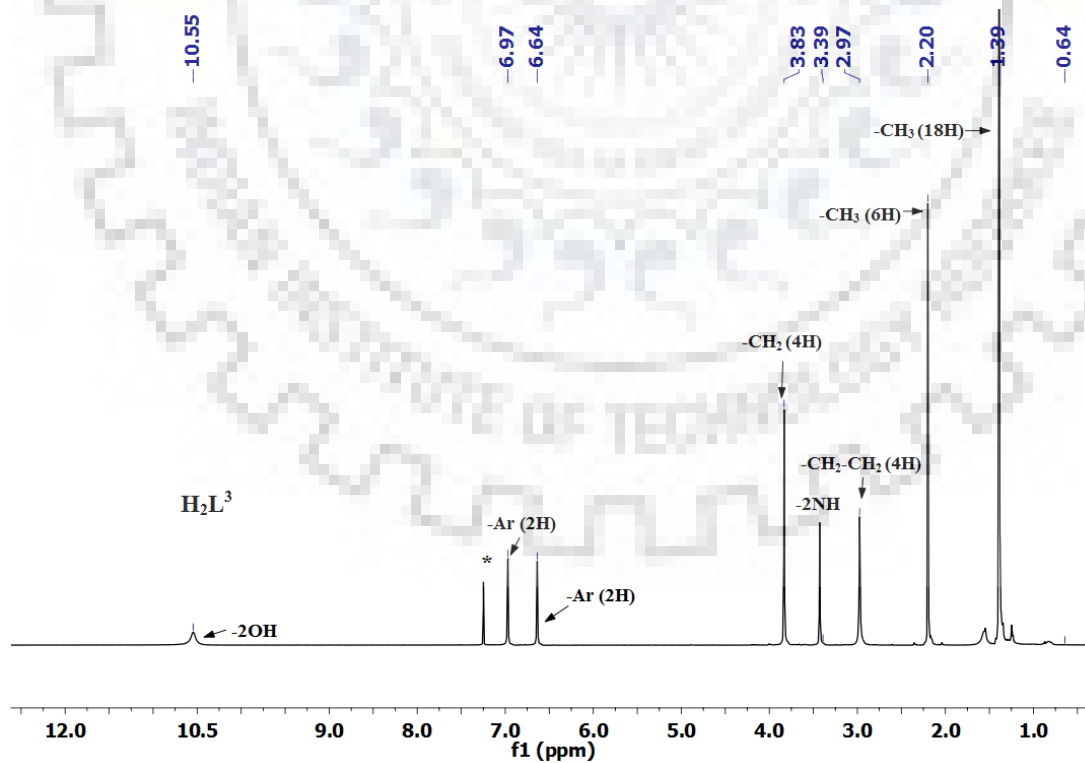


Fig. 2.14. ^1H NMR spectrum of H_2L^3 in CDCl_3 .

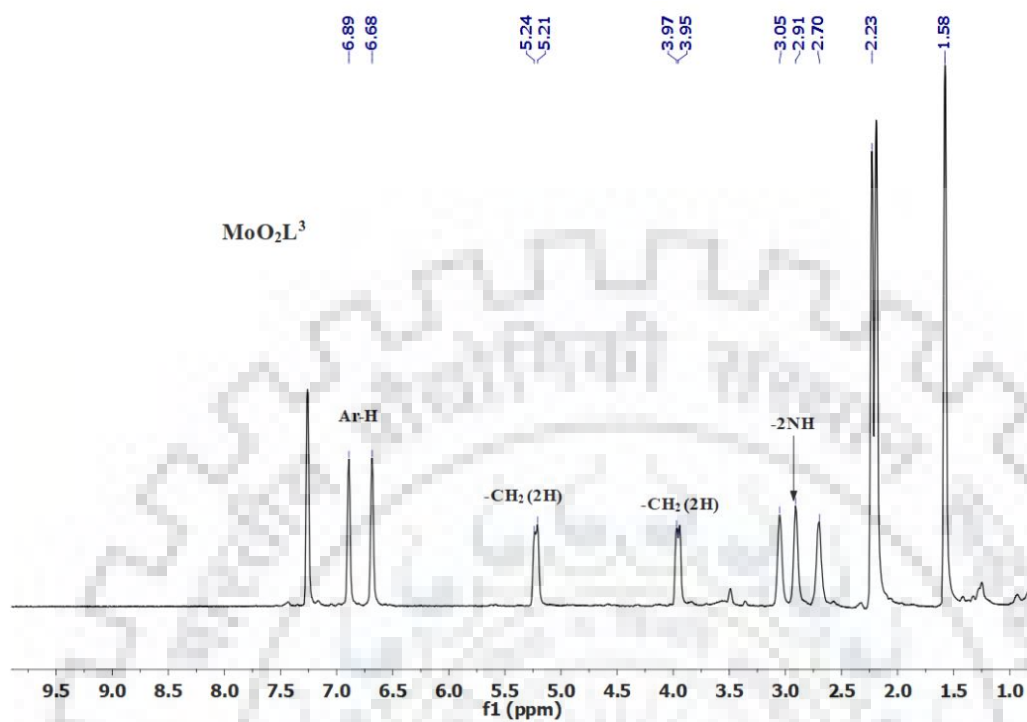


Fig. 2.15. ^1H NMR spectrum of $[\text{Mo}^{\text{VI}}\text{O}_2\text{L}^3]$ in CDCl_3 .

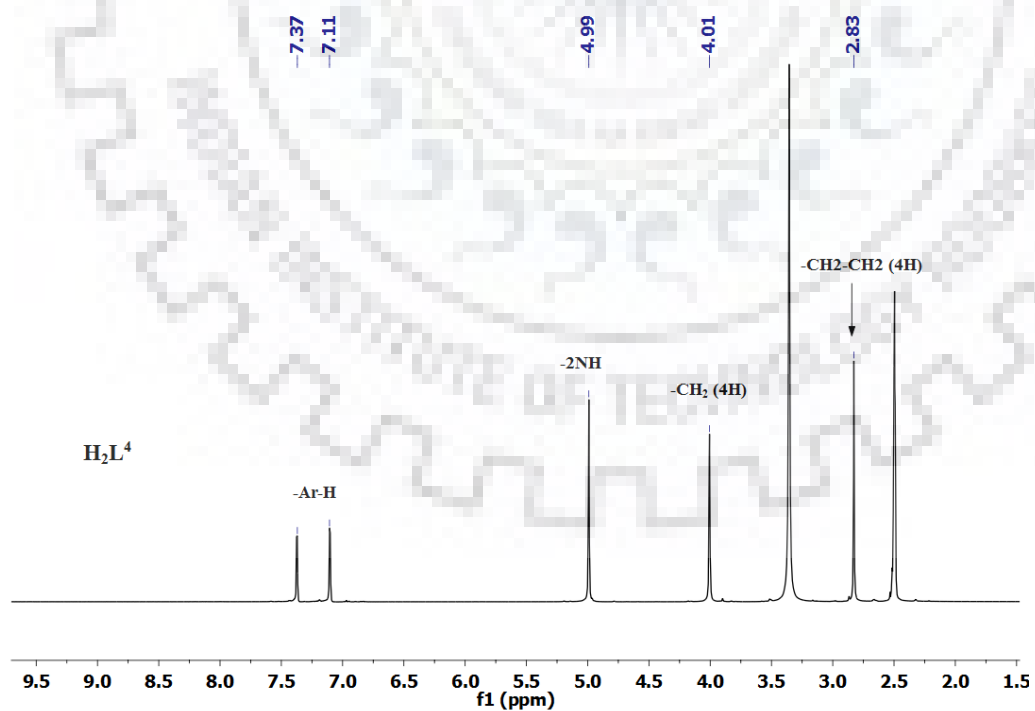


Fig. 2.16. ^1H NMR spectrum of H_2L^4 in DMSO-d_6 .

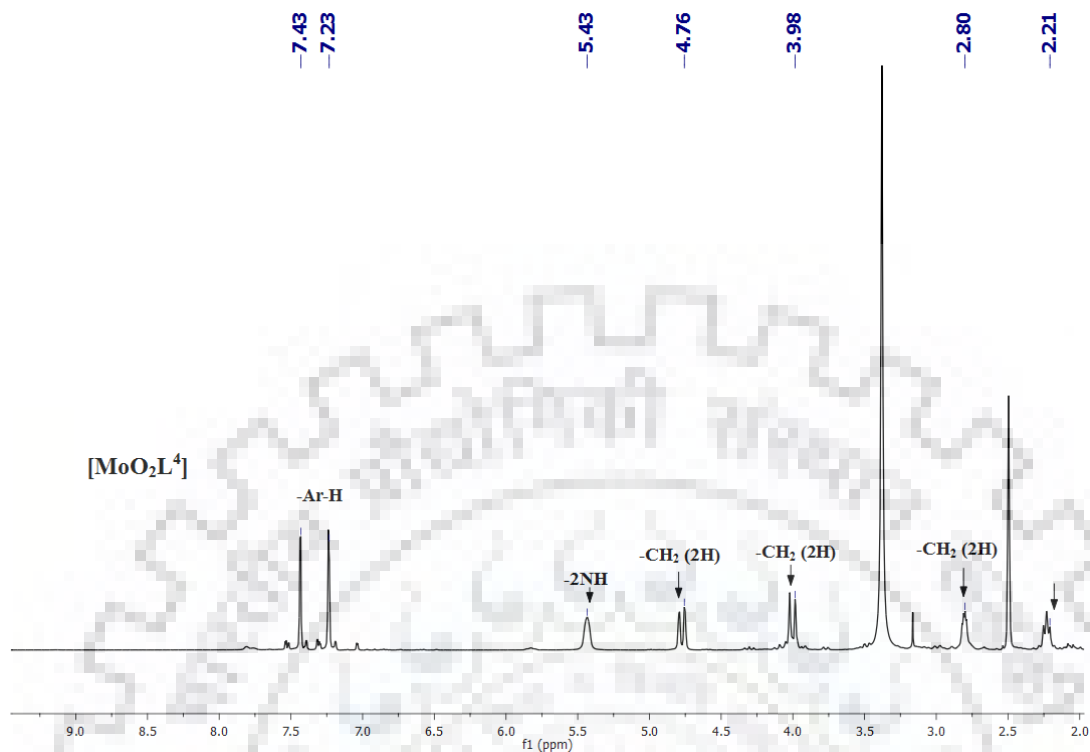


Fig. 2.17. ^1H NMR spectrum of $[\text{Mo}^{\text{VI}}\text{O}_2\text{L}^4]$ in DMSO-d_6 .

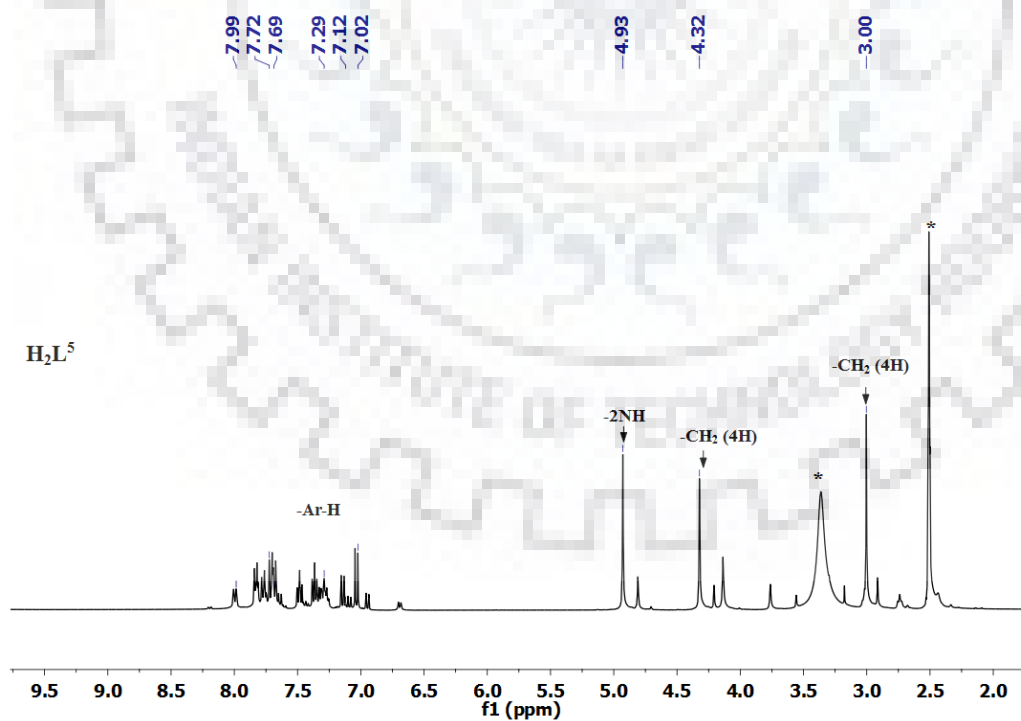


Fig. 2.18. ^1H NMR spectrum of H_2L^5 in DMSO-d_6 .

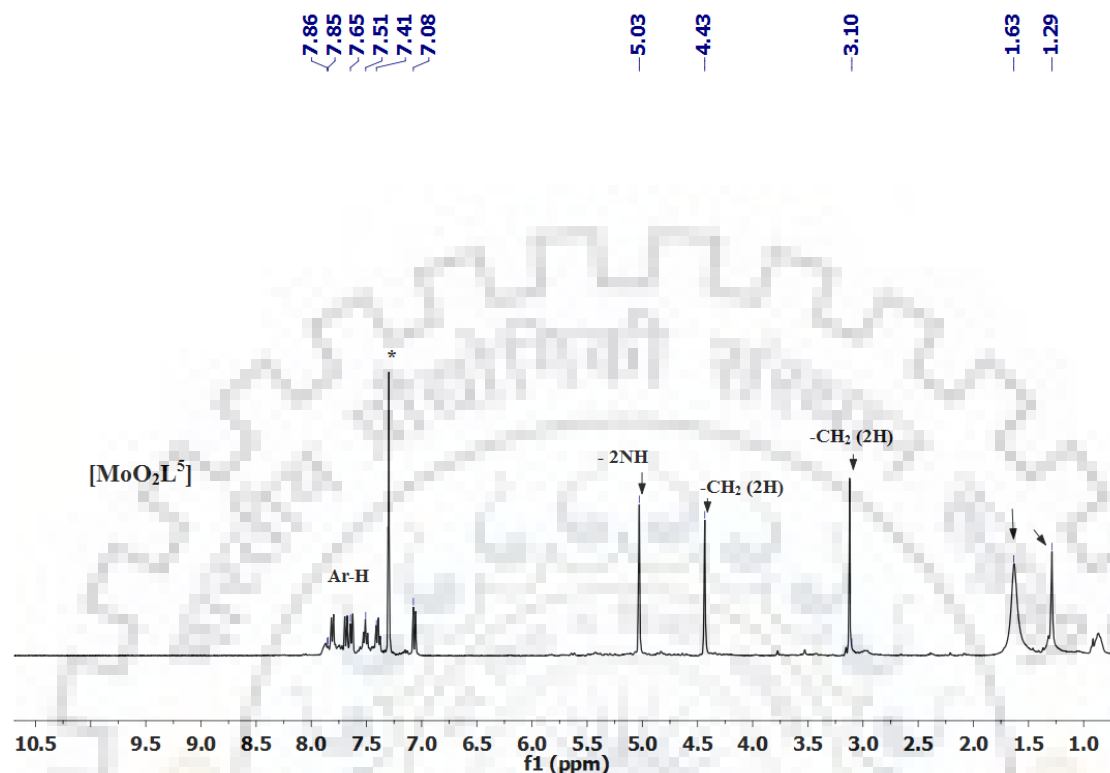
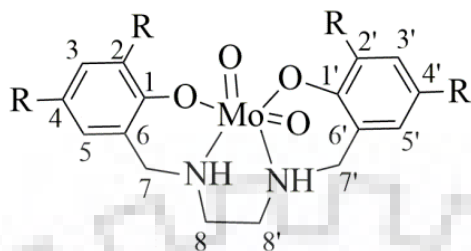


Fig. 2.19. ^1H NMR spectrum of $[\text{Mo}^{\text{VI}}\text{O}_2\text{L}^5]$ in CDCl_3 .

2.3.5. ^{13}C NMR spectral studies

The binding modes of the ligands were further supported by the study of the coordination-induced ^{13}C NMR chemical shifts. The spectra were recorded in $\text{CDCl}_3/\text{DMSO-d}_6$ and the relevant data are presented in Table 2.6. All carbons resonate well within the expected regions; however, significant shifts, $\Delta\delta = [\delta(\text{complex}) - \delta(\text{ligand})]$, were observed in the signals of the carbon atoms in the vicinity of the coordinating atoms. Thus, the carbons bearing the phenolic oxygens undergo a shift, $\Delta\delta$ between ~ 3.4 to -0.68 ppm (see Table 2.6). Similarly, the effect of coordination is also well pronounced on the ethylene protons, and they resonate with an average shift of $\Delta\delta$ between -11.48 to 7.99 ppm. A complete list of all peaks is included in the experimental section (see Fig. 2.20 as a representative).

Table 2.6. ^{13}C NMR spectral data (δ in ppm) of ligands and complexes.

Compound ^a	C ₁ /C _{1'}	C ₄ /C _{4'}	C ₇ /C _{7'}	C ₈ /C _{8'}
H ₂ L ¹ (I)	150.83	142.17	49.69	51.35
[Mo ^{VI} O ₂ L ¹] (2.1)	154.23	140.84	51.87	59.34
($\Delta\delta$)	(3.4)	(2.03)	(2.18)	(7.99)
H ₂ L ² (II)	153.13	131.24	58.36	51.77
[Mo ^{VI} O ₂ L ²] (2.2)	156.49 (3.36)	130.58	53.59	45.63
($\Delta\delta$)		(-0.66)	(-4.77)	(-11.48)
H ₂ L ³ (III)	154.21	136.07	58.05	50.89
[Mo ^{VI} O ₂ L ³] (2.3)	156.71	138.5	53.20	45.71
($\Delta\delta$)	(2.5)	(2.43)	(-4.85)	(-5.18)
H ₂ L ⁴ (IV)	154.43	128.17	52.31	45.72
[Mo ^{VI} O ₂ L ⁴] (2.4)	153.75	127.40	50.20	45.97
($\Delta\delta$)	(-0.68)	(-0.77)	(-2.11)	(0.25)

^a $\Delta\delta = [\delta(\text{complex}) - \delta(\text{free ligand})]$.

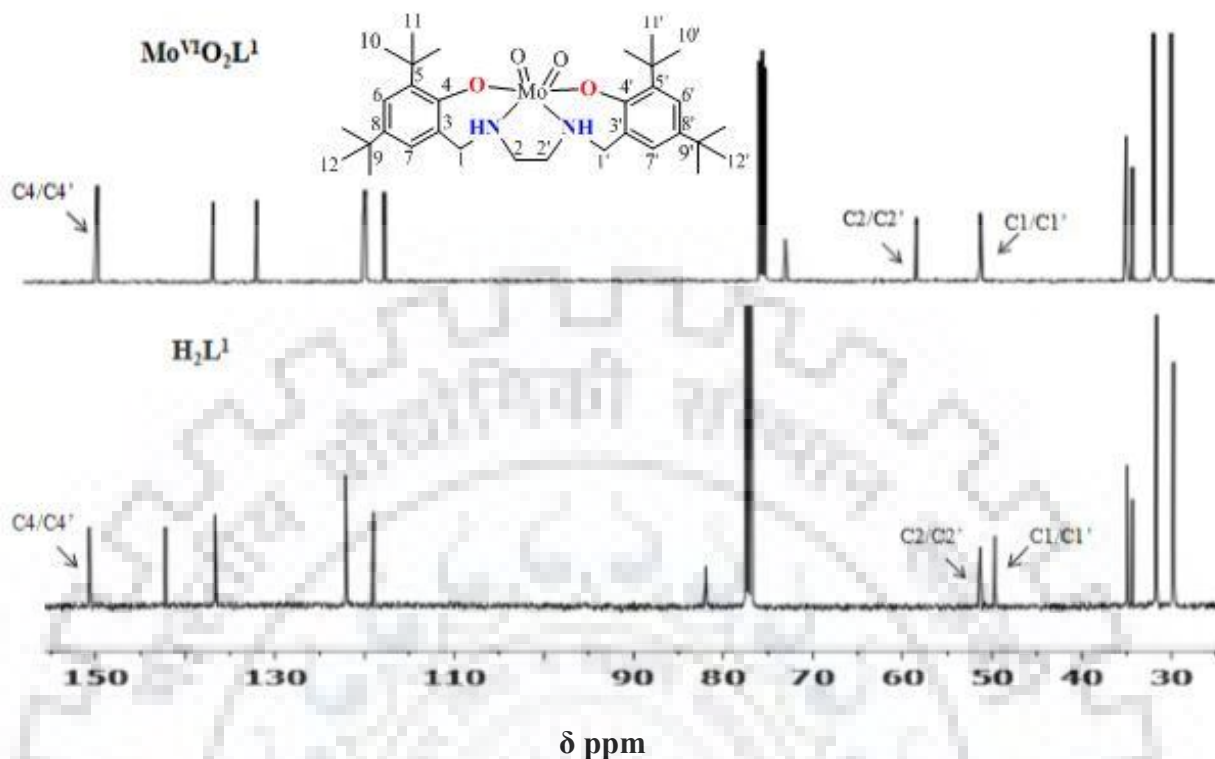


Fig. 2.20. ^{13}C NMR spectra [chemical shifts (δ) in ppm] of H_2L^1 and **2.1** in CDCl_3 .

2.3.6. Oxygen atom transfer between benzoin and DMSO

Cis-dioxidomolybdenum(VI) complexes are known to catalyze oxygen atom transfer (OAT) in the presence of DMSO in a fashion similar to DMSO reductases. Most of these reactions reported in literature, are based on oxygen atom transfer between phosphines and/ or DMSO[57,88,89,125-129] and only a few reports are available where OAT has been explored with a suitable organic substrate [29,30,91,130]. In our recent studies, we have reported the oxygen atom transfer ability of *cis*-dioxidomolybdenum(VI) complexes between DMSO and benzoin in acetonitrile at 80 °C. We have also proposed an overall steric control over the reaction mechanism, and identified suitable reaction intermediates [29]. The present study further explores the mechanistic details involving the oxygen atom transfer between DMSO and benzoin, catalyzed by *cis*-dioxidomolybdenum(VI) complexes. As the *cis*-dioxidomolybdenum (VI) complexes reported here are built on amino bisphenols, we have evaluated their electronic environment effect on OAT reactions between DMSO and benzoin in acetonitrile at 80 °C.

The reaction was monitored over a period of 24 h, and the maximum conversion of 99 % to benzil selectively was achieved within 18 h at 80 °C using $[\text{Mo}^{\text{VI}}\text{O}_2\text{L}^5]$ (**2.5**) as a representative catalyst. The reaction was followed by measuring the decrease in the concentration of benzoin and formation of benzil via periodic HPLC analysis of the reaction mixture, eluted with water-acetonitrile-trifluoroacetic acid mixture (60:40:02) (Fig. 2.21).

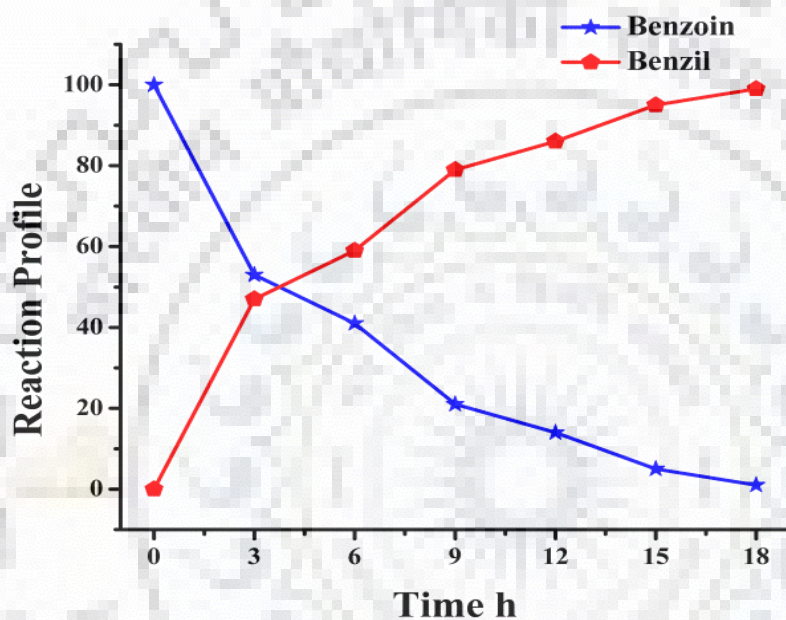


Fig. 2.21. The progress of the reaction as monitored by HPLC analysis of the reaction mixture at different time intervals using $[\text{Mo}^{\text{VI}}\text{O}_2(\text{L}^5)]$ (**2.5**) as the catalyst. Mobile phase: MeCN : H₂O : TFA 60 : 40 : 0.02 (for details, see text).

The reaction was initiated by taking benzoin (1.00 g, 5 mmol), DMSO (1 mL, 14 mmol) and the complex **2.5** as catalyst (3.00 mg, 6.02 μmol) in 10 mL of acetonitrile in a two neck 50 mL round bottom flask. DMSO was always taken in excess with respect to benzoin as well as the catalyst in all the reactions. The temperature of the reaction mixture was maintained at 80 °C for a period of 24 h, and the progress of the reaction was monitored by withdrawing small aliquots of the reaction mixture periodically and analyzing the same by HPLC analysis. A maximum of 99% conversion was achieved in 18 h and after that no

further conversion was noted. Under the same reaction conditions, the other four complexes were also tested and the obtained results are collected in Table 2.7 and Fig. 2.22. Thus, the best conversion of 99 % was achieved by using 3.00 mg (6.02 μmol) of **2.5**.

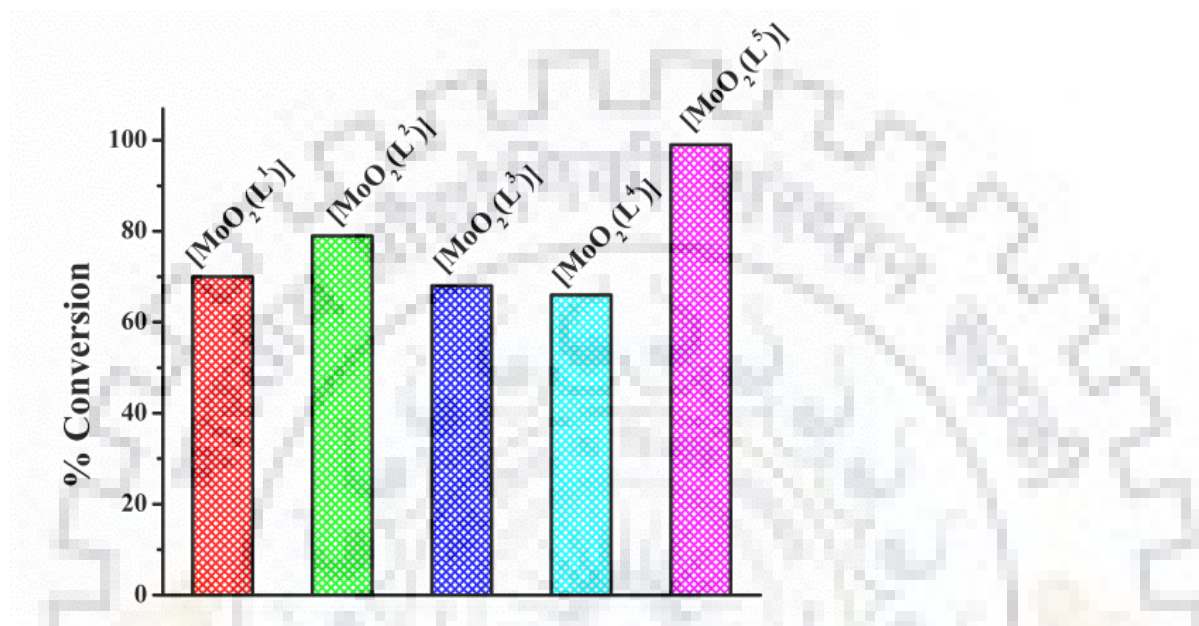


Fig. 2.22. Results for oxygen atom transfer reaction between DMSO and benzoin catalyzed by *cis*-[MoO₂]²⁺ complexes (for details, see text).

Table 2.7. Dioxidomolybdenum(VI) complexes catalyzed oxygen atom transfer between benzoin and DMSO in acetonitrile at 80 °C in 18 h of reaction time; conversion, TOF and selectivity data.

Entry	Catalyst	Catalyst [mg, μmol]	Conv. [%]	Selectivity [%]	TOF [h ⁻¹]
1	[Mo ^{VI} O ₂ (L ¹)] (2.1)	3.76, 6.02	70	100	33
2	[Mo ^{VI} O ₂ (L ²)] (2.2)	2.73, 6.02	79	100	37
3	[Mo ^{VI} O ₂ (L ³)] (2.3)	3.24, 6.02	68	100	31
4	[Mo ^{VI} O ₂ (L ⁴)] (2.4)	3.22, 6.02	66	100	31
5	[Mo ^{VI} O ₂ (L ⁵)] (2.5)	3.00, 6.02	99	100	46

The results of the catalytic OAT reaction between DMSO and benzoin using different catalysts, show a stark variation while changing the substituent on the phenol rings. Therefore, the complex with naphthyl rings, i.e. $[\text{Mo}^{\text{VI}}\text{O}_2(\text{L}^5)]$ (**2.5**) renders an excellent conversion of 99 %. This conversion drops to 70 – 80 % with alkyl substitution while the chloro substitution further slows down the reaction, and the overall conversion drops to 66 % in 18 h of reaction time for $[\text{Mo}^{\text{VI}}\text{O}_2(\text{L}^4)]$ (**2.4**). These results can directly be correlated with the electronic environment of the *cis*- $[\text{MoO}_2]^{2+}$ core of the catalyst during the catalytic process and its consequences on the reaction mechanism. Most OAT reactions are thought to proceed via an associative mechanism; the reaction being initiated by the nucleophilic attack of the substrate (DMS in case of DMSO reductase) onto one of the more labile oxido groups of *cis*- $[\text{MoO}_2]^{2+}$ moiety [127, 142, 143]. Thus, the substitutions on the ligands can affect the OAT reactions in two ways: (i) the electronic effect caused by the *para* substituent, and (ii) the steric effect caused by the *ortho* substituent. A bulky *ortho* substitution would hinder the approach of the incoming nucleophile, thus inhibiting the reaction. On the other hand, an electron donating *para* substitution would facilitate the nucleophilic attack of the substrate by compensating the electron density on the metal center because of the +I effect. Thus, when the *ortho* and *para* positions are substituted by chloro group, the reaction conversion drops to lowest, since the electron withdrawing chloro group exerts an –I effect, thus destabilizing the reaction intermediate. Consequently, complex **2.4** delivers the lowest conversion of 66 %. However, when the phenolic rings are replaced with naphthyl rings, the steric hindrance is reduced to minimal at the *ortho* positions, enabling an effective and strong interaction of the nucleophile with the metal center. Further, they also contribute towards stabilization of the reaction intermediate due to enhanced conjugation. Thus, the maximum conversion of 99 % is achieved with complex **2.5**. The results obtained with the other three catalysts are also in line with the *ortho* effects of alkyl substitution [29]. The Hammett plot also shows a good correlation for all the four electronic *para* substitutions ($R^2 = 0.98$ and $\rho = -1.78$) (Fig. 2.23). This further substantiates our hypothesis of an electron deficient transition state during the reaction mechanism.

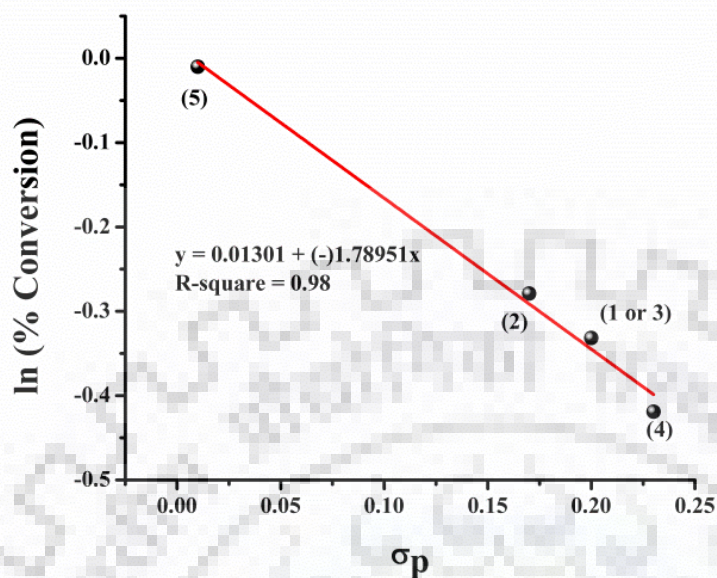


Fig. 2.23. Hammett plot for OAT reaction between DMSO and benzoin catalyzed by *cis*-[MoO₂]²⁺ complexes.

Dioxidomolybdenum(VI) complexes catalyzed oxygen atom transfer between 4-chlorobenzoin and DMSO have also been carried out in acetonitrile at 80 °C in 18 h of reaction time (Table 2.8 and Fig. 2.24). The results of the catalytic OAT reaction between DMSO and 4-chlorobenzoin using different catalysts, show a stark variation while changing the substituent on the phenol rings. Therefore, the complex with naphthyl rings, i.e. [MoO₂(L⁵)] (**2.5**) renders an excellent conversion of 100 %. This conversion drops to 95 – 100 % with alkyl substitution while the chloro substitution further slows down the reaction, and the overall conversion drops to 89 % in 18 h of reaction time for [Mo^{VI}O₂(L⁴)] (**2.4**). These results again can directly be correlated with the electronic environment of the *cis*-[MoO₂]²⁺ core of the catalyst during the catalytic process and its consequences on the reaction mechanism.

The electron withdrawing chloro group exerts an –I effect, destabilizing the reaction intermediate and consequently complex **2.4** gives the lowest conversion of 89 %. The naphthyl ring reduces the steric hindrance at the *ortho* position, stabilizing the reaction intermediate due to enhanced conjugation and consequently complex **2.5** gives highest

conversion of 100 %. Other substituents have intermediate effect. In 4-chlorobenzoin the reaction intermediate is more stable due to presence of –chloro group at para position which enhance the electron donation through conjugation. Because of that we get the excellent conversion which supports the mechanism.

Table 2.8. Dioxidomolybdenum(VI) complexes catalyzed oxygen atom transfer between 4-chlorobenzoin and DMSO in acetonitrile at 80 °C in 18 h of reaction time; conversion, TOF and selectivity data.

Entry	Catalyst	Catalyst [mg, μmol]	Conv. [%]	Selectivity [%]	TOF [h^{-1}]
1	$[\text{Mo}^{\text{VI}}\text{O}_2(\text{L}^1)]$ (2.1)	3.76, 6.02	99	100	46
2	$[\text{Mo}^{\text{VI}}\text{O}_2(\text{L}^2)]$ (2.2)	2.73, 6.02	97	100	45
3	$[\text{Mo}^{\text{VI}}\text{O}_2(\text{L}^3)]$ (2.3)	3.24, 6.02	98	100	45
4	$[\text{Mo}^{\text{VI}}\text{O}_2(\text{L}^4)]$ (2.4)	3.22, 6.02	89	100	41
5	$[\text{Mo}^{\text{VI}}\text{O}_2(\text{L}^5)]$ (2.5)	3.00, 6.02	100	100	46

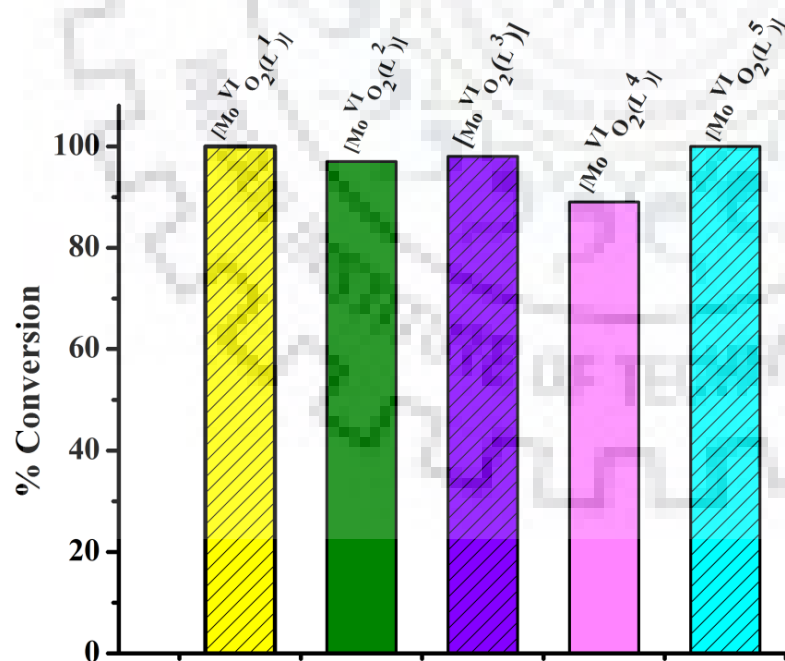


Fig. 2.24. Results for oxygen atom transfer reaction between DMSO and 4-chlorobenzoin catalyzed by *cis*- $[\text{MoO}_2]^{2+}$ complexes (for details, see text).

We have performed a detailed kinetic analysis using the most active complex, **2.5** as the representative catalyst and deduced the rate equation for oxygen atom transfer between DMSO and benzoin. For this, a solution of **2.5** (3.00 mg, 6.02 μmol), benzoin (5 mmol) and DMSO (1 mL) in 10 mL MeCN was maintained at 80 °C. The reaction was performed for a period of 18 h and reaction mixture was analyzed as mentioned earlier.

The integrated rate equation for the OAT reaction between catalyst, benzoin and DMSO can be represented by equation 2. Since, the effective concentration of the catalyst does not change during the reaction, the reaction may be assumed to be following pseudo first order reaction kinetics. This was confirmed by the pseudo first order straight line plot obtained between log of decrease in concentration of benzoin vs time (Fig. 2.25). Equation 3 represents the resulting pseudo first order rate equation. The pseudo first order rate constant for **2.5** was found to be 0.0998 h^{-1} .

$$\text{Rate} = k_{\text{obs}}[\text{Benzoin}]^x[\text{Catalyst}]^y \quad (2)$$

$$\text{Rate} = k_1[\text{Benzoin}] \quad (3)$$

$$\text{where } k_1 = k_{\text{obs}} [\text{Catalyst}]^y \quad (4)$$

$$\ln k_1 = \ln k_{\text{obs}} + y \ln [\text{Catalyst}] \quad (5)$$

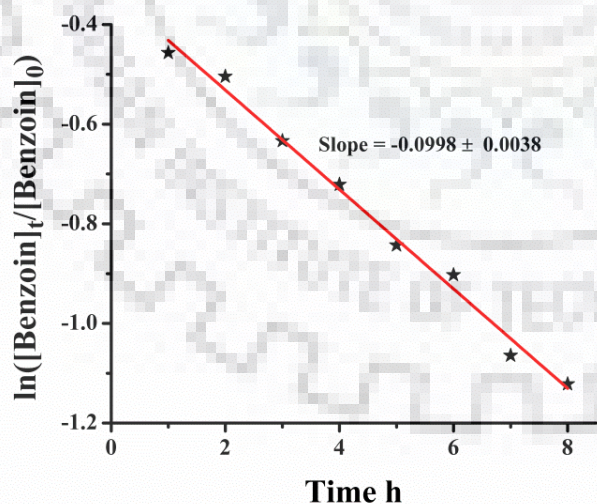


Fig. 2.25. Variation of $[\text{Benzoin}]$ with time for the *cis*- $[\text{Mo}^{\text{VI}}\text{O}_2 (\text{L}^5)]$ (**2.5**) catalyzed oxygen atom transfer reaction in the presence of DMSO. Reaction conditions: $[\text{Benzoin}]_0$ (5 mmol), DMSO (1.00 mL), catalyst (3.00 mg) and MeCN (10 mL).

The order of the reaction with respect to catalyst concentration was determined by solving equation 5, using the data inferred from Fig. 2.25. Thus, the rate of decrease in benzoin concentration after 18 h of reaction time at 80 °C in acetonitrile was monitored using different concentrations of the catalyst, $[\text{Mo}^{\text{VI}}\text{O}_2(\text{L}^5)]$. The relevant plot ($\ln k_1$ vs $\ln[\text{catalyst}]$) is shown in Fig. 2.26 and the observed order with respect to catalyst is found to be 0.94 and k_{obs} is $0.038 \text{ M}^{-1}\text{h}^{-1}$. Therefore, the overall rate equation may be represented as:

$$\begin{aligned} \text{Rate} &= k_{\text{obs}}[\text{Benzoin}][\text{Catalyst}] & (6) \\ k_{\text{obs}} &= 0.038 \text{ M}^{-1} \text{ h}^{-1} \end{aligned}$$

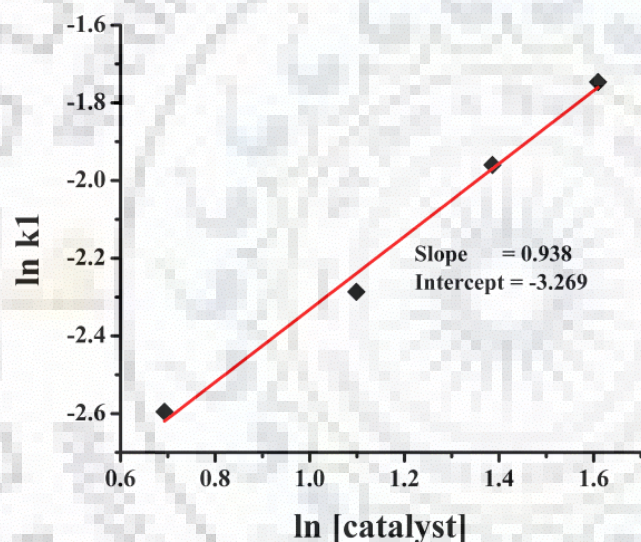


Fig. 2.26. Plot of $\ln k_1$ vs $\ln[\text{catalyst}]$ for oxido transfer reaction between benzoin and DMSO catalysed by $[\text{Mo}^{\text{VI}}\text{O}_2(\text{L}^5)]$ (2.5) at 80 °C for 18 h reaction time.

Most oxygen transfer reactions are thought to proceed via the formation of a Mo(V) dinuclear intermediate $[\text{LMo}^{\text{V}}-\mu-\text{O}-\text{Mo}^{\text{V}}\text{L}]$ (equations 7–8) [29]. However, its formation is fast and reversible, and irreversible binuclear formation is often related to catalyst poisoning. During our studies, the formation of the binuclear intermediate and its fast decay into the initial dioxidomolybdenum(VI) complex was established by time dependent UV–

Visible studies (Fig. 2.27). The reversible nature of the process is also authenticated by the fact that the order of the reaction in terms of catalyst was found to be unity.

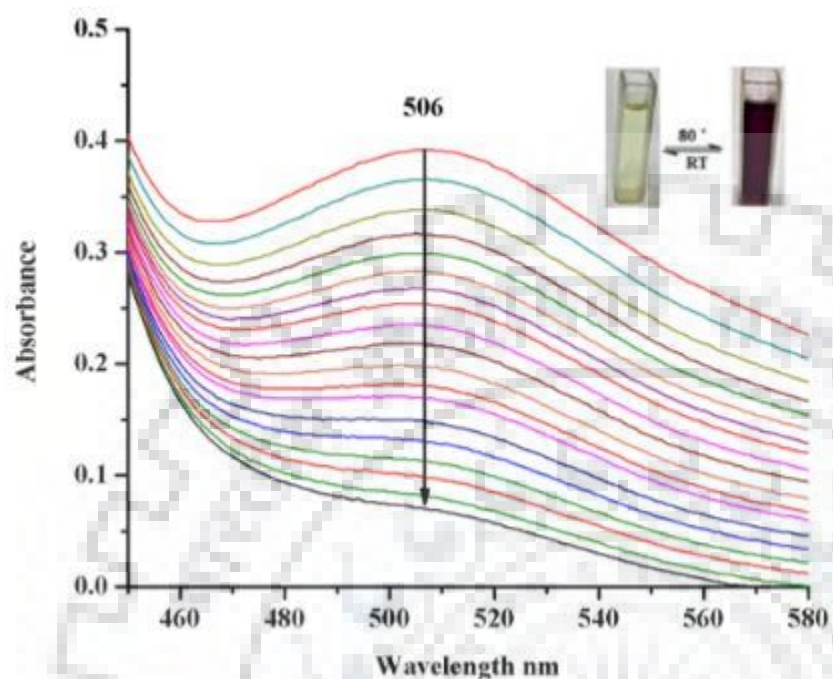


Fig. 2.27. Time-dependent spectral changes observed in the OAT reaction between **2.4**, benzoin and DMSO in acetonitrile after 8 h of reaction time. The spectra were recorded every 10 s from 80 °C to room temperature.



2.4. Conclusions

Five dibasic tetra dentate ONNO donor Mannich bases H_2L^{1-5} derived from ethylenediamine and 2, 4-di-*tert*-butylphenol, 2, 4-di-methylphenol, 2-*tert*-butyl-4-methylphenol, 2, 4-di-chlorophenol and 2-naphthol and their corresponding *cis*- MoO_2 complexes, $[\text{Mo}^{\text{VI}}\text{O}_2(\text{L}^{1-5})]$ have been isolated and characterized. The isolated complexes have successfully been used as catalysts for oxygen atom transfer between benzoin or 4-chlorobenzoin and dimethyl sulfoxide (DMSO) in acetonitrile at 80 °C, similar to DMSO

reductase. As high as 100% conversion, monitored by HPLC was achieved with complex **2.5**. The electron withdrawing chloro group exerts an $-I$ effect, destabilizing the reaction intermediate and consequently complex **2.4** gives the lowest conversion of 66% for benzoin and 89% for 4-chlorobenzoin. The naphthyl ring reduces the steric hindrance at the *ortho* position, stabilizing the reaction intermediate due to enhanced conjugation and consequently complex **2.5** gives highest conversion. Other substituents have intermediate effect. The Hammett plot also presents a good correlation for all the four para substitutions ($R^2 = 0.98$ and $\rho = -1.78$). A detailed kinetic study supports the pseudo first order reaction; the obtained pseudo first order rate constant for **2.5** is 0.0998 h^{-1} . UV/Vis spectroscopy suggested the plausible formation of the binuclear intermediate $[\text{LMo}^{\text{V}}-\mu\text{-O}-\text{Mo}^{\text{V}}\text{L}]$ during catalytic action and its fast decay to the initially taken monomeric complex.

3.1. Introduction

Amongst the actinides, uranium can exist in five oxidation states, +2, +3, +4, +5 and +6 but only the +4 and +6 states are stable enough to be of practical importance. Uranium complexes are generally dominated by the $[U^{VI}O_2]^{2+}$ moiety in +6 oxidation state and forms complexes very similar to group 6 transition metal analogues $[M^{VI}O_2]^{2+}$ (M = Cr, Mo and W) and even similar to $[VO_2]^+$. However, the basic difference between $[MO_2]^{2+}/[VO_2]^+$ and $[U^{VI}O_2]^{2+}$ moieties is that former ones have *cis*- MO_2 group while dioxido group in uranyl ion in their complexes is essentially *trans*; the angle being close to 180° . Further, depending upon the reaction conditions and ligand used the equatorial plane of uranyl complexes can further extend the coordination number by four, five or six resulting in the formation of complexes of varied geometries.¹

During past one decade, a good number of papers on $[U^{VI}O_2]^{2+}$ - complexes of polydentate ligands have appeared [19, 77 - 80, 144-149] but the catalytically potentials of these complexes have narrowly been explored [150]. Since such complexes are generally associated with one solvent/neutral donor molecule in equatorial position which is flexible in nature and may play an important role in catalytic reactions like vanadium, molybdenum and tungsten complexes [54, 138, 151 - 155]. Adam in 2015 has reported dioxidouranium(VI) complexes catalyzed oxidation of various alkenes using H_2O_2 and TBHP as oxidant [150] and showed that these complexes can act as potential oxidation catalysts but oxidative halogenation of organic substrates has not been explored. Such catalytic reaction is generally observed by model vanadium complexes in the presence of oxidant, halide ion and acid, and considered as a functional mimic of enzymes halo peroxidases [138, 151 - 153,]. Recently, we explored $[MO_2]^{2+}$ - complexes (M = Mo and W) as functional models of vanadium dependent halo peroxidases and successfully reported oxidative bromination of thymol, styrene and *trans*-stilbene [54,154 - 156].

Herein we have now prepared and characterized dioxidouranium(VI) $\{trans-[U^{VI}O_2]^{2+}\}$ complexes of ligands derived from Mannich bases of ethylene diamine and 2,4-substituted phenols (H_2L^{1-4} , Scheme 3.1), and report our findings on the oxidative bromination of thymol and styrene in the line of functional models of vanadium dependent

halo peroxidases. Very recently, we observed that dioxidomolybdenum(VI) complexes of these ligands catalyze oxygen atom transfer (OAT) between benzoin and dimethyl sulfoxide (DMSO) in acetonitrile at 80 °C and achieved almost 99 % conversion in only 18 h of reaction time [138].

3.2. Experimental section

3.2.1. Materials and general methods

Uranyl acetate dihydrate (Loba chemie, India), thymol, KBr (S.D. fine chemicals, India), methanol (SRL, India), n-Hexane, perchloric acid, 30% H₂O₂, and DMSO (Rankem, India) were used as obtained. Other chemicals and solvents were of AR grade. Ligands **I** to **IV** were prepared as reported in previous chapter.

¹H and ¹³C NMR spectra were recorded in CDCl₃/DMSO-d₆ on a JEOL ECX 400 MHz spectrometer. The catalytic activity of the metal complexes were studied using Shimadzu 2010 gas chromatogram with an Rtx-1 capillary column (30 m × 0.25 mm × 0.25 μm), and their % conversion and product selectivity were calculated using peak area of substrate and respective products. Other instrumentation details are given in chapter 2.

3.2.2. Preparation of complexes [U^{VI}O₂L¹⁻⁴(MeOH)] (**3.1** – **3.4**)

A representative method for [U^{VI}O₂L¹(MeOH)] (**3.1**) is given here. A solution of U^{VI}O₂(CH₃COO)₂·2H₂O (0.424 g, 1 mmol) in 20 mL MeOH was added to the stirred suspension of ligand H₂L¹ (0.496 g, 1 mmol) in MeOH (100 mL) (1:1 molar ratio) and the resulting reaction mixture was heated under reflux on a water bath for 10 h. During this period ligands slowly dissolved and red-brown coloured complexes precipitated instead. After reducing the solvent volume to ca. 40 mL and cooling to room temperature, the precipitated solid was collected by filtration, washed with MeOH (2 × 5 mL) and dried under vacuum.

Complexes **3.2–3.4** were prepared similarly using U^{VI}O₂(CH₃COO)₂·2H₂O (0.424 g, 1.0 mmol) in 20 mL MeOH and respective ligands (1 mmol) in 100 mL MeOH. All analytical measurements were made after drying the metal complexes at 110 °C for 5 h.

Data for [U^{VI}O₂L¹ (MeOH)] (3.1). Yield: 0.605 g (76%). (Found: C, 49.3; H, 7.0; N, 3.6%. Calcd for C₃₃H₅₄N₂O₅U (796.83 g mol⁻¹): C, 49.74; H, 6.83; N 3.52%). ¹H NMR (400 MHz, CDCl₃): δ 7.33 (s, 2H), 6.86 (s, 2H) (aromatic), 2.51 (s, 2H, -NH), 3.87 (s, 2H), 2.93 (s, 2H) (-CH₂-), 1.63 (s, 4H) (-CH₂CH₂-), 1.34 (s, 18H), 1.19 (s, 18H) (-CH₃). ¹³C NMR (400 MHz, DMSO-d₆): δ 166.65, 138.16, 136.31, 128.97, 125.88, 124.24, 22.57, 122.33, 57.54, 52.84, 35.57, 33.88, 32.57, 31.04

Data for [U^{VI}O₂L² (MeOH)] (3.2). Yield: 0.515 g (82.0%). (Found: C, 40.47; H, 4.65; N 4.55%. Calcd for C₂₁H₃₀N₂O₅U (628.51 g mol⁻¹): C, 40.13; H, 4.81; N, 4.46%). ¹H NMR (400 MHz, CDCl₃): δ 6.99 (s, 1H), 6.92 (s, 3H) (aromatic), 5.40 (s, 2H, -NH), 4.71-4.69 (dd, 2H), 4.18-4.15 (dd, 2H) (-CH₂-), 3.90 (t, 2H), 3.70 (t, 2H) (-CH₂CH₂-), 3.25 (s, 3H) (CH₃ of MeOH), 2.32 (s, 3H), 2.12 (s, 3H) (CH₃). ¹³C NMR (400 MHz, DMSO-d₆): δ 165.88, 130.50, 127.78, 127.29, 126.55, 123.27, 56.30, 52.82, 20.47, 17.24

Data for [U^{VI}O₂L³ (MeOH)] (3.3). Yield: 565 g (79%). (Found: C, 45.2; H, 5.8; N, 4.0%. Calcd for C₂₇H₄₂N₂O₅U (712.67 g mol⁻¹): C, 45.50; H, 5.94; N, 3.93%). ¹H NMR (400 MHz, CDCl₃): δ 6.85 (s, 2H), 6.64 (s, 2H) (aromatic), 3.81 (s, 2H), 2.94 (s, 2H) (-CH₂-), 3.25 (s, 3H) (CH₃ of MeOH), 2.51 (s, -NH), 2.12 (s, 4H) (-CH₂CH₂-), 1.61s, 9H) 1.32 (s, 9H) (CH₃). ¹³C NMR (400 MHz, DMSO-d₆): δ 153.69, 135.49, 127.31, 126.84, 126.54, 122.33, 57.58, 56.82, 34.65, 34.36, 30.86, 29.59, 20.69.

Data for [U^{VI}O₂L⁴ (MeOH)] (3.4). Yield: 0596 g (84%). (Found: C, 28.6; H, 2.4; N, 4.1%. Calcd for C₁₇H₁₈Cl₄N₂O₅U (710.17 g mol⁻¹): C, 28.75; H, 2.55; N 3.94%). ¹H NMR (400 MHz, CDCl₃): δ 7.49 (s, 2H), 7.33 (s, 2H) (aromatic), 6.10 (s, 2H, -NH), 4.65 (dd, 2H) (-CH₂-), 4.36 (dd, 2H) (-CH₂CH₂-), 3.30 (s, 3H) (CH₃ of MeOH). ¹³C NMR (400 MHz, DMSO-d₆): δ 163.14, 130.61, 127.58, 123.55, 117.60, 55.21, 52.55.

3.2.3. X-Ray crystal structure determination

Three-dimensional X-ray data were collected on a Bruker Kappa Apex CCD diffractometer at room temperature for **3.3** and at low temperature for **3.4**, by the ϕ - ω scan method. Reflections were measured from a hemisphere of data collected from frames, each of them covering 0.3° in ω . A total of, 81578 for **3.3** and 87961 for **3.4**, reflections measured were corrected for Lorentz and polarization effects and for absorption by multi-scan methods based on symmetry-equivalent and repeated reflections. Of the total, 6254 for **3.3** and 8678 for **3.4**, independent reflections exceeded the significance level $(|F|/\sigma|F|) > 4.0$. After data collection an empirical absorption correction (SADABS) [132] was applied, and the structures were solved by direct methods and refined by full matrix least-squares on F^2 data using SHELX suite of programs [133, 157] In **3.3**, hydrogen atoms were included in calculation position and refined in the riding mode, except for O(1M), which was located in difference Fourier map and freely refined and for O(2M) and N(1), which were located in difference Fourier map and fixed to the atoms. In **3.4**, were included in calculation position and refined in the riding mode, except for O(1M), O(2M), N(1), N(2), N(3) and N(4) which were located in difference Fourier map and fixed to the atoms. A final difference Fourier map showed a high residual density outside: 3.252 and -1.426 e. \AA^{-3} for **3.3** and 2.009 and -2.378 e. \AA^{-3} for **3.4**, next to the uranium atoms. A weighting scheme $w = 1/[\sigma^2(F_o^2) + (0.036900 P)^2 + 61.142097 P]$ for **3.3**, and $w = 1/[\sigma^2(F_o^2) + (0.000000 P)^2 + 39.040199 P]$ for **3.4**, where $P = (|F_o|^2 + 2|F_c|^2)/3$, were used in the latter stages of refinement. Further details of the crystal structures determination are given in Table 3.1.

Table 3.1. Crystal Data and Structure Refinement for [U^{VI}O₂L³(MeOH)] (**3.3**) and [U^{VI}O₂L⁴(EtOH)] (**3.4**).

	3.3	3.4
Formula	C ₂₇ H ₄₂ N ₂ O ₅ U	C ₁₈ H ₂₀ Cl ₄ N ₂ O ₅ U
Formula weight	712.66	724.19
T, K	296(2)	100(2)
Wavelength, Å	0.71073	0.71073
Crystal system	Monoclinic	Monoclinic
Space group	P2 ₁ /n	P2 ₁ /n
a/Å	14.3077(12)	10.6553(6)
b/Å	16.2307(13)	24.9128(15)
c/Å	24.925(2)	16.9982(10)
β/°	92.714(4)	97.998(2)
V/Å ³	5781.7(8)	4468.3(5)
Z	8	8
F ₀₀₀	2800	2736
D _{calc} /g cm ⁻³	1.637	2.153
μ/mm ⁻¹	5.651	7.776
θ/°	1.50 to 28.62	1.46 to 27.86
R _{int}	0.1152	0.0715
Crystal size/ mm ³	0.21 x 0.16 x 0.05	0.38 x 0.28 x 0.23
Goodness-of-fit on F ²	1.061	1.115
R ₁ [I>2σ(I)] ^a	0.0675	0.0387
wR ₂ (all data) ^b	0.1730	0.0832
Largest differences peak and hole (eÅ ⁻³)	3.252 and -1.426	2.009 and -2.378

$${}^a R_1 = \frac{\sum ||F_o| - |F_c||}{\sum |F_o|} \quad {}^b wR_2 = \left\{ \frac{\sum [w(|F_o|^2 - |F_c|^2)]^2}{\sum [w(F_o^2)]^2} \right\}^{1/2}$$

3.2.4. Catalytic activity study

3.2.4.1. Oxidative bromination of thymol

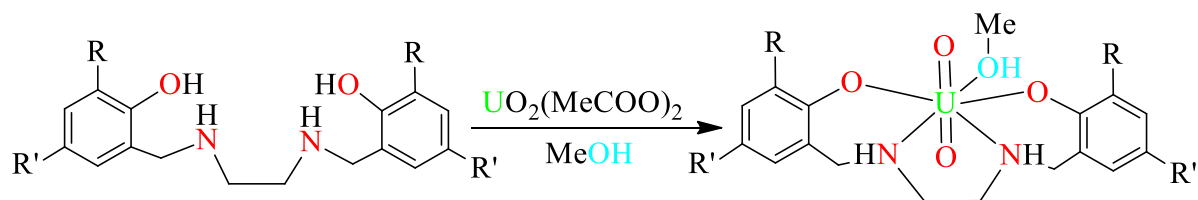
Thymol (1.50 g, 10 mmol), 30% aqueous H_2O_2 (2.27 g, 20 mmol) and KBr (2.38 g, 20 mmol), were mixed in a flask containing 20 mL water and stirred at room temperature. The catalyst (0.001 g, 1.6×10^{-3} mmol) and 70% HClO_4 (10 mmol, 1.43 g) was then added to it and the reaction mixture was stirred at room temperature for 2h at room temperature. A small aliquot at every 30 min was withdrawn, extracted with n-hexane, dried over anhydrous Na_2SO_4 and analyzed quantitatively by gas chromatograph on the basis of their relative peak area of the respective product. The confirmation of products was carried out by GC-MS after their separations.

3.2.4.2. Oxidative bromination of styrene

Styrene (1.04 g, 10 mmol), 30% aqueous H_2O_2 (2.27 g, 20 mmol) and KBr (2.38 g, 20 mmol), were mixed in a flask containing 20 mL water and stirred at room temperature. The catalyst (0.001 g, 1.6×10^{-3} mmol) and 70% HClO_4 (20 mmol, 2.86 g in 2 equal portions, one at $t = 0$ min and other at $t = 30$ min) was then added to it and the reaction mixture was stirred at room temperature for 2h at room temperature. A small aliquot at every 30 min was withdrawn, extracted with n-hexane, dried over anhydrous Na_2SO_4 and analyzed quantitatively by gas chromatograph as mentioned above. The confirmation of products was carried out by GC-MS after their separations.

3.3. Results and discussion

Preparation of Ligands **I – IV** (H_2L^{1-4}) are given in Chapter 2. Reaction of these ligands with $\text{U}^{\text{VI}}\text{O}_2(\text{CH}_3\text{COO})_2 \cdot 2\text{H}_2\text{O}$ in 1:1 molar ratio in MeOH (Scheme 3.1), results in the formation of the corresponding dioxidouranium(VI) complexes, $[\text{U}^{\text{VI}}\text{O}_2(\text{L}^{1-4})(\text{MeOH})]$ (**3.1–3.4**) in good yields. All complexes are air stable dark red solids and soluble in common organic solvents such as MeOH, CHCl_3 , MeCN, DMSO, DMF etc.



R	R'	Ligands	Complexes
tert-butyl	tert-butyl	H ₂ L ¹	[U ^{VI} O ₂ L ¹ (MeOH)] (3.1)
Me	Me	H ₂ L ²	[U ^{VI} O ₂ L ² (MeOH)] (3.2)
tert-butyl	Me	H ₂ L ³	[U ^{VI} O ₂ L ³ (MeOH)] (3.3)
Cl	Cl	H ₂ L ⁴	[U ^{VI} O ₂ L ⁴ (MeOH)] (3.4)

Scheme 3.1. Structure ligands and synthetic route to prepare uranium complexes reported in this study.

3.3.1. Solid state characterization

ORTEP diagram for the complexes [U^{VI}O₂L³(MeOH)] (3.3) and [U^{VI}O₂L⁴(EtOH)] (3.4) are shown in Figs.3.1 and 3.2, respectively and their crystal packing are presented in Figs. 3.3 and 3.4, respectively. Selected bond distances and angles are given in Table 3.2. Both compounds are mononuclear complexes, which crystallize in a monoclinic space group P2₁/n. The structures adopt a distorted pentagonal bipyramidal geometry around of metal centre. The ligands act as tetra dentate, coordinated through two phenoxido oxygen and two amine nitrogen atoms. The amine nitrogen atoms present a distorted sp³ hybridized bonding network. U centres complete the coordination sphere bonding to two O_{oxido} terminal oxygen atoms and one oxygen atom from solvent molecules (MeOH or EtOH). The U^{VI}=O bond lengths [1.770(8)-1.764(2) Å in compound 3.3 and 1.766(4)-1.797(4) in compound 3.4] are similar to other in the literature [158] The two distances U^{VI}=O_{phenoxido} [2.217(8)-2.234(9) Å in compound 3.3 and 2.304(4)-2.203(4) Å in compound 3.4] are shorter than the U^{VI}=O_{solvent} [2.566(9) Å in compound 3.3 and 2.455(4) Å in compound 3.4]. The equatorial plane is occupied by the O_{phenoxido} atoms, O(3) and O(4), by the N_{amine} atoms, N(1) and N(2) and by the oxygen atom (O1M) of MeOH or ETOH molecules. They

are distorted respect to the planarity, [mean deviation from the plane 0.0843(60) Å in compound **3.3** and 0.0959(29) Å in compound **3.4**]. The terminal oxido atoms occupy the axial sites. The crystal packing present hydrogen bonds between the electronegative atoms (see Table 3.3 and Figs. 3.3 and 3.4). π - π Interactions are not present in the structures.

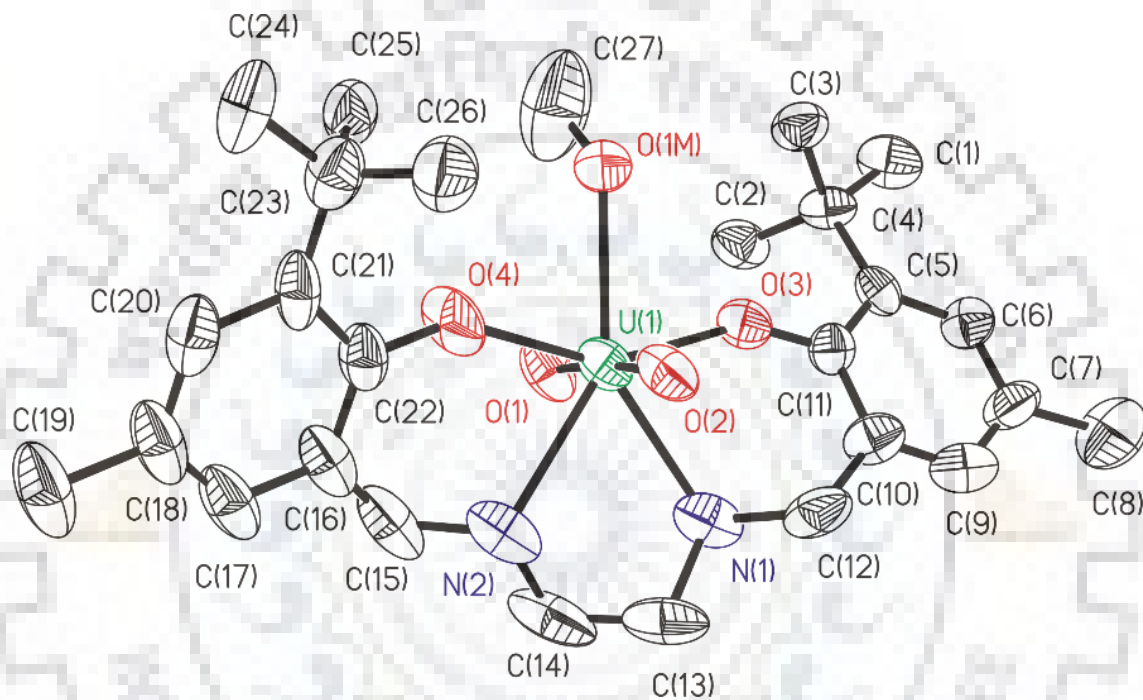


Fig. 3.1. ORTEP for the compound $[U^{VI}O_2(L^3)(MeOH)]$ (**3.3**). All the non-hydrogen atoms are presented by their 50% probability ellipsoids. Hydrogen atoms are omitted for clarity.

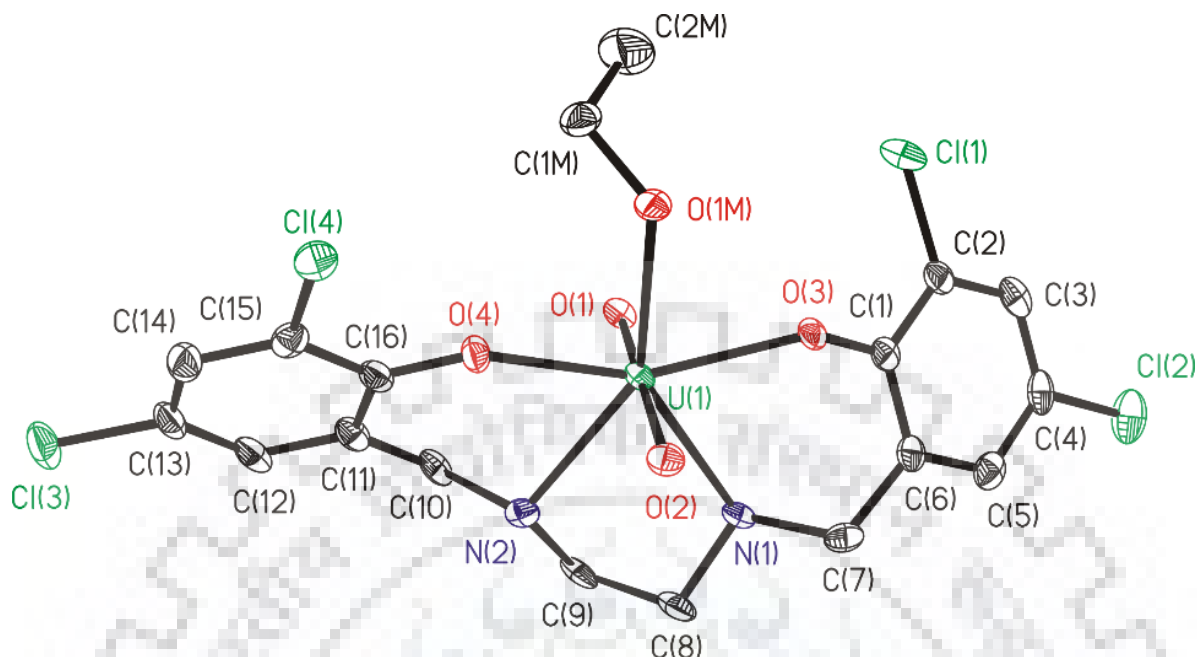


Fig. 3.2. ORTEP for the compound $[U^{VI}O_2(L^4)(EtOH)]$ (3.4). All the non-hydrogen atoms are presented by their 50% probability ellipsoids. Hydrogen atoms are omitted for clarity.

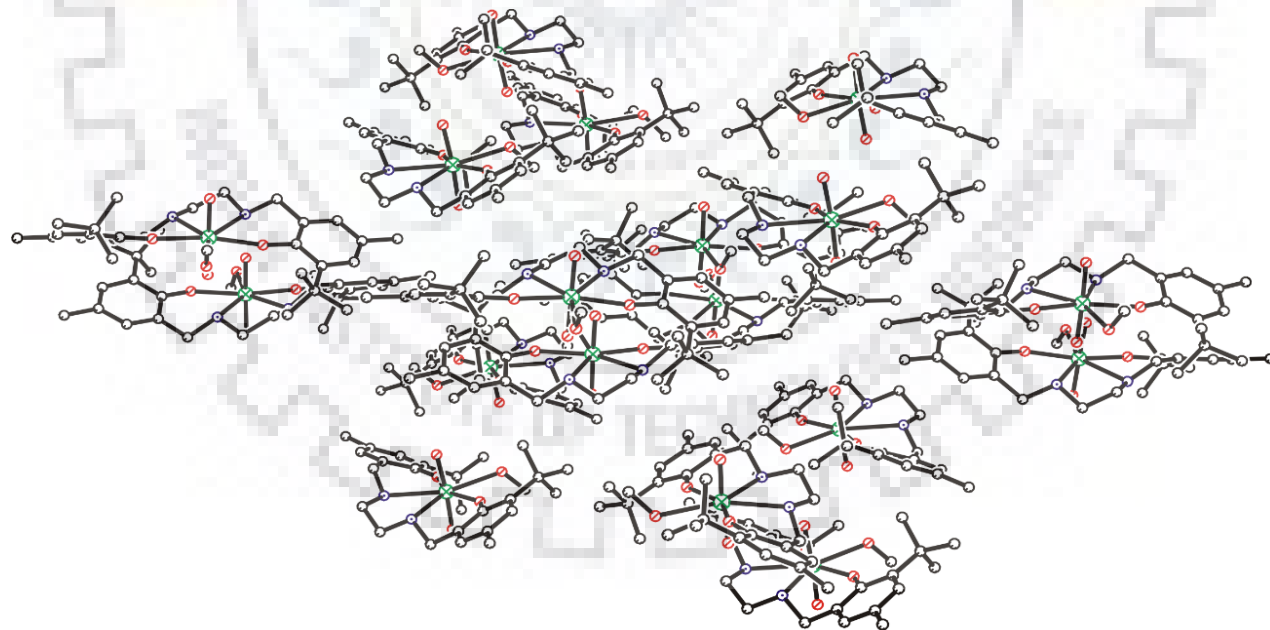


Fig. 3.3. Crystal packing in the compound $[U^{VI}O_2(L^3)(MeOH)]$ (3.3). Drawing was done in ball and sticks.

Table 3.2. Bond lengths [\AA] and angles [$^\circ$] for the compounds for $[\text{U}^{\text{VI}}\text{O}_2\text{L}^3(\text{MeOH})]$ (**3.3**) and $[\text{U}^{\text{VI}}\text{O}_2\text{L}^4(\text{EtOH})]$ (**3.4**).

Bond lengths	3.3	3.4
U(1)-O(1)	1.770(8)	1.766(4)
U(1)-O(2)	1.764(9)	1.797(4)
U(1)-O(3)	2.217(8)	2.304(4)
U(1)-O(4)	2.234(9)	2.203(4)
U(1)-O(1M)	2.566(9)	2.455(4)
U(1)-N(1)	2.526(12)	2.624(5)
U(1)-N(2)	2.581(10)	2.604(5)
Angles	3.3	3.4
O(2)-U(1)-O(1)	173.8(4)	173.46(19)
O(2)-U(1)-O(3)	94.2(3)	89.39(17)
O(1)-U(1)-O(3)	87.1(3)	90.16(17)
O(2)-U(1)-O(4)	89.7(4)	89.81(18)
O(1)-U(1)-O(4)	92.0(4)	93.49(18)
O(3)-U(1)-O(4)	151.9(3)	153.55(15)
O(2)-U(1)-O(1M)	93.2(3)	95.28(17)
O(1)-U(1)-O(1M)	93.0(4)	90.91(17)
O(3)-U(1)-O(1M)	77.0(3)	75.17(15)
O(4)-U(1)-O(1M)	75.0(3)	78.58(15)
O(2)-U(1)-N(2)	88.2(3)	91.53(17)
O(1)-U(1)-N(2)	86.7(3)	84.39(17)
O(3)-U(1)-N(2)	137.2(4)	137.24(15)
O(4)-U(1)-N(2)	70.7(4)	69.22(16)

O(1M)-U(1)-N(2)	145.6(4)	147.04(15)
O(2)-U(1)-N(1)	87.82(9)	84.44(17)
O(1)-U(1)-N(1)	89.12(9)	89.27(18)
O(3)-U(1)-N(1)	72.60(8)	70.19(15)
O(4)-U(1)-N(1)	129.14(8)	135.97(16)
O(1M)-U(1)-N(1)	145.5(3)	145.36(15)
N(2)-U(1)-N(1)	68.8(4)	67.36(15)

Table 3.3. Hydrogen bonds in the compounds $[U^{VI}O_2L^3(MeOH)]$ (**3.3**) and $[U^{VI}O_2L^4(EtOH)]$ (**3.4**).

D-H...A	compound	d(D-H)	d(H...A)	d(D...A)	<(DHA)
N(2)-H(2)...O(9)	3.3	0.91	2.48	3.289(13)	147.7
O(1M)-H(1M)...O(8)	3.4	0.85	2.00	2.760(6)	148.8
N(2)-H(2N)...O(5)#1	3.4	0.93	2.21	3.049(6)	151.0
O(2M)-H(2M)...O(3)	3.4	0.91	1.80	2.645(6)	152.7
N(3)-H(3N)...O(2)#2	3.4	1.11	1.99	2.935(6)	140.1

Symmetry transformations used to generate equivalent atoms: #1 $x-1,y,z$ #2 $x+1,y,z$.

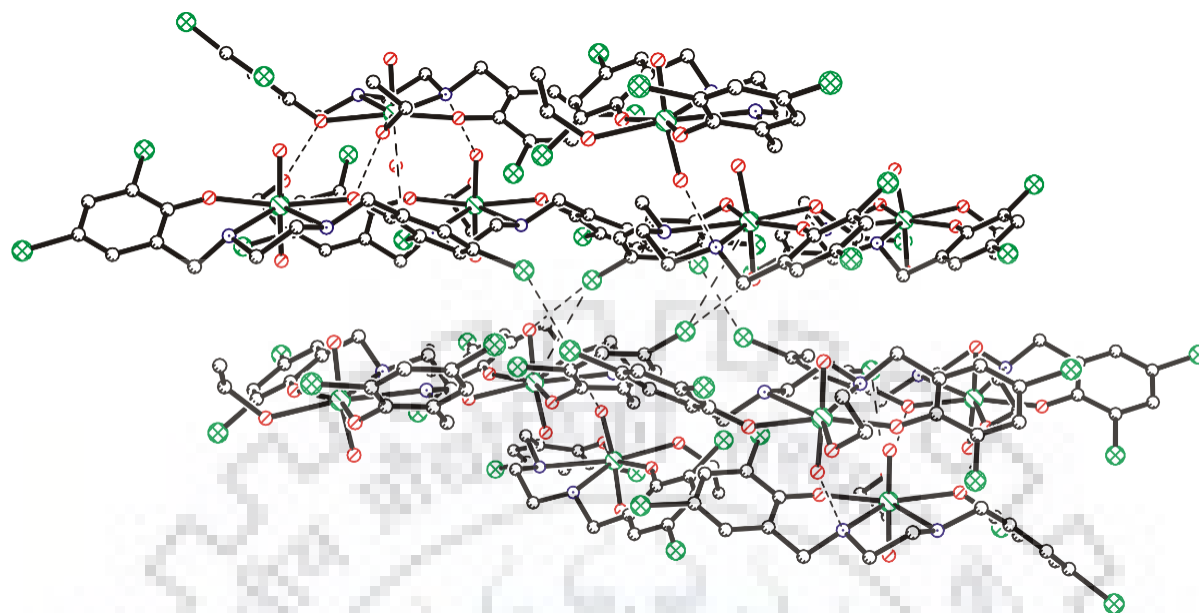


Fig. 3.4. Crystal packing in the compound $[U^{VI}O_2(L^4)(EtOH)]$ (**3.4**). Drawing was done in ball and sticks. Dashed lines show hydrogen bonding.

3.3.2. Spectral studies

3.3.2.1. FT-IR spectral study

IR spectroscopic analyses of all the ligands and the uranium complexes were carried to confirm the coordination modes of ligands. The IR spectra of all complexes exhibits one sharp IR bands around 879-921 and other band in the lower region around 850-868 cm^{-1} (Table 3.4), due to the respective symmetric and asymmetric stretching of *trans*- $[UO_2]$ core, respectively. Coordination of phenolate oxygen and nitrogen functionalities could not be ascertained unequivocally by IR spectral study because the spectra of the ligands as well as complexes both exhibit $\nu(\text{OH})$ and $\nu(\text{NH})$ bands around 3400 and 3100 cm^{-1} , respectively. The former band may be only due to the coordinated MeOH. However, coordination of these functionalities are well supported by single crystal X-ray study (vide supra). The characteristic band due to methylene group appears in the spectra of the ligands as well as the complexes around 2800–3000 cm^{-1} .

Table 3.4 Selected IR data (in cm^{-1}) for the ligands and complexes with tentative assignments.

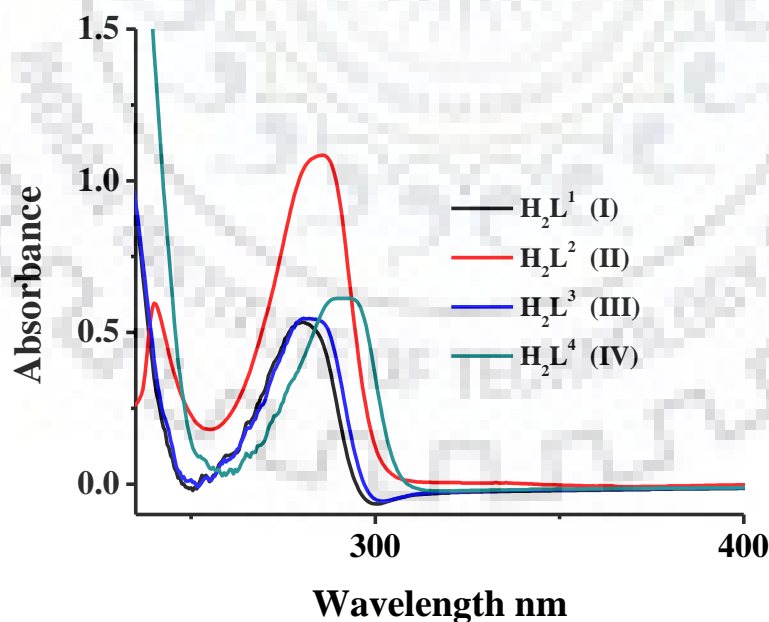
Entry	Compounds	$\nu(\text{OH})$	$\nu(\text{N-H})$	$\nu_{\text{asym}}(\text{O=U=O})$	$\nu_{\text{sym}}(\text{O=U=O})$
1	H_2L^1 (I)	3440 (b)	3130	-	-
2	$[\text{U}^{\text{VI}}\text{O}_2\text{L}^1(\text{MeOH})]$ (3.1)	3450 (b)	2834, 3099	879	850
3	H_2L^2 (II)	3270 (b)	3000	-	-
4	$[\text{U}^{\text{VI}}\text{O}_2\text{L}^2(\text{MeOH})]$ (3.2)	3430 (b)	2960, 3015	921	868
5	H_2L^3 (III)	3425 (b)	3050	-	-
6	$[\text{U}^{\text{VI}}\text{O}_2\text{L}^3(\text{MeOH})]$ (3.3)	3450 (b)	2865, 2953	900	868
7	H_2L^4 (IV)	3440 (b)	2990, 3128	-	-
8	$[\text{U}^{\text{VI}}\text{O}_2\text{L}^4(\text{MeOH})]$ (3.4)	3470 (b)	2899, 3066	905	863

3.3.2.2. UV-Visible spectral study

Table 3.5 collects UV/Vis spectral data of ligands and their *trans*- $[\text{UO}_2]^{2+}$ complexes recorded in MeCN and Fig. 3.5 (and Fig. 3.6) gives detail of their spectral profiles. The detail interpretation of spectral data of ligands is reported earlier. UV-Vis spectra of complexes also display same two bands at nearly same positions as observed in corresponding ligands are attributed to $\pi \rightarrow \pi^*$ and $n \rightarrow \pi^*$ transitions. In addition these complexes show a very low intensity broad band at 380 - 400 nm due to $1^1\epsilon_g^+ \rightarrow 3^3\pi_u$ transition [48].

Table 3.5. UV/Vis spectral data of ligands and complexes.

Entry	Compound	λ [nm] (ϵ , liter mole ⁻¹ cm ⁻¹)
1.	H ₂ L ¹ (I)	234 (2.48×10^3), 294 (1.22×10^3)
2.	[U ^{VI} O ₂ L ¹ (MeOH)] (3.1)	242 (5.63×10^3), 281 (4.45×10^3), 394 (3.62×10^3), 474 (3.41×10^3)
3.	H ₂ L ² (II)	224 (1.46×10^3), 286 (4.73×10^3)
4.	[U ^{VI} O ₂ L ² (MeOH)] (3.2)	242 (6.76×10^3), 290 (4.31×10^3), 402 (3.5×10^3), 490 (3.82×10^3)
5.	H ₂ L ³ (III)	226 (1.75×10^3), 286 (1.02×10^3)
6.	[U ^{VI} O ₂ L ³ (MeOH)] (3.3)	242 (broad) (5.4×10^3), 272 (5.95×10^3), 391 (3.08×10^3), 474 (2.3×10^3)
7.	H ₂ L ⁴ (IV)	237 (1.43×10^3), 295 (6.66×10^2)
8.	[U ^{VI} O ₂ L ⁴ (MeOH)] (3.4)	241 (5.53×10^3), 273 (4.22×10^3), 374 (3.4×10^3), 466 (2.6×10^3)

**Fig. 3.5.** UV-Visible spectra of I – IV recorded in MeCN.

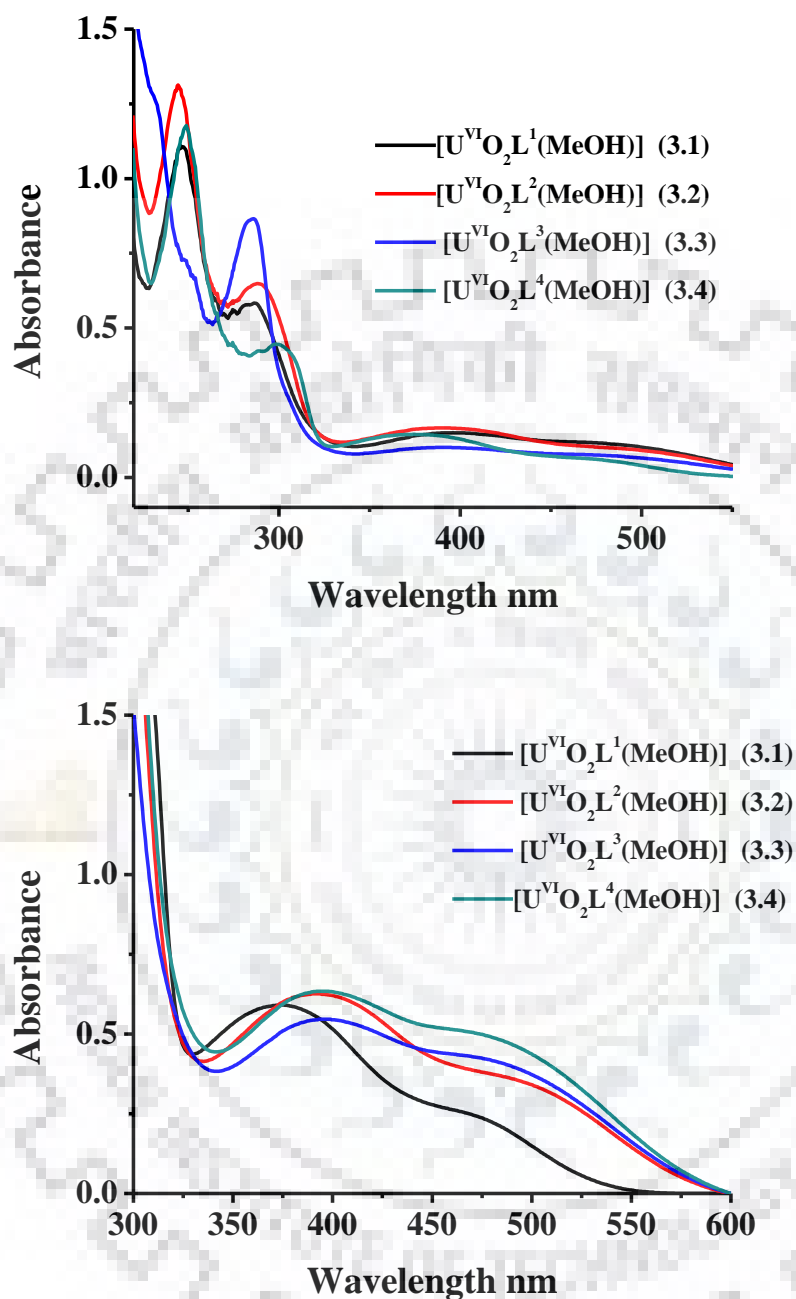


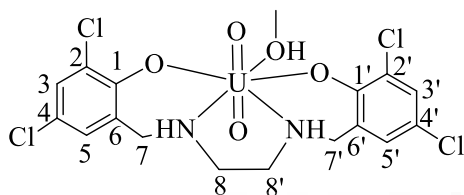
Fig. 3.6. UV-Visible spectra of dioxidouranium(VI) complexes **3.1** – **3.4** recorded in MeCN. (a) Recorded in the region 250-550 nm and (b) Expanded region of 300-600 nm with more concentrated solution.

3.3.2.3. ^1H NMR spectral study

^1H NMR spectra of ligands and complexes recorded in CDCl_3 , presented in the experimental section also supplement the coordinating modes of ligand to the metal complex. Thus, the absence of the signal due to two equivalent nature of phenolic $-\text{OH}$ protons, which appears in ligands at $\delta = 10.25\text{--}10.73$ ppm, in complexes indicates the coordination of the phenolic oxygen after its deprotonation (see Chapter 2). Signals due to methylene groups, connecting to $-\text{N}$ and aromatic ring and $-\text{NH}$ protons have no systematic trend but are observed in ligands as well as in complexes. Protons of methyl group of MeOH appear at ca. 3.3 ppm. Aromatic protons of all ligands and complexes and methyl protons on ligands **I**, **II** and **III** and their corresponding complexes appear in the expected region with slight variations.

3.3.2.4. ^{13}C NMR spectral study

The ^{13}C NMR data recorded in DMSO-d_6 are listed in the experimental section; a ^{13}C NMR spectrum of complex **3.4** is presented here as a representative (Fig. 3.7). The coordination-induced ^{13}C NMR chemical shifts due to coordination of phenolic oxygens and imino nitrogens further supplement the binding mode of the ligands. A significant shifts, $\Delta\delta = [\delta(\text{complex}) - \delta(\text{ligand})]$ was observed for the signals of the carbon atoms in the vicinity of the coordinating atoms (Table 3.6). Thus, the carbons bearing the phenolic oxygens (C_1/C_1') with a $\Delta\delta$ value of -0.52 to 15.82 ppm, ethylene carbons (connecting to $-\text{NH}$ and aromatic, C_7/C_7') with a $\Delta\delta$ value of -2.06 to 6.19 ppm and ethylene carbons ($-\text{CH}_2\text{CH}_2-$, C_8/C_8') with a $\Delta\delta$ value of 1.05 to 6.83 ppm confirm the coordination of the corresponding accompanying functionalities to uranium. Other signals in the spectra of complexes are well within expected region.

Table 3.6. ^{13}C NMR spectral data (δ in ppm) of ligands and complexes.

Compound ^{a,b}	C ₁ /C _{1'}	C ₇ /C _{7'}	C ₈ /C _{8'}
H ₂ L ¹ (I)	150.83	51.35	49.69
[U ^{VI} O ₂ L ¹ (MeOH)] (3.1)	166.65	57.54	52.84
($\Delta\delta$)	(15.82)	(6.19)	(3.15)
H ₂ L ² (II)	153.13	58.36	51.77
[U ^{VI} O ₂ L ² (MeOH)] (3.2)	165.88	56.30,	52.82
($\Delta\delta$)	(12.75)	(-2.06)	(1.05)
H ₂ L ³ (III)	154.21	58.05	50.89
[U ^{VI} O ₂ L ³ (MeOH)] (3.3)	153.69	57.58	56.82
($\Delta\delta$)	(-0.52)	(-0.47)	(5.93)
H ₂ L ⁴ (IV)	154.43	52.31	45.72
[U ^{VI} O ₂ L ⁴ (MeOH)] (3.4)	163.14	55.21	52.55
($\Delta\delta$)	(9.11)	(2.90)	(6.83)

^a $\Delta\delta = [\delta(\text{complex}) - \delta(\text{free ligand})]$.

^b recorded in CDCl₃ at room temperature.

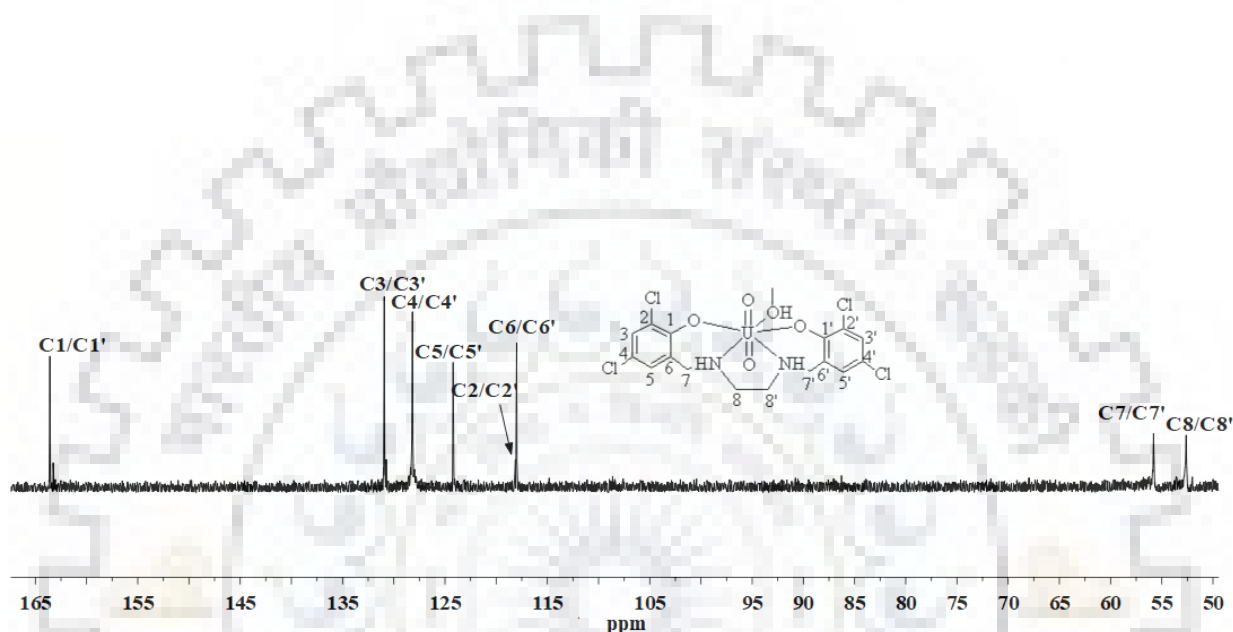


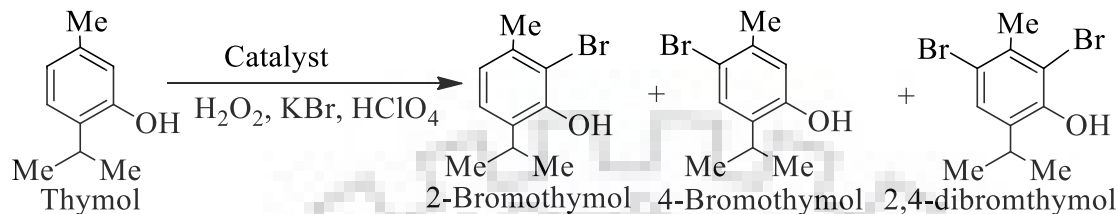
Fig. 3.7. ¹³C NMR spectrum of [U^{VI}O₂L⁴(EtOH)] (3.4). Spectrum below 50 ppm is not shown as this region mostly have solvent and water signals.

3.3.3. Catalytic activity study

3.3.3.1. Oxidative bromination of thymol

The synthesized complexes **3.1**, **3.2**, **3.3** and **3.4** have been used as catalyst to study catalytic oxidative bromination of thymol (a monoterpene) in the presence of KBr, 70% aqueous HClO₄ and 30% H₂O₂ in aqueous solution under appropriate reaction conditions. All reactions were carried out in a 100 mL reaction flask in aqueous medium at room temperature. The bromination reaction takes place on the most activated site as a result of electrophilic aromatic substitution in the phenolic ring. Thus, the oxidative bromination of thymol led to the formation of 2-bromothymol and 4-bromothymol while further

bromination of these also gave 2,4- dibromothymol (Scheme 3.2). In fact, these products are usual and reported in the literature [156,159 - 162].



Scheme 3.2. Products of the oxidative bromination of thymol.

In order to obtain best suited reaction conditions for the maximum oxidative bromination products, reaction conditions were optimized considering $[\text{U}^{\text{VI}}\text{O}_2(\text{eda-2,4-dmp})(\text{MeOH})]$ (**3.2**) as a representative catalyst. Thus, for 10 mmol of thymol (1.50 g), four different amounts of catalyst (0.0005, 0.001, 0.002, 0.003 g), three different amounts of 30% aqueous H_2O_2 (10, 20 and 30 mmol), three different amounts of KBr (10, 20 and 30 mmol) and three different amounts of 70% aqueous HClO_4 (10, 20 and 30 mmol, added in three equal portions to the reaction mixture, first portion at $t = 0$ and other two portions after every 30 min intervals) were taken in 20 mL water and the reaction was carried out at room temperature for 2h. The amount of HClO_4 and its addition to the reaction was found to be crucial to bring out effective catalytic bromination and selectivity of products. The complexes slowly decompose during the reaction when entire required amount of HClO_4 was added in one portion while this decomposition was almost stopped, if it was successively added in three equal portions during 2h of reaction time.

Details of all reaction conditions and the corresponding conversions of thymol are summarized in Figs. 3.8-3.11 and Table 3.7. It may be concluded from the data presented in Table 3.7 that the optimized reaction conditions (entry no. 10) for the best conversion of 10 mmol (1.50 g) of thymol with the catalyst **3.1** are those using 0.002 g catalyst, 30 mmol 30% H_2O_2 , 30 mmol KBr, and 30 mmol 70% HClO_4 .

Under these conditions the obtained conversion is 99% where the selectivity of different major products follows the order: 4-bromothymol (91%) > 2,4-dibromothymol (5%) > 2-bromothymol (4%).

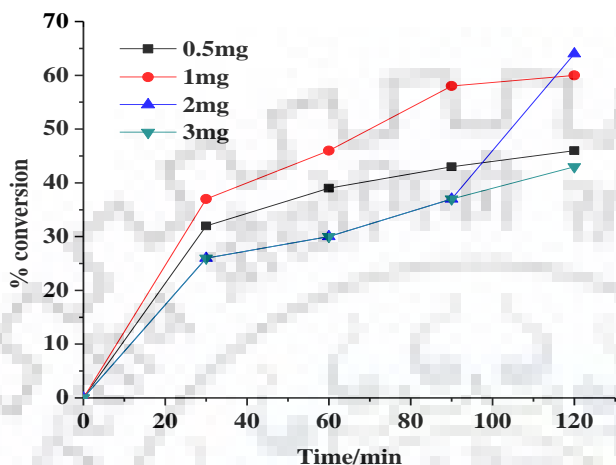


Fig. 3.8. Effect of variation of amount of catalyst on the oxidative bromination of thymol. Reaction conditions: thymol (1.5g, 10 mmol), 30% aqueous H_2O_2 (10 mmol, 1.13 g), KBr (10 mmol, 1.19 g), and HClO_4 (10 mmol, 1.43 g) at room temperature.

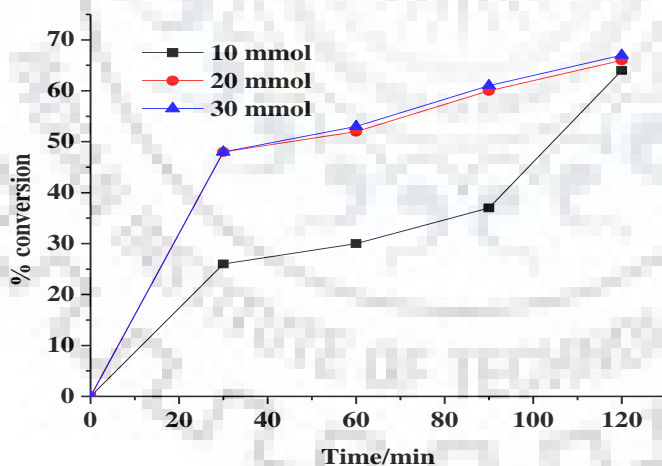


Fig. 3.9. Effect of variation of amount of oxidant on the oxidative bromination of thymol. Reaction conditions: thymol (1.5g, 10 mmol), catalyst $[\text{U}^{\text{VI}}\text{O}_2\text{L}^2(\text{MeOH})]$ (3.20 (0.002 g, 3.2×10^{-3} mmol), KBr (10 mmol, 1.19 g), and HClO_4 (10 mmol, 1.43 g) at room temperature.

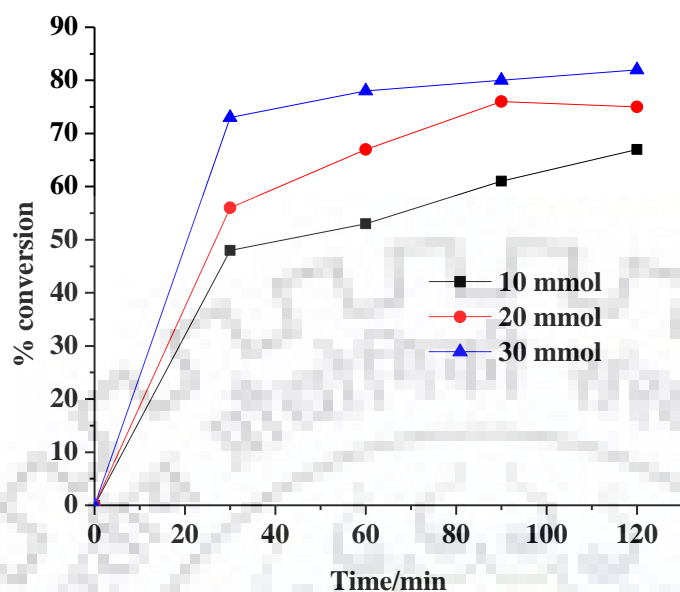


Fig. 3.10. Effect of varying amount of additive (KBr) on the oxidative bromination of thymol. Reaction conditions: thymol (1.5g, 10 mmol), catalyst [$U^{VI}O_2L^2(MeOH)$] (**3.2**) (0.002 g, 3.2×10^{-3} mmol), 30% aqueous H_2O_2 (30 mmol, 3.39 g), and $HClO_4$ (10 mmol, 1.43 g) at room temperature.

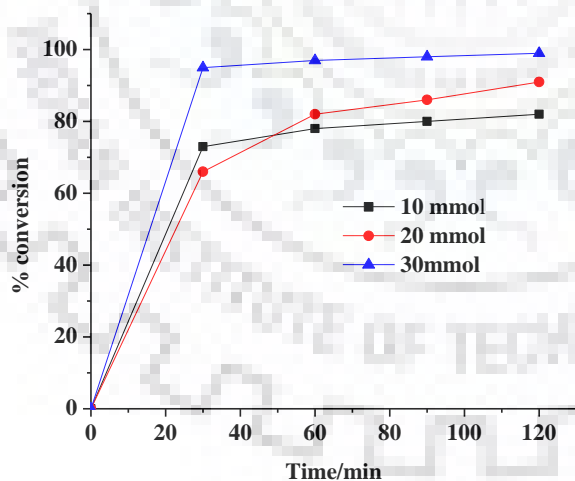


Fig. 3.11. Effect of varying amount of $HClO_4$ on oxidative bromination of thymol. Reaction conditions: thymol (1.5g, 10 mmol), catalyst [$U^{VI}O_2L^2(MeOH)$] (**3.2**) (0.002 g, 3.2×10^{-3} mmol), 30% aqueous H_2O_2 (30 mmol, 3.39 g), and KBr (30 mmol, 3.57 g), at room temperature.

Table 3.7. Conversion of thymol (1.5 g, 0.010 mol) using [U^{VI}O₂(eda-2,4-dmp)(MeOH)] (**3.2**) as a catalyst, turn over frequency, and selectivity of different products for 2 h of reaction time under different reaction conditions.

Entry	KBr [g (mmol)]	H ₂ O ₂ [g (mmol)]	HClO ₄ [g (mmol)]	Catalyst [mg (mmol)]	Conv. [%]	TOF [h ⁻¹]	Selectivity [%]		
							2-Brth	4-Brth	2,4-diBrth
1	1.19 (10)	1.13 (10)	1.43 (10)	0.5 (8.0 × 10 ⁻⁴)	46	2875	11	68	21
2	1.19 (10)	1.13 (10)	1.43 (10)	1 (1.6 × 10 ⁻³)	60	1875	13	78	9
3	1.19 (10)	1.13 (10)	1.43 (10)	2 (3.2 × 10 ⁻³)	64	1000	12	76	12
4	1.19 (10)	1.13 (10)	1.43 (10)	3 (4.8 × 10 ⁻³)	43	448	12	81	7
5	1.19 (10)	2.26 (20)	1.43 (10)	2 (3.2 × 10 ⁻³)	66	1031	13	70	17
6	1.19 (10)	3.39 (30)	1.43 (10)	2 (3.2 × 10 ⁻³)	67	1046	12	67	21
7	2.38 (20)	3.39 (30)	1.43 (10)	2 (3.2 × 10 ⁻³)	75	1172	12	66	22
8	3.57 (30)	3.39 (30)	1.43 (10)	2 (3.2 × 10 ⁻³)	82	1281	9	60	31
9	3.57 (30)	3.39 (30)	2.86 (20)	2 (3.2 × 10 ⁻³)	91	1422	3	85	12
10 ^a	3.57 (30)	3.39 (30)	4.29 (30)	2 (3.2 × 10 ⁻³)	99	1547	4	91	5
11	3.57 (30)	3.39 (30)	4.29 (30)	blank	32		4	90	6

^a The optimized conditions mentioned here are the best among the different sets of reactions carried out.

Other three catalysts i.e. **3.1**, **3.3** and **3.4** were also tested under the above optimized reaction conditions and the results are presented in Table 3.8. It is clear from the data of Table 3.8 that all the four complexes show comparable catalytic activity between 97-99% (also see Fig. 3.8) along with high turnover frequency. Again 4-bromothymol is highest in selectivity. Blank reaction under above reaction conditions gave only 32 % conversion (Table 3.8).

Table 3.8. Conversion, turn over frequency and selectivity parameters for various catalysts for the oxidative bromination of thymol.

Catalyst	TOF [h ⁻¹] ^a	Conv. [%]	Selectivity [%]		
			2- Brth	4-Brth	2,4-diBrth
[U ^{VI} O ₂ L ¹ (MeOH)] (3.1)	1515	97	5	90	5
[U ^{VI} O ₂ L ² (MeOH)] (3.2)	1547	99	4	91	5
[U ^{VI} O ₂ L ³ (MeOH)] (3.3)	1515	97	4	90	6
[U ^{VI} O ₂ L ⁴ (MeOH)] (3.4)	1531	98	6	89	5
Without catalyst		32	0	97	2

^aTOF values calculated at 2 h reaction time.

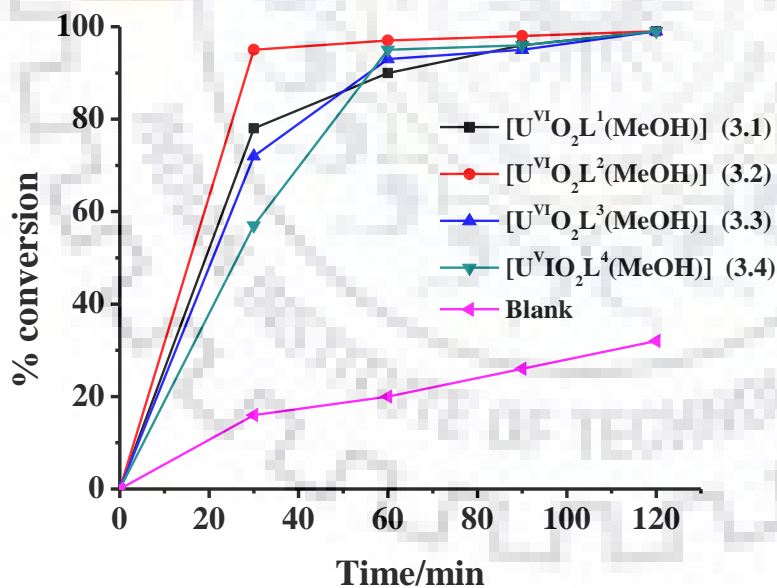


Fig. 3.12. Plot representing conversion of thymol in the presence of different [UO₂]²⁺ complexes and without catalyst.

We have also studied the catalytic potential of complex **3.2** towards the oxidative bromination of thymol in different biphasic solvent systems and their effect on the selectivity of different products. The catalytic potential of **3.2** is almost the same in most mixed solvent systems studied here (Table 3.9) but the selectivity of products slightly varies. The selectivity of 4-bromothymol is as highest (95%) in CHCl₃-H₂O followed by 93% in Hexane-H₂O and 91% in water. Thus, it seems that 4-bromothymol is the preferred product over 2,4-dibromothymol possibly due to steric hindrance and/or further bromination of monobromothymol species in aprotic solvents.

Table 3.9. Solvent effect on the oxidative bromination of thymol and selectivity of products catalysed by complex **3.2**.

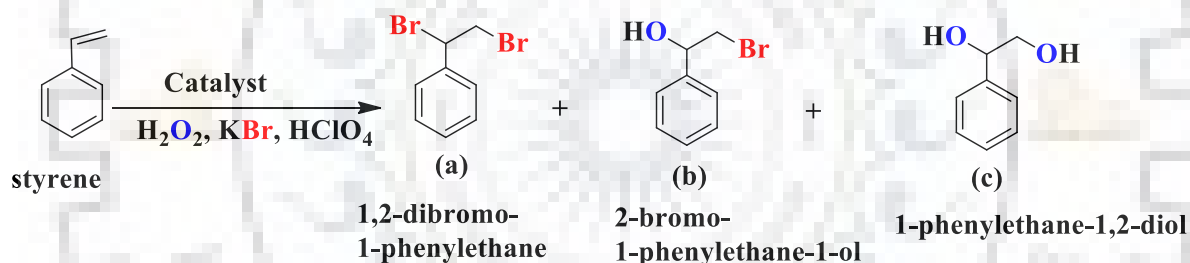
Entry	Solvents	Conv. [%]	Selectivity [%]		
			2- Brth	4-Brth	2,4-diBrth
1	Water	99	4	91	5
2	MeOH-H ₂ O	95	3	90	7
3	CH ₂ Cl ₂ -H ₂ O	99	5	88	7
4	MeCN-H ₂ O	99	5	90	5
5	CHCl ₃ -H ₂ O	93	2	95	3
6	Hexane-H ₂ O	98	3	93	4

These complexes show almost similar conversion as reported for [V^{VO}(OMe)(MeOH)(L)] [H₂L = 6,6'-(2-(pyridin-2-yl)ethylazanediyl)bis(methylene)-bis(2,4-di-*tert*-butylphenol)] (ca. 99%)¹⁶ and [Mo^{VI}O₂]²⁺ complexes of Schiff base ligands derived from 8-formyl-7-hydroxy-4-methylcoumarin and hydrazides (94-99%) [54]. but little better to [W^{VI}O₂]²⁺ complexes (91-96%) [156]. However, the selectivity of 4-bromothymol is relatively high (more than 90%) for uranium complexes over other catalysts. In case of [U^{VI}O₂]²⁺ complexes, under optimized reaction conditions higher amounts of KBr, H₂O₂ and HClO₄ (3 equivalent each for 10 mmol of substrate) versus

lower amounts of these reagents for vanadium, molybdenum and tungsten complexes have been used and this might be responsible for higher amount of 4-bromothymol.

3.3.3.2. Oxidative bromination of styrene

The synthesized complexes **3.1**, **3.2**, **3.3** and **3.4** have also been used as a catalyst to study the oxidative bromination of styrene. We have considered $[U^{VI}O_2(eda-2,4-dmp)(MeOH)]$ (**3.2**), complex as a representative catalyst again and the oxidative bromination of styrene was carried out at room temperature in the presence of KBr, 70% aqueous $HClO_4$ and 30% aqueous H_2O_2 in water led to the formation of (a) 2-bromo-1-phenylethanol and (b) 1-phenylethane-1,2-diol along with some minor oxidized products (totaling ca. 1%), though literature reports the formation of one more product i.e. 1,2-dibromo-1-phenylethane (Scheme 3.3) [154, 160, 163].



Scheme 3.3. Expected products upon oxidative bromination of styrene: (a) 1,2-dibromo-1-phenylethane, (b) 2-bromo-1-phenylethane-1-ol and (c) 1-phenylethane-1,2-diol.

Consequently, the reaction was investigated by changing different parameters that may affect the rate of styrene bromination and the selectivity of different products. Thus, for 10 mmol of styrene (1.04 g, 10 mmol), four different amounts of catalyst (0.0005, 0.001, 0.002, 0.003 g), three different amounts of 30% aqueous H_2O_2 (10, 20 and 30 mmol), three different amounts of KBr (10, 20 and 30 mmol) and three different amounts of 70% aqueous $HClO_4$ (10, 20 and 30 mmol, added in three equal portions to the reaction mixture as mentioned above). Details of all reaction conditions and the corresponding conversion

of styrene are summarized in Table 3.10. From the data presented in Table 3.10 it is clear that the optimized reaction conditions (entry no. 9) for the maximum conversion of 10 mmol (1.04 g) of styrene are those using 0.001 g (1.6×10^{-3} mmol) of catalyst, 2.26 g (20 mmol) of 30% H_2O_2 , 3.57 g (30 mmol) of KBr, and 2.86 g (20 mmol) of 70% HClO_4 . Under these conditions the obtained conversion is 99% where the selectivity of the two products follows the order: 1-phenylethane-1,2-diol (69%) > 2-bromo-1-phenylethanol (31%).

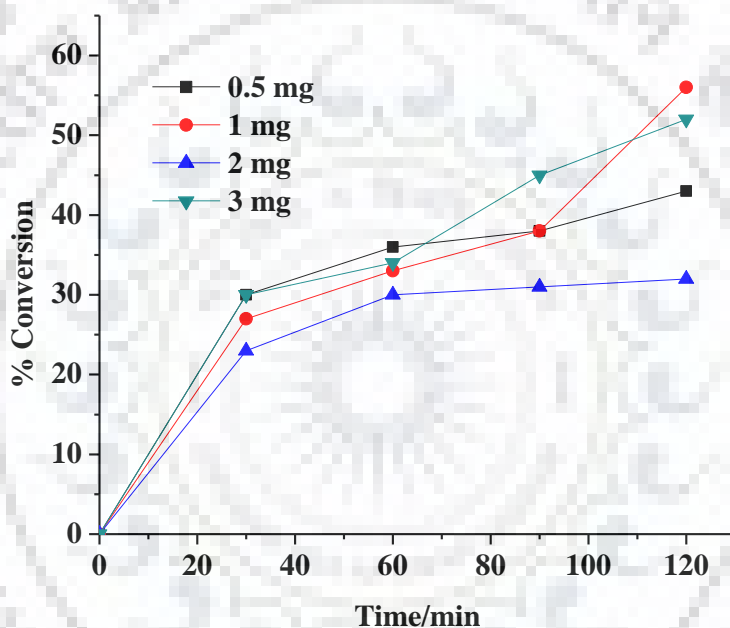


Fig. 3.13. Effect of variation of amount of catalyst on the oxidative bromination of styrene. Reaction conditions: styrene (1.04 g, 10 mmol), 30% aqueous H_2O_2 (10 mmol, 1.13 g), KBr (10 mmol, 1.19 g), and HClO_4 (10 mmol, 1.43 g) at room temperature.

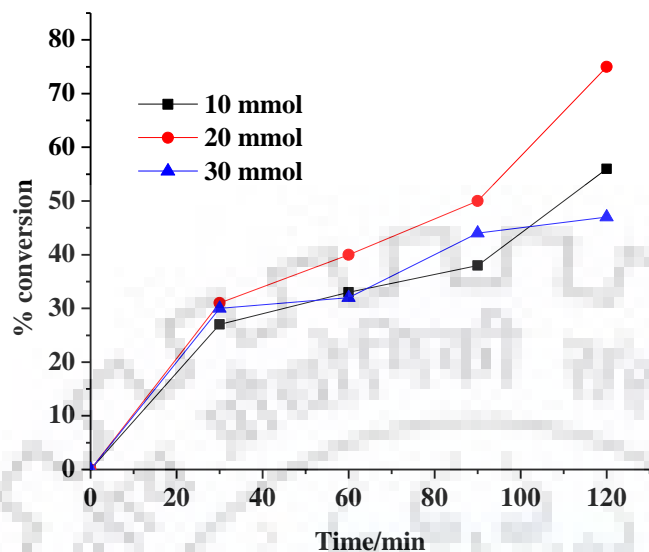


Fig. 3.14. Effect of variation of amount of oxidant on the oxidative bromination of styrene. Reaction conditions: styrene (1.04g, 10 mmol), catalyst $[U^{VI}O_2L^2(MeOH)]$ (**3.2**) (0.001g, 1.6×10^{-3} mmol), KBr (10 mmol, 1.19 g), and $HClO_4$ (10 mmol, 1.43 g) at room temperature.

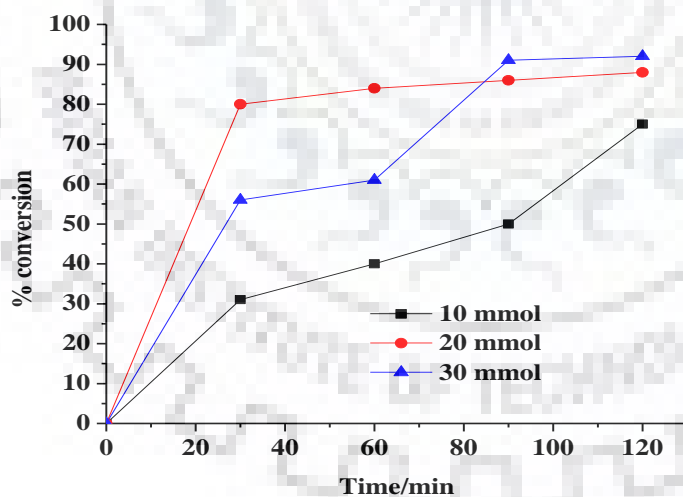


Fig. 3.15. Effect of varying amount of additive (KBr) on the oxidative bromination of styrene. Reaction conditions: styrene (1.04 g, 10 mmol), catalyst $[U^{VI}O_2L^2(MeOH)]$ (**3.2**) (0.001 g, 1.6×10^{-3} mmol), 30% aqueous H_2O_2 (20 mmol, 2.26 g), and $HClO_4$ (10 mmol, 1.43 g) at room temperature.

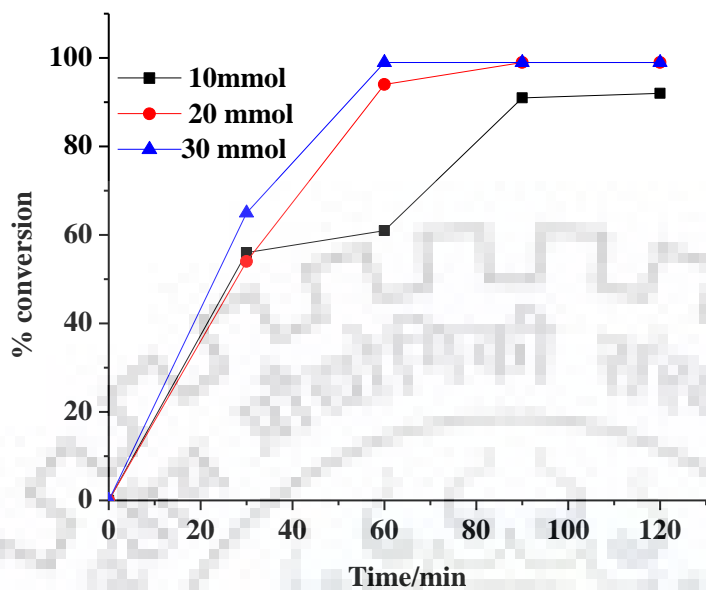


Fig. 3.16. Effect of varying amount of HClO_4 on oxidative bromination of styrene. Reaction conditions: styrene (1.04g, 10 mmol), catalyst $[\text{U}^{\text{VI}}\text{O}_2\text{L}^2(\text{MeOH})]$ (3.2) (0.001g, 1.6×10^{-3} mmol), 30% aqueous H_2O_2 (20 mmol, 2.26 g), and KBr (30 mmol, 3.57 g), at room temperature.

Table 3.10. Conversion of styrene (1.04 g, 10 mmol), using complex **3.2** as a catalyst, turn over frequency, and product selectivity for 2 h of reaction time under different reaction conditions.

Entr y	KBr [g (mmol)]	H ₂ O ₂ [g (mmol)]	HClO ₄ [g (mmol)]	Catalyst [mg (mmol)]	Conv. [%]	Selectivity [%] ^a	
						<i>a</i>	<i>b</i>
1	1.19 (10)	1.13 (10)	1.43 (10)	0.5 (8×10^{-4})	43	12	88
2	1.19 (10)	1.13 (10)	1.43 (10)	1 (1.6×10^{-3})	56	19	81
3	1.19 (10)	1.13 (10)	1.43 (10)	2 (3.2×10^{-3})	32	13	87
4	1.19 (10)	1.13 (10)	1.43 (10)	3 (4.8×10^{-3})	52	13	87
5	1.19 (10)	2.26 (20)	1.43 (10)	1 (1.6×10^{-3})	75	17	83
6	1.19 (10)	3.39 (30)	1.43 (10)	1 (1.6×10^{-3})	47	12	88
7	2.38 (20)	2.26 (20)	1.43 (10)	1 (1.6×10^{-3})	88	25	75
8	3.57 (30)	2.26 (20)	1.43 (10)	1 (1.6×10^{-3})	92	4	96
9	3.57 (30)	2.26 (20)	2.86 (20)	1 (1.6×10^{-3})	99	31	69
10	3.57 (30)	2.26 (20)	4.29 (30)	1 (1.6×10^{-3})	99	32	68
11	3.57 (30)	2.26 (20)	4.29 (30)	blank	38	20	80

^a *a* = 2-bromo-1-phenylethanol and *b* = 1-phenylethane-1,2-diol.

Other three catalysts, i.e. **3.1**, **3.3** and **3.4** were also tested under the above optimized reaction conditions for the maximum conversion of styrene. The results are accessible in Fig. 3.8 and Table 3.11. It is clear from the data that all the four complexes show comparable catalytic activity (99%) along with high turnover frequency and within the two products, the selectivity of 1-phenylethane-1,2-diol is always higher than that of 2-bromo-1-phenylethanol. Blank reaction gave only 38% conversion

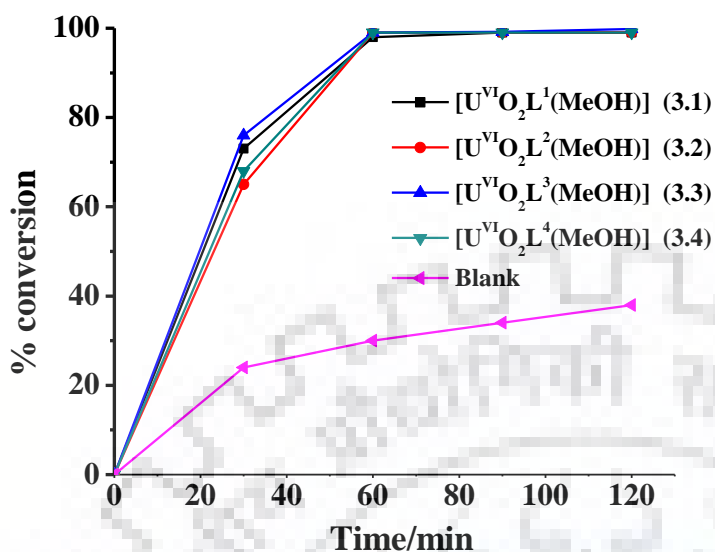


Fig. 3.17. Plot representing conversion of styrene in the presence of different $[\text{UO}_2]^{2+}$ complexes.

Table 3.11. Conversion, turn over frequency and selectivity parameters for various catalysts for the oxidative bromination of styrene.

Entry	Catalyst	Conv. [%]	TOF [h^{-1}] ^a	Selectivity [%]	
				2-bromo-1-phenylethanol	1-phenylethane-1,2-diol
1	$[\text{U}^{\text{VI}}\text{O}_2\text{L}^1(\text{MeOH})]$ (3.1)	99	3094	33	67
2	$[\text{U}^{\text{VI}}\text{O}_2\text{L}^2(\text{MeOH})]$ (3.2)	99	3094	31	69
3	$[\text{U}^{\text{VI}}\text{O}_2\text{L}^3(\text{MeOH})]$ (3.3)	99	3094	37	63
4	$[\text{U}^{\text{VI}}\text{O}_2\text{L}^4(\text{MeOH})]$ (3.4)	99	3094	38	62
5	Without catalyst	38		20	80

^a TOF values calculated at 2 h of reaction time.

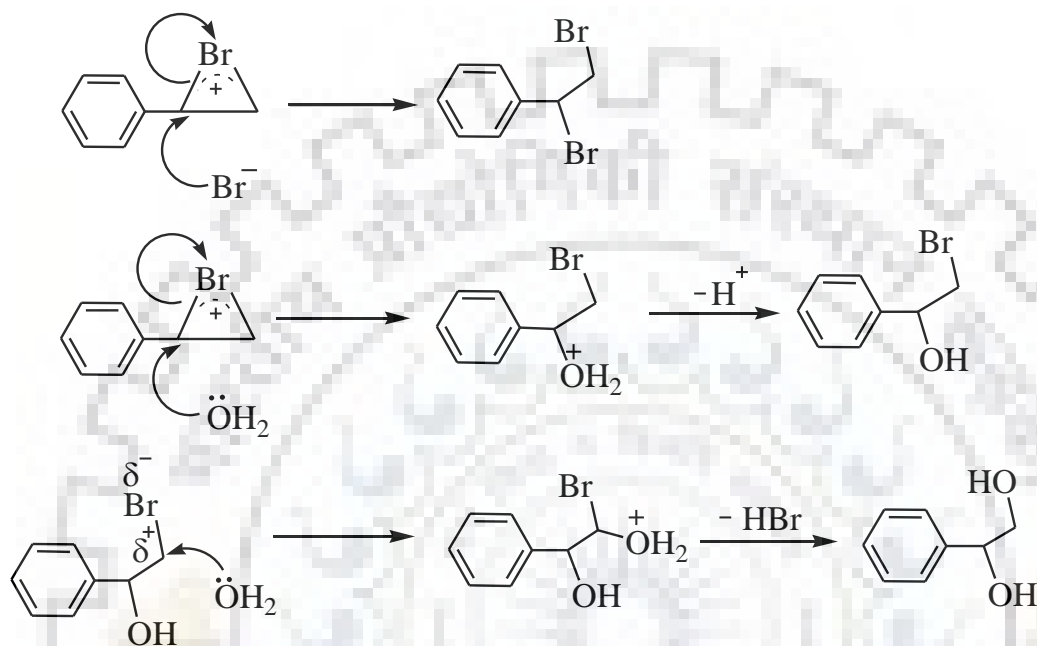
We have also studied the catalytic potential of complex **3.2** towards the oxidative bromination of styrene in different biphasic solvent systems and their effect on the selectivity of different products. Thus, catalytic potential of **3.2** is almost the same in all solvent systems (Table 3.12), except in CH₂Cl₂-H₂O where it is slightly lower. However, the selectivity of products varies. The selectivity 1-phenylethane-1,2-diol follows the order: is highest CH₃CN-H₂O = Hexane-H₂O (80 %) > CHCl₃-H₂O (79%) > CH₂Cl₂-H₂O (78%) > MeOH-H₂O = H₂O (67%). Thus, it seems that the expected product, 1,2-dibromo-1-phenylethane completely hydrolyses with water to 2-bromo-1-phenylethanol and 2-bromo-1-phenylethanol further hydrolyses to some extent to 1-phenylethane-1,2-diol possibly through the mechanism presented in Scheme 3.4.

Table 3.12. Solvent effect on the selectivity of products catalysed by complex (**3.2**).

Entry	Solvents	Conv. [%]	Selectivity [%]	
			2-bromo-1-phenylethanol	1-phenylethane-1,2-diol
1	Water	99	33	67
2	MeOH-H ₂ O	98	33	67
3	CH ₂ Cl ₂ -H ₂ O	92	22	78
4	CH ₃ CN-H ₂ O	99	20	80
5	CHCl ₃ -H ₂ O	99	21	79
6	Hexane-H ₂ O	98	20	80

As observed in *cis*-[MO₂]- complexes (M = V, Mo and W) [19,20,26,29]. the reaction of complexes with KBr in the presence of H₂O₂ and HClO₄, catalytically generate HOBr and/or Br⁺, Br₂, Br³⁻ which react with styrene to give bromonium ion as an intermediate. A similar reaction may also be presumed by *trans*-[UO₂]²⁺- complexes (see next section). The nucleophile Br⁻ as well as H₂O both may attack on the α-carbon of the intermediate to give 1,2-dibromo-1-phenylethane and 2-bromo-1-phenylethane-1-ol,

respectively. The nucleophile H_2O may further attack on the α -carbon of 2-bromo-1-phenylethane-1-ol to give 1-phenylethane-1,2-diol (Scheme 3.4 also see Scheme 1.2) [54]. All these justify the formation of 1-phenylethane-1,2-diol in highest yield.



Scheme 3. 4. Mechanism of action of Br_2/HOBr on styrene and hydrolysis of the brominated products in the presence of water.

3.3.4. Reactivity

It was observed recently by ^{51}V NMR study by some of us that the $[\text{VO}(\text{O}_2)(\text{L})]$ -type species is an active intermediate during catalytic study of oxidative bromination of thymol in the presence of oxidant H_2O_2 [138]. Conte *et al.* have identified an oxidomonoperoxidovanadium(V) complex as the oxidant of the Br^- ion to HOBr/Br_2 by spectroscopic techniques [160]. The formations of similar monoperoxido species have also been suggested as an active intermediate by molybdenum and tungsten complexes [54,156]. In order to generate information for such an intermediate in *trans*- $[\text{UO}_2]$ -complexes, we have also treated these complexes with H_2O_2 and monitored the changes by UV-Vis spectroscopy. Thus, the sequential addition of a 30% H_2O_2 solution (0.108 g, 0.95 mmol) dissolved in 5 mL of MeCN to a 25 mL of 9.97×10^{-2} M solution of $[\text{U}^{\text{VI}}\text{O}_2(\text{eda-$

2,4-dmp)(MeOH)] (**3.2**) in MeCN resulted in the spectral changes as presented in Fig. 3.18. The band at 490 nm slowly disappears with a decrease in intensity while 402 nm band slowly becomes shoulder along with marginal increasing in intensity and shifting to 350 nm. The UV-band appearing at 290 nm shift to 286 along with only marginally decrease in intensity. These changes also generate two isosbestic points at 305 and 379 nm which suggest the transformation of dioxidouranium(VI) complex to its oxidoperoxido form (Eq. 1), based on the knowledge gathered from vanadium, molybdenum and tungsten complexes treated with H₂O₂ under similar conditions [54,156, 160, 163]. Other complexes show almost similar spectral changes upon treatment with H₂O₂ (Fig. 3.19-3.21).

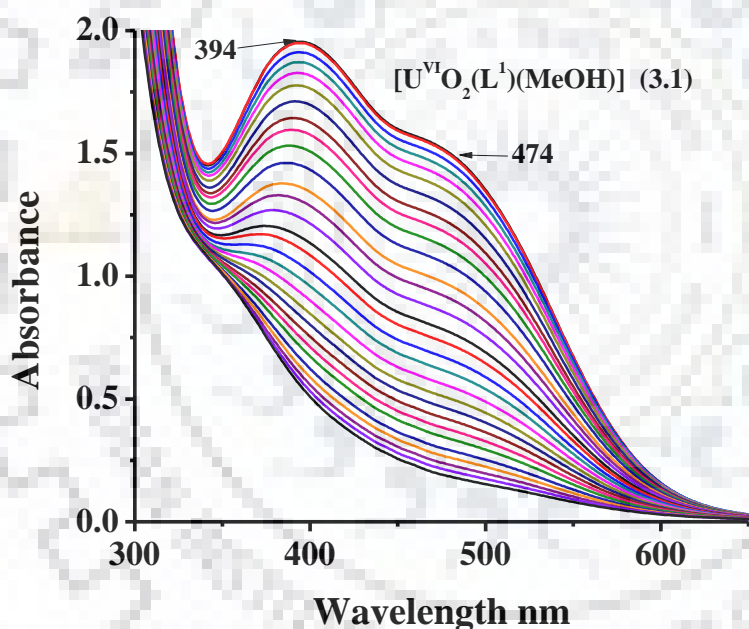


Fig. 3.18. Plots representing the Spectral changes during titration of [U^{VI}O₂L¹(MeOH)] (**3.1**) with H₂O₂. Spectra were obtained after successive addition of one drop portion 30% H₂O₂ (0.108 g, 0.95 mmol) dissolved in 5 mL of MeCN to 25 mL of 8.75 × 10⁻² M solution of **3.1** in MeCN.

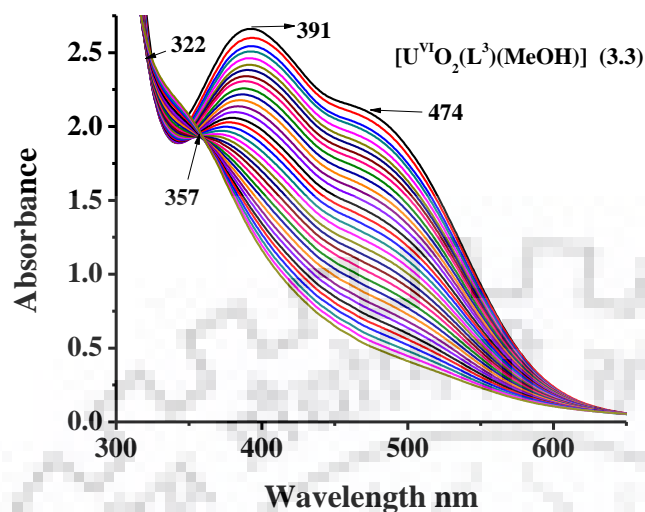


Fig. 3.19. Plots representing the Spectral changes during titration of $[U^{VI}O_2L^3(MeOH)]$ (3.3) with H_2O_2 . Spectra were obtained after successive addition of one drop portion 30% H_2O_2 (0.108 g, 0.95 mmol) dissolved in 5 mL of MeCN to 25 mL of 7.7×10^{-2} M solution of 3.3 in MeCN.

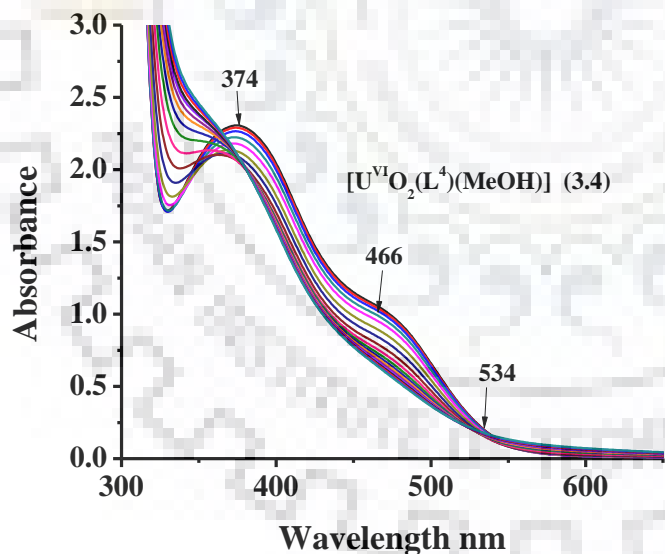


Fig. 3.20. Plots representing the Spectral changes during titration of $[U^{VI}O_2L^4(MeOH)]$ (3.4) with H_2O_2 . Spectra were obtained after successive addition of one drop portion 30% H_2O_2 (0.108 g, 0.95 mmol) dissolved in 5 mL of MeCN to 25 mL of 6.48×10^{-2} M solution of 3.4 in MeCN.

These spectral changes are similar to oxidoperoxido- vanadium, molybdenum- and tungsten complexes. Such oxidoperoxido intermediates in vanadium complexes finally form hydroperoxido species during the catalytic action as proposed for haloperoxidases which is responsible for the catalytic conversion of Br^- ion to HOBr/Br_2 [164]. A similar intermediate may also be proposed here.

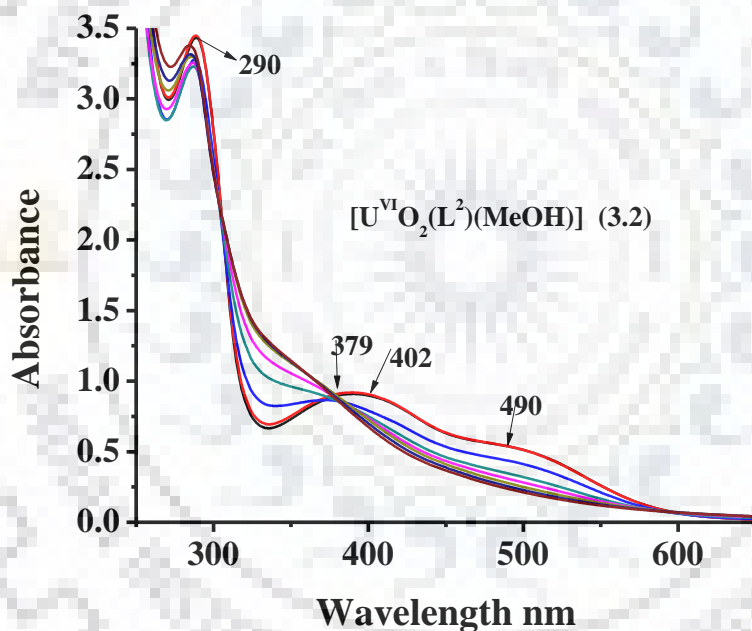
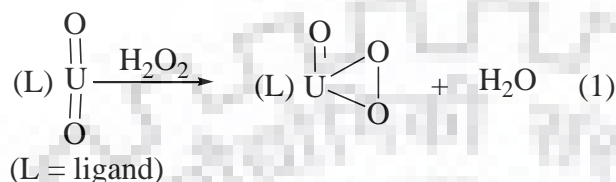


Fig. 3.21. Plots representing the spectral changes during titration of $[\text{U}^{\text{VI}}\text{O}_2\text{L}^2(\text{MeOH})]$ (3.2) with H_2O_2 . Spectra were obtained after successive addition of one drop portions of 30% H_2O_2 (0.108 g, 0.95 mmol) dissolved in 5 mL of MeCN to 25 mL of 9.97×10^{-2} M solution of 3.2 in MeCN.

3.4. Conclusions

Four *trans*-dioxidouranium(VI) complexes, *trans*-[U^{VI}O₂L¹⁻⁴(MeOH)] (**3.1**–**3.4**) have been prepared from potential dibasic tetra dentate ONNO type Manisch base ligands derived from ethylenediamine and 2,4-di-*tert*-butylphenol(H₂L¹) (**I**) and 2,4-dimethylphenol (H₂L²) (**II**), , 2-*tert*-butyl-4-methylphenol (H₂L³) (**III**), and 2,4-dichlorophenol (H₂L⁴) (**IV**). All these complexes have been characterized by various spectroscopic techniques and two of them **3.3** and **3.4** by single crystal X-ray study. Oxidative bromination of thymol and styrene has successfully been carried out using these complexes as catalyst, signifying them useful functional model of vanadium dependent halo peroxidases. In the presence of H₂O₂, the formation of corresponding oxidoperoxidouranium(VI) complexes, similar to oxidoperoxido- vanadium, molybdenum- and tungsten complexes, have also been demonstrated in solution which may lead to the formation of similar hydroperoxido intermediate during the catalytic action as proposed for halo peroxidases. Therefore, a reaction mechanism similar to halo peroxidases may also be proposed here.

4.1. Introduction

Molybdenum is an essential metal which is capable of forming complexes with many compounds of biological importance such as carbohydrates, amino acids and other bioinspired ligands [87, 120, 165, and 166]. These model complexes can catalyze a wide variety of biochemical reactions. The most commonly studied reactions (other than biochemical) in which dioxidomolybdenum(VI) complexes act as catalysts are epoxidation of alkenes [18, 59, 117, 167-174], oxidation of alcohols [23, 104] and sulfur based compounds [103, 175, 176], and oxidative halogenation of organic substrates [45, 54, 153]. The nature of complex, oxidant and reaction conditions decide whether the reaction will proceed via a homolytic or electrophilic oxidation.

In current years artificial enzyme mimics have become a hot topic of research since they present many advantages over conventional enzymes, namely easier preparation, lower price and improved stability, overcoming the drawbacks of natural enzymes [151, 152, 155, and 177]. Dioxidomolybdenum(VI) complexes are air stable and show functional as well as structural similarity with vanadium based halo peroxidases, thus can be considered as artificial models for halo peroxidases [151 - 153].

Amongst the actinides, uranium is the only element being well known for their coordination chemistry. Like molybdenum, uranium in its *trans*-[UO₂] form forms stable complexes in higher oxidation state [19, 153] but their catalytic activities are not much explored [19, 74, 80, 84, 148, 149, 153, 178, and 179]. Therefore, the objective of the present work is to prepare dioxidomolybdenum(VI) and dioxidouranium(VI) complexes of stable dibasic tetra dentate ligand, 1,4-bis-(2-hydroxy-3,5-dimethylbenzyl)piperazine (abbreviated as H₂pip-2,4-dmp, Scheme 1) and study their catalytic activity as homogeneous catalysts for the oxidative bromination of thymol, an essential catalytic reaction observed by many model vanadium complexes [151 - 153]. It has been observed that both complexes mimic similar catalytic activity as shown by vanadium based halo peroxidases and show very good conversion of thymol to the corresponding oxidative brominated products.

4.2. Experimental

4.2.1. Materials

MoO₃ (S.D. fine, India), uranyl acetate dihydrate (Loba chemie, India), piperazine, 2,4-dimethylphenol (Aldrich Chemicals, USA) and thymol (Himedia, India) were used as obtained. [Mo^{VI}O₂(acac)₂] was prepared following the method reported in literature [131]. Ligand 1,4-bis-(2-hydroxy-3,5-dimethylbenzyl)piperazine (H₂pip-2,4-dmp) (**4.I**) was prepared following the method reported in literature [180]. All other chemicals and solvents used were of AR grade.

4.2.2. General procedures and techniques

Electronic spectra of ligands and complexes were measured in MeCN with a Shimadzu 2600 UV-Vis spectrophotometers. The ¹H and ¹³C NMR spectra of ligand and complexes were taken in CDCl₃/ DMSO-d₆ using a JEOL ECX 400 MHz spectrometer. The thermogravimetric analysis of the complexes was carried out under oxygen atmosphere using a TG Stanton Redcroft STA 780 instrument. A Shimadzu 2010 plus gas-chromatograph fitted with an Rtx-1 capillary column (30 m × 0.25 mm × 0.25 μm) and a FID detector was used to analyze the reaction products and their quantification was made based of the relative peak area of each product. The identity of the products was confirmed using a GC-MS model Perkin-Elmer, Clarus 500 and comparing the fragments of each product with the library available. Other instrumentation details are given in chapter 2.

4.2.3. Synthesis of [Mo^{VI}O₂(pip-2,4-dmp)] (**4.1**)

The ligand H₂pip-2, 4-dmp (1.77 g, 5 mmol) was dissolved in 80 mL methanol by refluxing on a water bath for 2 h. A solution of [Mo^{VI}O₂(acac)₂] (1.625 g, 5 mmol) in methanol (15 mL) was added to the solution of ligand and the reaction mixture was allowed to reflux for 24 h, whereupon a yellow precipitate separated out. The solution volume was reduced to ca. 20 mL and the separated product was collected by filtration, washed with methanol and dried in vacuum desiccator. Yield: 33.1% (0.792 g) Cal. For C₂₂H₂₈N₂O₄Mo (480); C, 55.0; H, 5.83; N, 5.83. Obs. C, 54.6; H, 5.9; N, 5.8%.

4.2.4. Synthesis of [U^{VI}O₂(pip-2,4-dmp)(MeOH)] (4.2)

A solution of U^{VI}O₂(CH₃COO)₂.2H₂O (2.125 g, 5 mmol) in 10 mL methanol was added to the stirred solution of ligand (1.77 g, 5 mmol) in 80 mL MeOH prepared as mentioned above and the resulting reaction mixture was refluxed on a water bath for 24 h as a result of which a yellow-orange precipitate appeared. The solution volume was reduced to ca. 20 mL and the separated product was filtered, washed with methanol and dried in vacuo. Yield: 40.8% (1.27 g). Cal. For C₂₂H₃₂N₂O₅U (642); C, 41.12; H, 4.98; N, 4.36. Obs. C, 40.6; H, 4.9; N, 4.5%. Crystals of the complex suitable for X-ray study were grown in DMSO and obtained complex is now abbreviated as [U^{VI}O₂(pip-2,4-dmp)(DMSO)] (4.2a).

4.2.5. X-Ray crystal structure determination

Three-dimensional X-ray data of [U^{VI}O₂(pip-2,4-dmp)(DMSO)] (4.2a) were collected on a Bruker Kappa Apex CCD diffractometer at room temperature by the ϕ - ω scan method. Reflections were measured from a hemisphere of data collected from frames, each of them covering 0.3° in ω . A total of 26,000 reflections measured were corrected for Lorentz and polarization effects and for absorption by multi-scan methods based on symmetry-equivalent and repeated reflections. Of the total, 5271 independent reflections exceeded the significance level ($|F|/\sigma|F|$) > 4.0. After data collection an empirical absorption correction (SADABS) [157] was applied, and the structure was solved by direct methods and refined by full matrix least-squares on F^2 data using SHELX suite of programs [132, 133]. Hydrogen atoms were included in calculated position and refined in the riding mode, except for C(3), C(5) and C(16), which were located in difference Fourier map and freely refined. A final difference Fourier map showed no residual density outside: 0.912 and -0.668 e.Å⁻³ for 4.2a. Due to disorder in DMSO molecule bonded to U(1) atom, two positions for sulfur atom of DMSO molecule were refined with anisotropic atomic displacement parameters. The site occupancy factor was 0.91716 for S(1A). A weighting scheme $w = 1/[\sigma^2(F_o^2) + (0.018900 P)^2 + 2.237600 P]$, where $P = (|F_o|^2 + 2|F_c|^2)/3$, was used

in the latter stages of refinement. Further details of the crystal structure determination are given in Table 4.1.

Table 4.1. Crystal Data and Structure Refinement for [U^{VI}O₂ (pip-2,4-dmp)(DMSO)] (4.2a).

Formula	C ₂₄ H ₃₄ N ₂ O ₅ SU
Formula weight	700.62
T, K	293(2)
Wavelength, Å	0.71073
Crystal system	Monoclinic
Space group	P2 ₁ /c
a/Å	11.6974(10)
b/Å	14.5623(12)
c/Å	15.2257(12)
β/°	95.112(4)
V/Å ³	2583.2(4)
Z	4
F ₀₀₀	1360
D _{calc} /g cm ⁻³	1.801
μ/mm ⁻¹	6.400
θ/ (°)	2.53 to 28.61
R _{int}	0.0292
Crystal size/ mm ³	0.09 × 0.06 × 0.05
Goodness-of-fit on F ²	1.059
R ₁ [I>2σ(I)] ^a	0.0210
wR ₂ (all data) ^b	0.0525
Largest differences peak and hole (eÅ ⁻³)	0.912 and -0.668

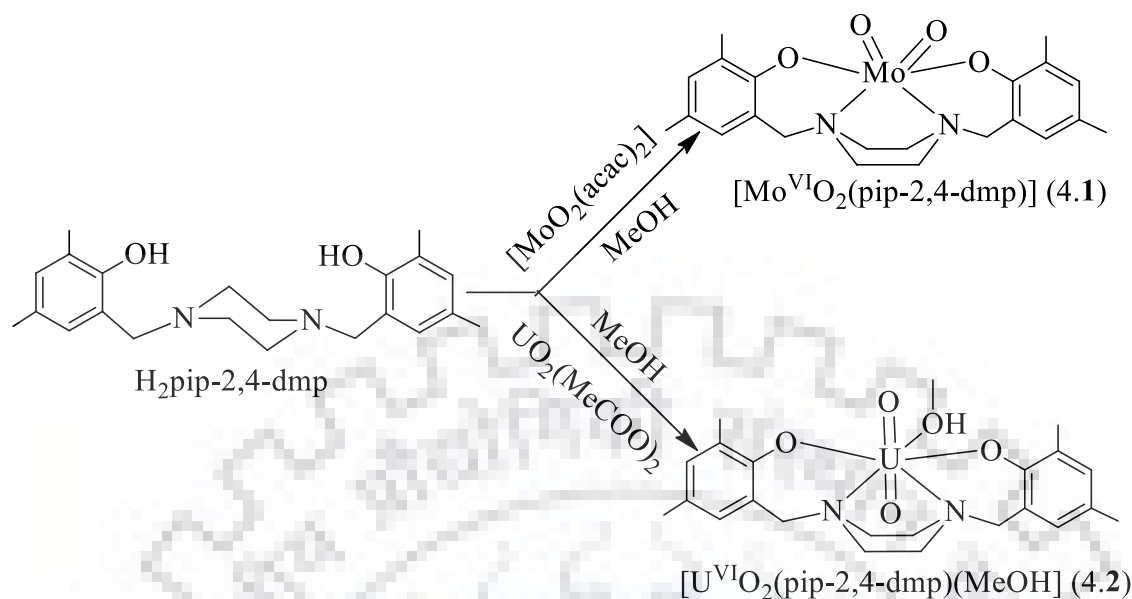
$${}^a R_1 = \frac{\sum ||F_o| - |F_c||}{\sum |F_o|}, \quad {}^b wR_2 = \left\{ \frac{\sum [w(|F_o|^2 - |F_c|^2)]^2}{\sum [w(F_o^2)]^2} \right\}^{1/2}$$

4.2.6. Catalytic activity study: Oxidative bromination of thymol

All the reactions were carried out in a 100 mL two-necked round bottom flask. In a typical reaction, thymol (1.5 g, 10 mmol) and aqueous 30% H₂O₂ (1.13 g, 10 mmol) and KBr (1.19 g, 10 mmol) were added in 20 mL water. After adding the metal-complex (i.e. catalyst) (0.002 g), 70% HClO₄ (1.43 g, 10 mmol) was added to the reaction flask and the reaction mixture was stirred for 2 h at room temperature. The reaction mixture was then extracted with *n*-hexane where the products moved into the *n*-hexane layer. The oxidized products were analyzed quantitatively by withdrawing small aliquots from the *n*-hexane and subjected to GC and their quantifications were made on the basis of the relative peak area of the respective product. The obtained main products were further confirmed by ¹H NMR spectroscopy as well as GC–MS after their separations.

4.3. Results and discussion

A Mannich condensation between piperazine, 40% formaldehyde and 2,4-dimethyl phenol (1 : 2 : 2 molar ratio) in refluxing MeOH yields the Mannich base ligands, H₂pip-2,4-dmp (**4.I**) in excellent yield [180]. Reaction of **4.I** with [Mo^{VI}O₂(acac)₂] and U^{VI}O₂(CH₃COO)₂·2H₂O in refluxing methanol resulted in the formation of [Mo^{VI}O₂(pip-2,4-dmp)] (**4.1**) (yellow) and [U^{VI}O₂(pip-2,4-dmp)(MeOH)] (**4.2**) (reddish-brown), respectively, as stable solid. Idealized structures of the complexes are shown in Scheme 4.1. which are based on the spectroscopic (IR, UV/Vis and ¹H NMR) data, elemental and thermal analyses, and X-ray diffraction study of [U^{VI}O₂(pip-2,4-dmp)(DMSO)] (**4.2a**, a DMSO coordinated complex **4.2**). Both complexes are soluble in methanol, dichloromethane, dimethyl sulfoxide and acetonitrile.



Scheme 4.1. Synthetic route to prepare $[\text{Mo}^{\text{VI}}\text{O}_2(\text{pip-2,4-dmp})]$ (4.1) and $[\text{U}^{\text{VI}}\text{O}_2(\text{pip-2,4-dmp})(\text{MeOH})]$ (4.2).

4.3.1. Thermogravimetric analysis study

Thermogravimetric analysis (TGA) profile of $[\text{Mo}^{\text{VI}}\text{O}_2(\text{pip-2,4-dmp})]$ (4.1) under an oxygen atmosphere shows a mass loss of ca. 2.0% between 60 to 100 °C which is possibly due to moisture or traces of water/methanol of crystallization. The complex is then stable up to ca. 200 °C. Above this temperature complex starts decomposing in three exothermic steps and stabilizes at ca. 500 °C. The obtained residue of 31.1% at this temperature is equivalent to the formation of stable MoO_3 (Cal for $\text{MoO}_3 = 30\%$). The residue is stable up to 710 °C and then volatilizes beyond this temperature. TGA profile of $[\text{U}^{\text{VI}}\text{O}_2(\text{pip-2,4-dmp})(\text{MeOH})]$ (4.2) shows a mass loss (Fig. 4.1) between 60 °C to 285 °C equivalent to 4.9% which is equal to one methanol (Cal. 4.98%) coordinated to uranium. Increasing temperature further, it decomposes in three exothermic steps and stabilizes at ca. 525 °C. The residue obtained (42.9%) at this temperature equals to U_3O_8 (Cal. 43.41%). This residue is stable up to 1000 °C.

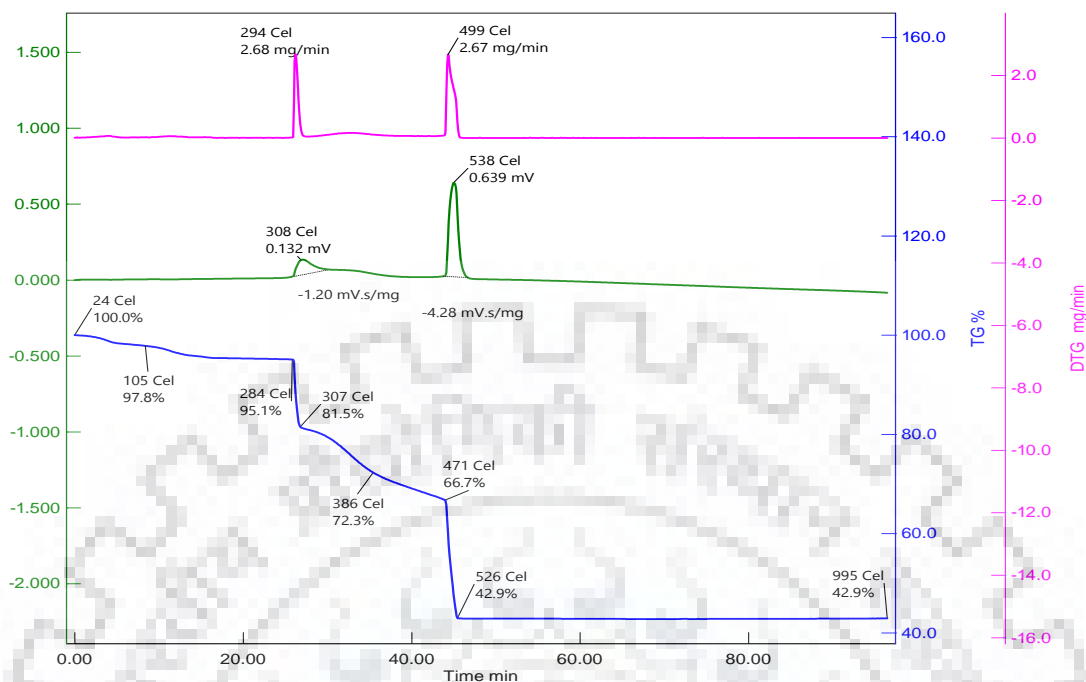


Fig. 4.1. TGA, DTA and DTG profiles of $[U^{VI}O_2(\text{pip-2,4-dmp})(\text{MeOH})]$ (4.2) under air atmosphere.

4.3.2. Description of structure of $[U^{VI}O_2(\text{pip-2,4-dmp})(\text{DMSO})]$ (4.2a)

Fig. 4.2. Selected bond distances and angles are given in Table 4.2. It is a mononuclear complex, which crystallizes in a monoclinic space group $P2_1/c$. The structure adopts a distorted pentagonal bipyramidal geometry around of metal centre. The ligand acts as tetra dentate, coordinated through two phenoxido oxygen and two piperazine nitrogen atoms. The piperazine nitrogen atoms present a distorted sp^3 hybridized bonding network. U centre completes the coordination sphere by bonding to two O_{oxido} terminal oxygen atoms and one oxygen atom from solvent molecule (DMSO). The $U^{VI} = O$ bond lengths [1.788(2)-1.792(2) Å] are similar to other in the literature [158]. The two distances $U^{VI} = O_{\text{phenoxido}}$ [2.225(2) and 2.234(2) Å] are shorter than the $U^{VI} = O_{\text{DMSO}}$ [2.446(2) Å] and are trans to each other. The equatorial plane is occupied by the $O_{\text{phenoxido}}$ atoms, O(3) and O(4), by the $N_{\text{piperazine}}$ atoms, N(1) and N(2) and by the oxygen atom (O1S) of DMSO molecule. They are distorted respect to the planarity, [mean deviation from the plane 0.0857(14) Å]. The terminal oxido atoms occupy the axial sites. The crystal packing (Fig.

4.3) does not present hydrogen bonds between the electronegative atoms. π - π Interactions are not present either.

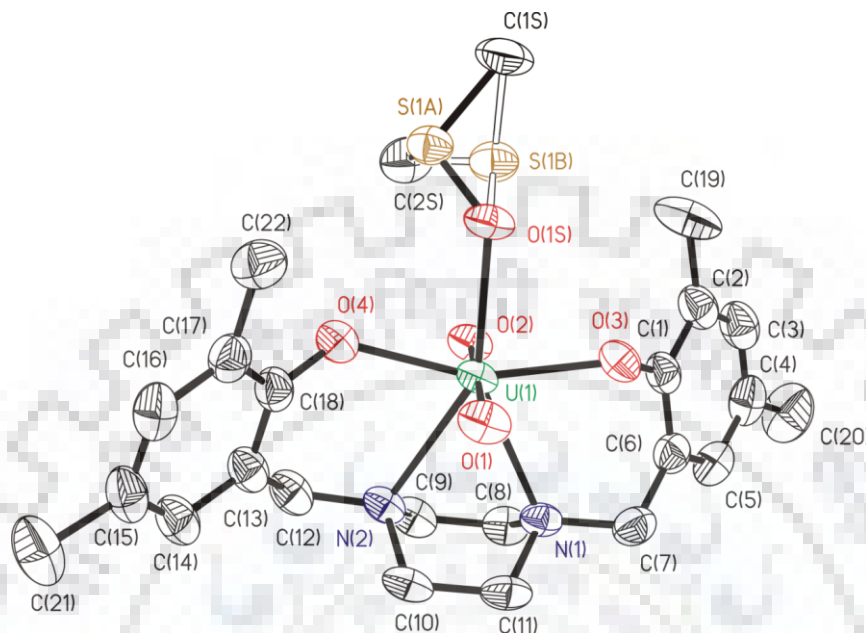


Fig. 4.2. ORTEP for the compound $[\text{U}^{\text{VI}}\text{O}_2(\text{pip-2,4-dmp})(\text{DMSO})]$ (**4.2a**). All the non-hydrogen atoms are presented by their 50% probability ellipsoids. Hydrogen atoms are omitted for clarity.

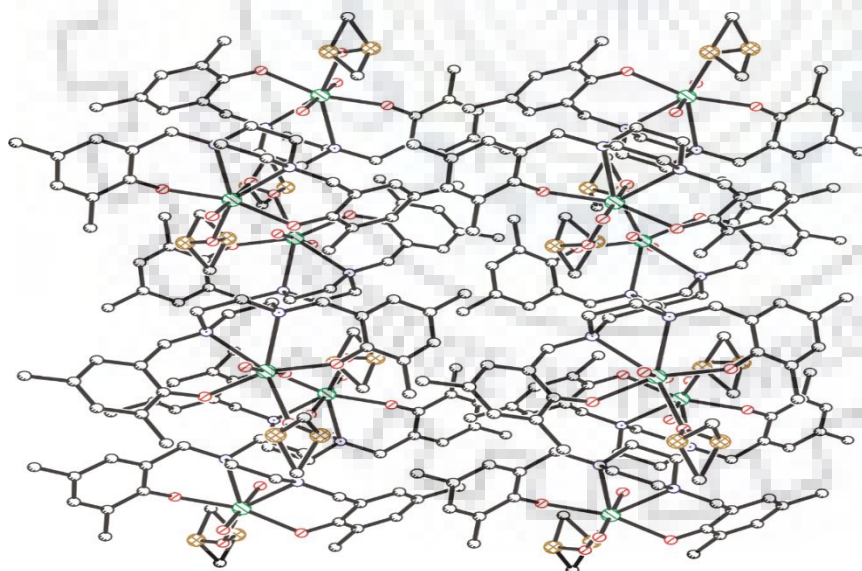


Fig. 4.3. Crystal packing of the compound $[\text{U}^{\text{VI}}\text{O}_2(\text{pip-2,4-dmp})(\text{DMSO})]$ (**4.2a**). Drawing was done in balls and sticks using SHELXL package. Hydrogen atoms are omitted for clarity.

Table 4.2. Bond lengths [\AA] and angles [$^\circ$] for the compounds $[\text{U}^{\text{VI}}\text{O}_2(\text{pip-2,4-dmp})(\text{DMSO})]$ (**4.2a**).

Bond lengths			
U(1)-O(1)	1.792(2)	N(1)-C(7)	1.481(4)
U(1)-O(2)	1.788(2)	N(1)-C(8)	1.477(4)
U(1)-O(3)	2.225(2)	N(1)-C(11)	1.479(4)
U(1)-O(4)	2.234(2)	N(2)-C(9)	1.485(4)
U(1)-O(1S)	2.446(2)	N(2)-C(10)	1.483(4)
U(1)-N(1)	2.640(3)	N(2)-C(12)	1.484(4)
U(1)-N(2)	2.639(2)		
Angles			
O(2)-U(1)-O(1)	176.48(10)	C(8)-N(1)-C(11)	107.0(2)
O(2)-U(1)-O(3)	89.86(9)	C(8)-N(1)-C(7)	110.5(3)
O(1)-U(1)-O(3)	90.88(10)	C(11)-N(1)-C(7)	109.8(2)
O(2)-U(1)-O(4)	91.25(10)	C(8)-N(1)-U(1)	106.85(18)
O(1)-U(1)-O(4)	89.33(10)	C(11)-N(1)-U(1)	105.69(19)
O(3)-U(1)-O(4)	158.26(9)	C(7)-N(1)-U(1)	116.45(19)
O(2)-U(1)-O(1S)	87.95(9)	C(10)-N(2)- C(12)	111.3(2)
O(1)-U(1)-O(1S)	95.56(9)	C(10)-N(2)-C(9)	106.9(3)
O(3)-U(1)-O(1S)	80.24(8)	C(12)-N(2)-C(9)	109.2(2)
O(4)-U(1)-O(1S)	78.10(8)	C(10)-N(2)-U(1)	106.16(17)
O(2)-U(1)-N(2)	84.44(9)	C(12)-N(2)-U(1)	116.3(2)
O(1)-U(1)-N(2)	92.42(9)	C(9)-N(2)-U(1)	106.40(18)
O(3)-U(1)-N(2)	128.86(8)		
O(4)-U(1)-N(2)	72.83(9)		

O(1S)-U(1)-N(2)	149.72(8)
O(2)-U(1)-N(1)	87.82(9)
O(1)-U(1)-N(1)	89.12(9)
O(3)-U(1)-N(1)	72.60(8)
O(4)-U(1)-N(1)	129.14(8)
O(1S)-U(1)-N(1)	152.51(8)
N(2)-U(1)-N(1)	56.46(8)

4.3.3. IR spectral study

Table 4.3 presents IR spectral data of ligand and complexes. The ligand H₂pip-2,4-dmp exhibits a broad band at ca. 3440 cm⁻¹ due to the $\nu(\text{OH})$ of the phenol. Absence of this band in molybdenum complex suggests the deprotonation and coordination of phenolic oxygen to molybdenum while a weak band in the 3400 cm⁻¹ region in uranium complex possibly suggests the presence of coordinated methanol. The presence of several medium intensity bands between 2500 and 2800 cm⁻¹ in the ligand as well as in complexes suggest the existence of C–H stretching bands due to -CH₂. The $\nu(\text{C-N})$ of ring nitrogen has no systematic trend in ligand and complexes. The presence of two sharp peaks in molybdenum complex at 944 and 906 cm⁻¹ due to $\nu_{\text{asym}}(\text{O}=\text{Mo}=\text{O})$ and $\nu_{\text{sym}}(\text{O}=\text{Mo}=\text{O})$ stretches, respectively, confirm the presence of *cis*-[Mo^{VI}O₂] moiety. In uranium complex, one sharp band appears at 900 cm⁻¹ and other one appears in the lower region at 859 cm⁻¹, due to $\nu_{\text{asym}}(\text{O}=\text{U}=\text{O})$ and $\nu_{\text{sym}}(\text{O}=\text{U}=\text{O})$, respectively, indicate the presence of *trans*-[U^{VI}O₂] structure [19]. Thus, the spectral data confirms the coordination of the ligand to the metal in both complexes.

Table 4.3. IR spectral data (cm^{-1}) of ligand and complexes.

Compound	$\nu(\text{O-H})$	$\nu(\text{C-N})$	$\nu(\text{CH}_2)$	$\nu_{\text{asym}}(\text{O}=\text{M}=\text{O})$	$\nu_{\text{sym}}(\text{O}=\text{M}=\text{O})$
$\text{H}_2\text{pip-2,4-dmp}$ (4.1)	3440	1156	2932		
$[\text{Mo}^{\text{VI}}\text{O}_2(\text{pip-2,4-dmp})]$ (4.1)		1162	2923	944	906
$[\text{U}^{\text{VI}}\text{O}_2(\text{pip-2,4-dmp})(\text{MeOH})]$ (4.2)	3428	1150	2928	900	859

4.3.4. UV-Vis spectral study

Fig. 4.4 presents UV-visible spectra of ligand and complexes and Table 4.4 provides absorption *maxima* of ligands and complexes along with their extinction coefficients. The ligand shows three bands at 223, 286 and 330 nm in the UV region. Based on their molar extinction coefficient, the first band at 223 nm is assigned due to $\sigma \rightarrow \sigma^*$ transition whereas the band at 286 nm is due to $\pi \rightarrow \pi^*$ transition. The low intensity band at 330 nm is due to $n \rightarrow \pi^*$ transition. The 330 nm band shifts to higher wavelength i.e. at 353 and 389 nm in $[\text{Mo}^{\text{VI}}\text{O}_2(\text{Pip-2,4-dmp})]$ (**4.1**) and $[\text{U}^{\text{VI}}\text{O}_2(\text{pip-2,4-dmp})(\text{MeOH})]$ (**4.2**), respectively. An additional band at 425 nm in **4.1** arises due to the ligand to metal charge transfer from the filled π orbital of ligand to the vacant d orbital of the metal while such band at 510 nm in **4.2** is due to ${}^1\varepsilon_g^+ \rightarrow {}^3\pi_u$ transition [19,155].

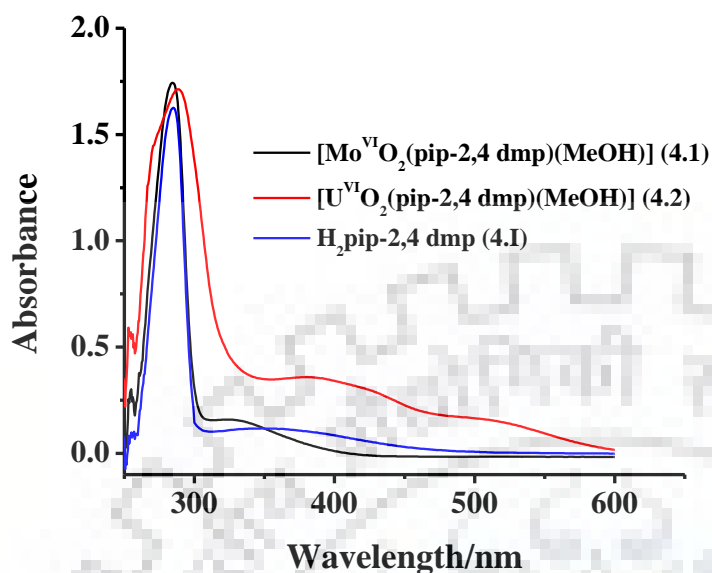


Fig. 4.4. UV-Visible spectra of $H_2pip-2,4$ dmp and complexes, $[Mo^{VI}O_2(pip-2,4$ dmp)(MeOH)] (4.1) and $[U^{VI}O_2(pip-2,4$ dmp)(MeOH)] (4.2) recorded in MeCN.

Table 4.4. UV-visible spectral data of ligand and complexes.

Compound	Solvent	λ (nm) ($\epsilon/M^{-1}cm^{-1}$)
$H_2Pip-2,4-dmp$ (4.I)	MeOH	223(682), 286(1252), 330(370)
$[Mo^{VI}O_2(pip-2,4-dmp)]$ (4.1)	MeOH	291(2072), 353(51), 425(110)
$[U^{VI}O_2(pip-2,4-dmp)(MeOH)]$ (4.2)	MeOH	222(690), 284(1812), 389(399), 510(178)

4.3.5. 1H NMR spectral study

The 1H NMR spectra of ligand and metal complexes were recorded in $CDCl_3$. The relevant spectral data are presented in Table 4.5 and spectra are accessible in the supporting information (Figs. 4.5 - 4.7). Ligand 4.I exhibits a broad band at 10.5 ppm due to phenolic protons and absence of this band in the spectra of complexes suggests coordination of phenolic oxygen to the metal after proton replacement. An up field shift of signals due to

-NCH₂ (piperazine) from 2.67 ppm (s, 8H) to 1.26 ppm (in **4.1**) and 2.15 ppm (in **4.2**) occurs which is possibly due to adjustment of ring current upon coordination of ring nitrogen to the metal. As expected signals due to aromatic, methylene and methyl protons are not much affected and appear at their expected positions.

Table 4.5. ¹H NMR (δ in ppm) of ligand and metal complexes.

Compound	OH	Aromatic H	-CH ₂	-CH ₃	-NCH ₂ (piperazine)
H ₂ pip-2,4-dmp (4.1)	10.5(2H)	6.63 (s, 2H), 6.87 (s, 2H)	3.66(s,4H)	2.21(s, 6H), 2.20(s, 6H)	2.67(s, 8H)
[Mo ^{VI} O ₂ (pip-2,4-dmp)] (4.1)	-	6.83 (s, 2H), 6.63 (s, 2H)	3.66(s,4H)	2.21(s, 6H), 2.19(s, 6H)	1.26(s, 8H)
[U ^{VI} O ₂ (pip-2,4-dmp)(MeOH)] (4.2)	-	6.84(s, 2H), 6.72 (s, 2H)	3.68(b,4H)	2.10(s, 6H), 2.08(s, 6H)	2.15(s, 8H)

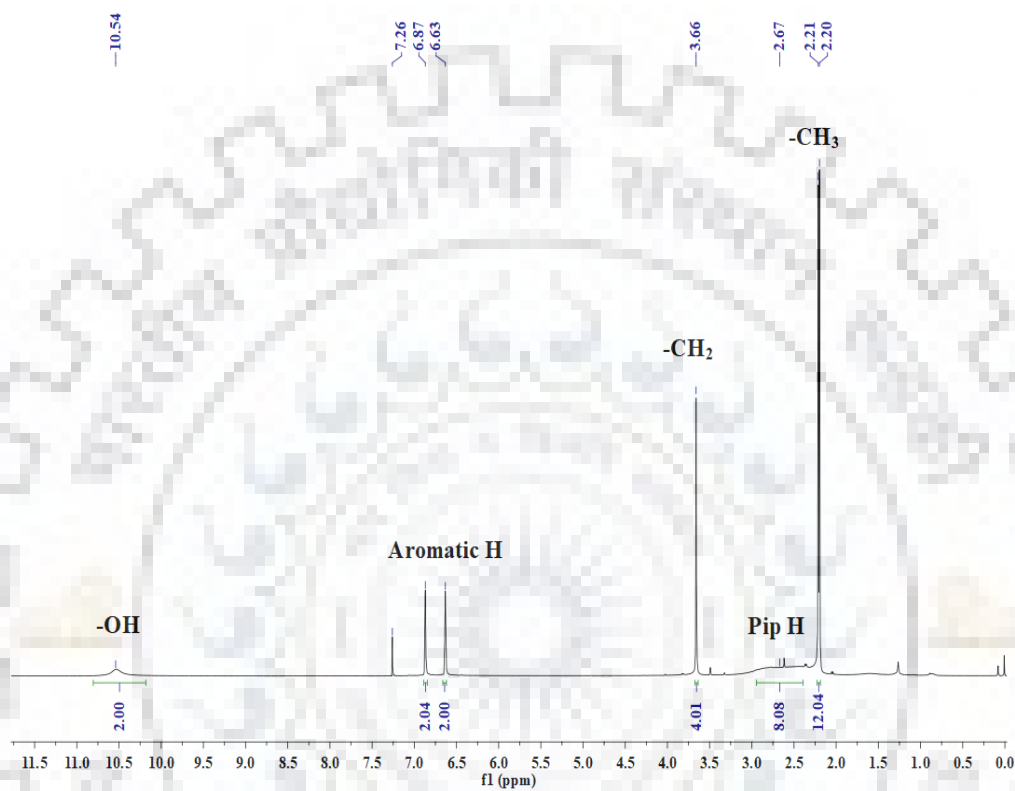


Fig. 4.5. ^1H NMR spectrum of ligand, $\text{H}_2\text{pip-2,4-dmp}$ (4.I).

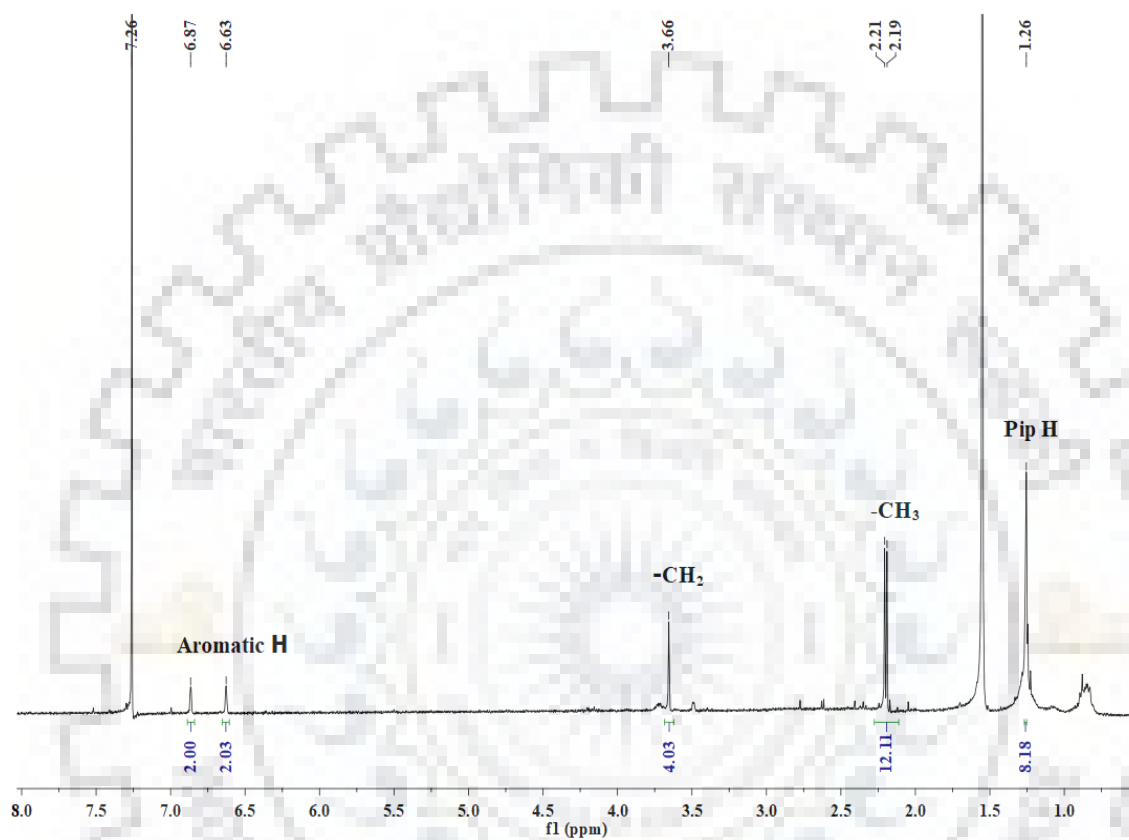


Fig. 4.6. ^1H NMR spectrum of $[\text{Mo}^{\text{VI}}\text{O}_2(\text{pip-2,4-dmp})]$ (4.1).

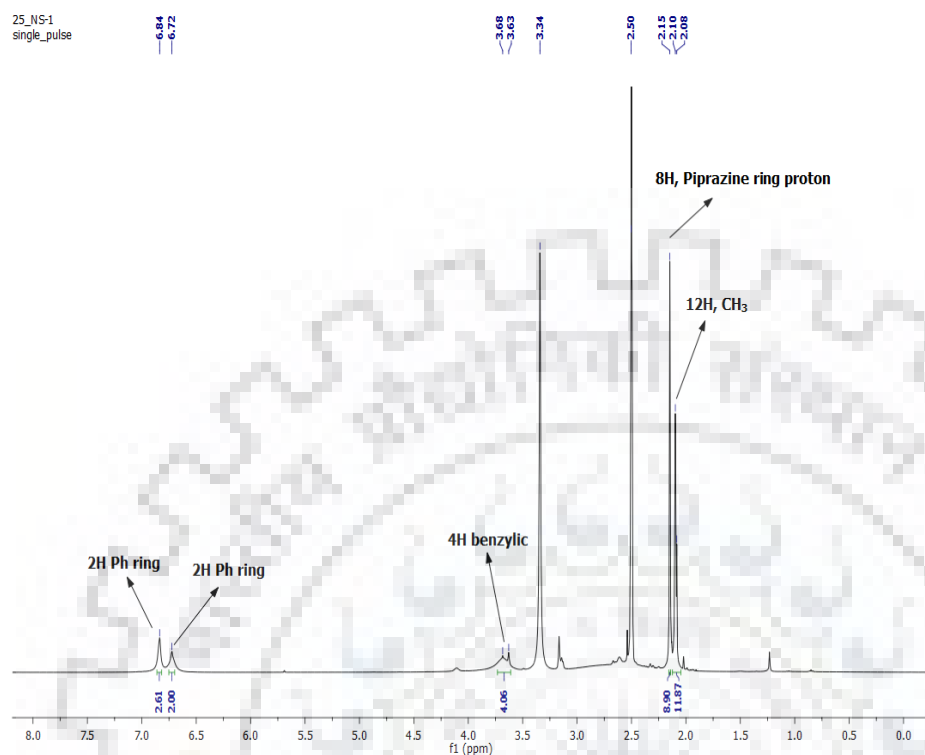


Fig. 4.7. ¹H NMR spectrum of [U^{VI} O₂ (pip-2,4-dmp)(MeOH)] (4.2).

4.3.6. ¹³C NMR spectral study

We have also recorded ¹³C NMR of ligand and complexes (Table 4.6) to ascertain the binding modes of the ligand towards complexes. The representative spectra (ligand and uranium complex) are presented in Fig. 4.8. The spectra recorded in DMSO-d₆ show considerable coordination-induced ¹³C NMR chemical shifts { $\Delta\delta = [\delta(\text{complex}) - \delta(\text{ligand})]$ } for those carbon atoms that are in the vicinity of the coordinating atoms like, C₁/C₁' (the carbon atoms close to phenolic oxygen), C₇/C₇' and C₈/C₈' (the carbon atoms close to the ring nitrogen). Even carbon atoms C₆/C₆' of benzene ring which are attached to C₇/C₇' are also affected. All these information supplement the conclusion drawn from ¹H NMR data. Other signals of ligand and complexes appear well within the expected region. We could not observe the signal due to methyl carbon of coordinated methanol in

complex **4.2**, possibly due to exchange of methanol with DMSO while recording the spectrum.

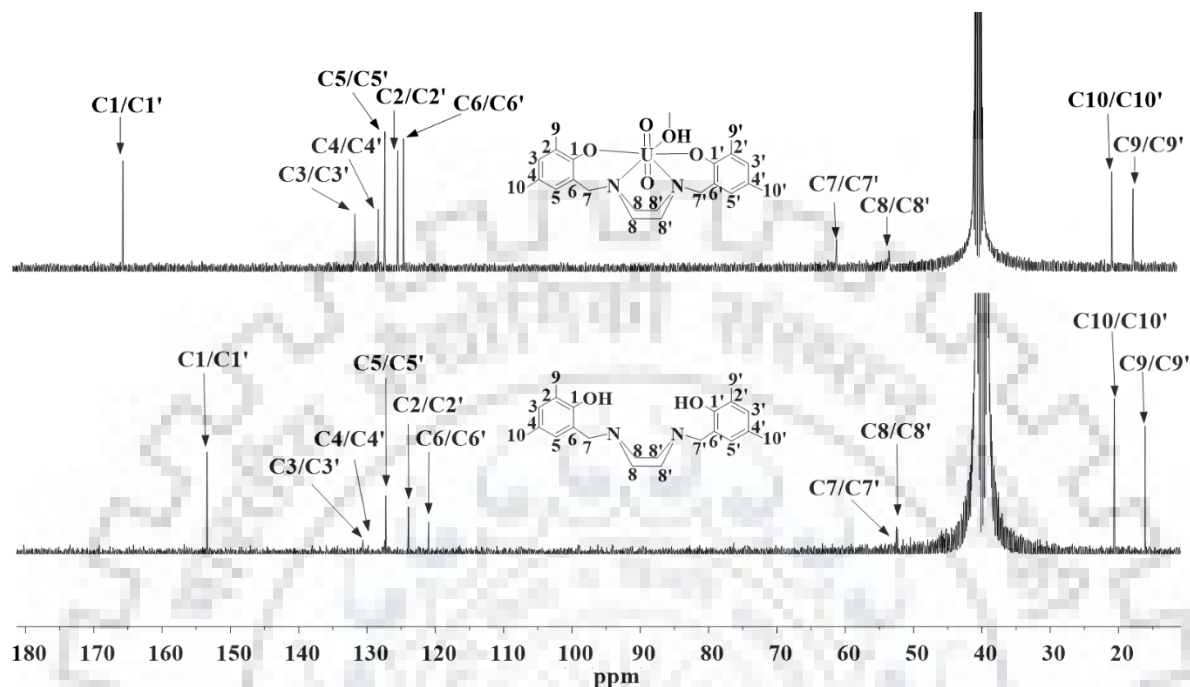


Fig. 4.8. ^{13}C NMR spectra of $\text{H}_2\text{pip-2,4-dmp}$ (**4.1**) and $[\text{U}^{\text{VI}}\text{O}_2(\text{pip-2,4-dmp})(\text{MeOH})]$ (**4.2**).

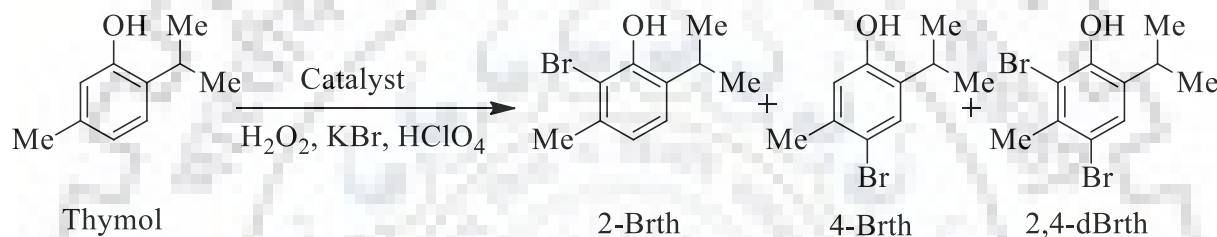
Table 4.6. ^{13}C NMR data (δ in ppm) of ligand and metal complexes.

Compound ^a										
	C ₁ /C ₁ '	C ₂ /C ₂ '	C ₃ /C ₃ '	C ₄ /C ₄ '	C ₅ /C ₅ '	C ₆ /C ₆ '	C ₇ /C ₇ '	C ₈ /C ₈ '	C ₉ /C ₉ '	C ₁₀ /C ₁₀ '
$\text{H}_2\text{Pip-2,4-dmp}$ (4.1)	153.4	123.9	131.0	129.8	127.3	121.0	52.6	52.3	16.1	20.6
$[\text{Mo}^{\text{VI}}\text{O}_2(\text{pip-2,4-dmp})]$ (4.1)	153.3	121.8	133.9	128.3	127.6	117.5	60.5	54.7	16.2	20.6
($\Delta\delta$)	(-0.1)					(-3.5)	(7.9)	(2.4)		
$[\text{U}^{\text{VI}}\text{O}_2(\text{pip-2,4-dmp})(\text{MeOH})]$ (4.2)	164.9	124.8	131.1	127.7	126.7	124.0	60.7	53.0	17.3	20.5
($\Delta\delta$)	(11.5)					(3.0)	(8.1)	(0.7)		

^a $\Delta\delta = [\delta(\text{complex}) - \delta(\text{free ligand})]$.

4.3.7. Catalytic activity study: Oxidative bromination of thymol

The oxidative bromination of thymol catalyzed by the metal complexes has been carried out using KBr, 30 % aqueous H₂O₂ and 70 % aqueous HClO₄ in aqueous medium. Acid is required to proceed the reaction. The electrophilic aromatic substitution in the phenolic ring led the bromination of thymol and formation of two isomers, 2-bromothymol and 4-bromothymol and further bromination of the *ortho/para* isomer led the formation of 2,4-dibromothymol (Scheme 4.2). Among these products, 2,4-dibromothymol was found in the highest yield, possibly because of the further bromination of the monobromo product(s).



Scheme 4.2. Products of the oxidative bromination of thymol. 2-Brth = 2-bromothymol, 4-Brth = 4-bromothymol, 2,4-dBrth = 2,4-dibromothymol.

To obtain the maximum yield of brominated products for both the catalysts, several parameters, such as, amounts of catalyst, 30% H₂O₂, KBr, and 70% HClO₄, were varied separately for both of them at room temperature. We have first optimized the reaction conditions considering different amounts of catalyst, H₂O₂, KBr and HClO₄ using [Mo^{VI}O₂(pip-2,4-dmp)] (**4.1**) as a catalyst. Thus, for 10 mmol (1.50 g) of thymol, three different amounts of catalyst viz. 0.001, 0.002 and 0.003 g and 1 : 1, 1 : 2 and 1 : 3 ratios each for substrate : H₂O₂, substrate : KBr and substrate : HClO₄ were taken in 20 mL water and the reaction was carried out at room temperature for 2 h. It was observed that HClO₄ added at a time in case of 20 and 30 mmol led to the partial decomposition of catalyst, therefore, in these cases HClO₄ was added in two and three equal portions, respectively, to the reaction mixture, first portion at t = 0 and other one/two portions after every 30 min intervals. Figs. 4.9 – 4.12 present time on analysis for different conditions and Table 4.7

summarizes details of all reaction conditions and the conversion of thymol at 2 h of reaction time.

As accessible in Table 4.7, the optimized reaction condition for the maximum conversion of 10 mmol (1.50 g) of thymol using **4.1** as catalyst is as presented in entry 8 i.e. those using catalyst : H₂O₂ : KBr : HClO₄ ratios (in mmol) of 10 : 4.16 × 10⁻³ : 10 : 20. Under these conditions a maximum of 99% conversion of thymol was achieved where products 2-bromothymol, 4-bromothymol and 2,4-dibromothymol with the percentage selectivity of 1, 2 and 97, respectively were obtained. Turn over frequency calculated at 2 h of reaction is 1198 h⁻¹ for this condition. Higher amount of KBr (30 mmol) and lower amount of acid (10 mmol) favors the formation of monobromo derivatives (see entry 7) to some extent while higher amount of acid (30 mmol) and lower amount (10 mmol) of KBr favors the formation of dibromo derivative (entry 9). However, at any reaction conditions (Table 4.7), the yield of 2,4-dibromo derivative is always higher. Further, no trace of substrate was observable in GC profile under the conditions mentioned in entry 9 of Table 4.7, suggesting the complete conversion of thymol to products. Blank reaction i.e. without catalyst but in the presence of substrate : H₂O₂ : KBr : HClO₄ ratios (in mmol) of 10: 10 : 10 : 20, a maximum of 45% conversion was noted, therefore the catalyst enhances the conversion of thymol.

Table 4.7. Conversion of 10 mmol (1.50 g) of thymol using [Mo^{VI}O₂(pip-2,4-dmp)] (**4.1**) complex as a catalyst precursor for 2h of reaction time under different reaction conditions.

Sr. No.	KBr [g(mmol)]	H ₂ O ₂ [g (mmol)]	HClO ₄ [g (mmol)]	Catalyst [mg (mmol)]	Conv. (%)	TOF	2-Brth	4-Brth	2,4-dBrth
1	1.19 (10)	1.13 (10)	1.43 (10)	1.0(2.08 × 10 ⁻³)	69	1658	10	22	67
2	1.19 (10)	1.13 (10)	1.43 (10)	2.0(4.16 × 10 ⁻³)	95	1141	10	21	69
3	1.19 (10)	1.13 (10)	1.43 (10)	3.0(6.24 × 10 ⁻³)	85	681	10	33	57
4	1.19 (10)	2.27 (20)	1.43 (10)	2.0(4.16 × 10 ⁻³)	79	949	12	18	69
5	1.19 (10)	3.39 (30)	1.43 (10)	2.0(4.16 × 10 ⁻³)	59	709	10	29	59
6	2.38 (20)	1.13 (10)	1.43 (10)	2.0(4.16 × 10 ⁻³)	90	1081	8	17	73
7	3.57 (30)	1.13 (10)	1.43 (10)	2.0(4.16 × 10 ⁻³)	92	1105	16	24	59
8	1.19 (10)	1.13 (10)	2.86 (20)	2.0(4.16 × 10 ⁻³)	99	1189	1	2	97
9	1.19 (10)	1.13 (10)	4.29 (30)	2.0(4.16 × 10 ⁻³)	100	1201	-	1	99
10	1.19 (10)	1.13 (10)	4.29 (30)	-	45	-	35	5	60

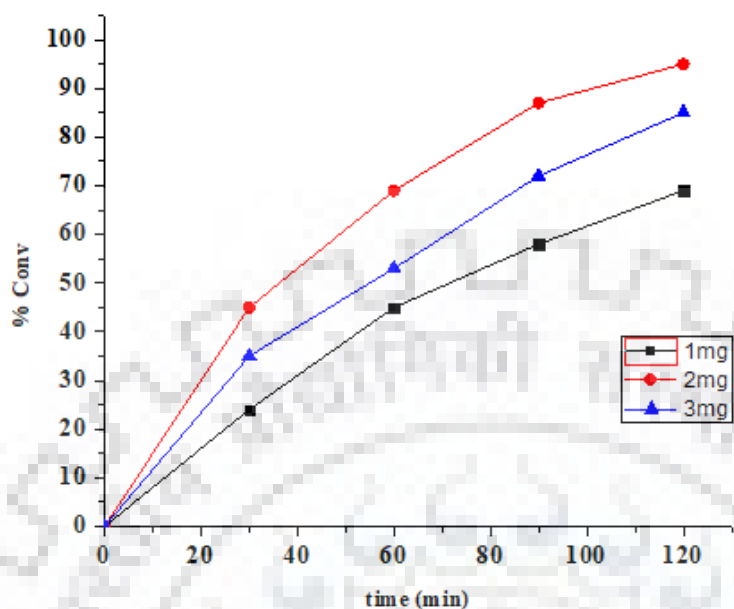


Fig. 4.9. Conversion of 10 mmol of thymol with varying amounts of $[\text{Mo}^{\text{VI}}\text{O}_2(\text{pip-2,4-dmp})]$ (**4.1**). Other reaction conditions (in mmol), substrate : H_2O_2 : KBr : HClO_4 ratios of 10 : 10 : 10 : 10.

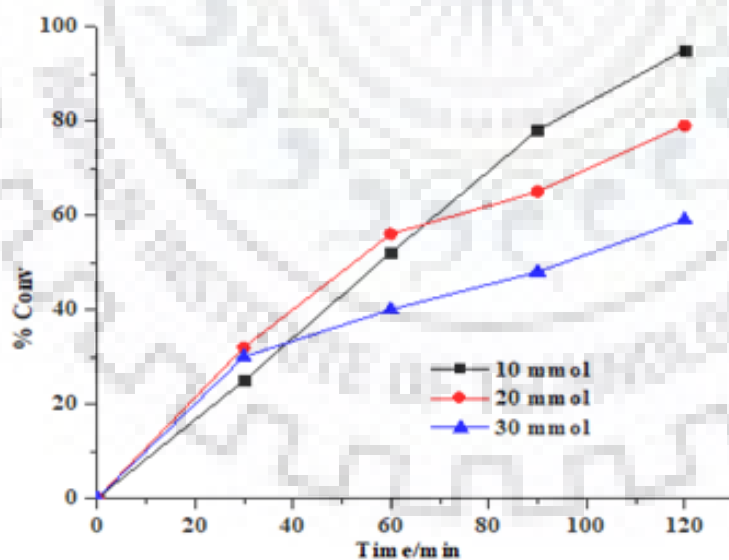


Fig. 4.10. Effect of oxidant on the oxidative bromination of 10 mmol of thymol using $[\text{Mo}^{\text{VI}}\text{O}_2(\text{pip-2,4-dmp})]$ (**4.1**) as catalyst. Other reaction conditions (in mmol), substrate : catalyst : KBr : HClO_4 ratios of 10 : 4.16×10^{-3} : 10 : 10.

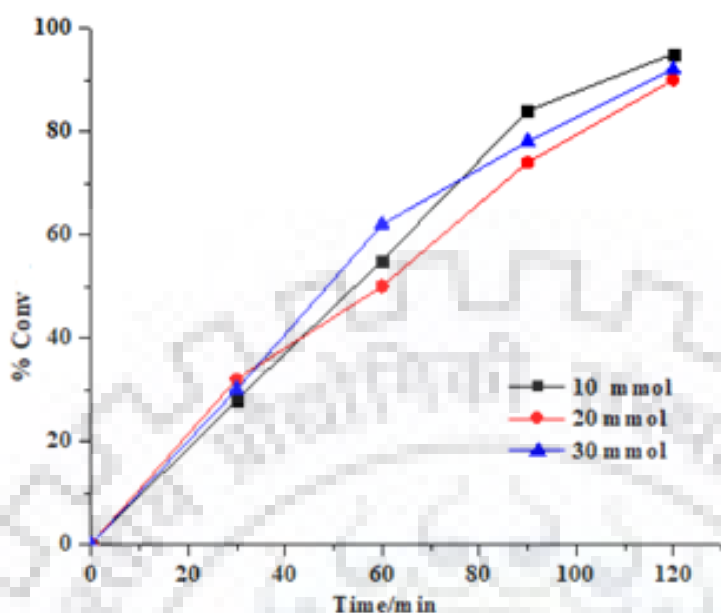


Fig. 4.11. Effect of variation of KBr on the oxidative bromination of thymol using $[\text{Mo}^{\text{VI}}\text{O}_2(\text{pip-2,4-dmp})]$ (**4.1**) complex as catalyst. Other reaction conditions (in mmol), substrate : oxidant : catalyst : HClO_4 ratios of 10 : 10 : 4.16×10^{-3} : 10.

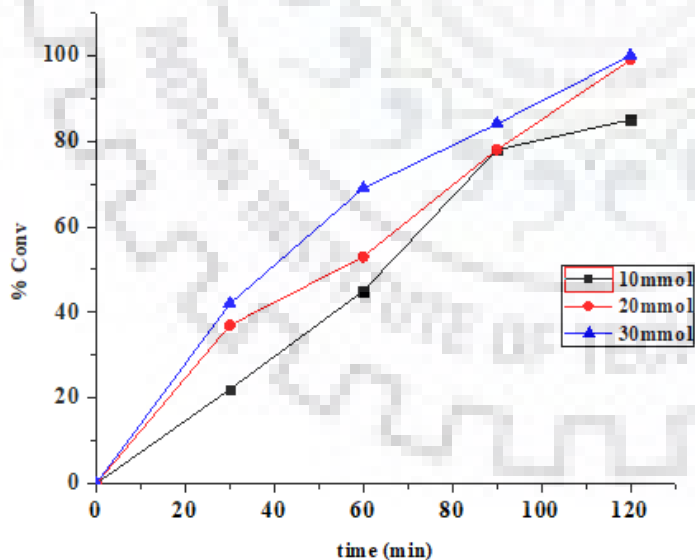


Fig. 4.12. Effect of variation of HClO_4 on the oxidative bromination of thymol using $[\text{Mo}^{\text{VI}}\text{O}_2(\text{pip-2,4-dmp})]$ (**4.1**) complex as catalyst. Other reaction conditions (in mmol), substrate : oxidant : catalyst : KBr ratios of 10 : 10 : 4.16×10^{-3} : 10 : 10.

We have also optimized all reaction parameters mentioned above in 20 mL water for catalyst (4.2). In this case also reaction acquires equilibrium in 2 h of reaction time at room temperature. Figs. 4.13 – 4.16 present time on analysis of conversion of thymol under various reaction conditions and Table 4.8 summarizes all the reactions conditions studied and the corresponding percentage of oxidative bromination of thymol along with TOF and the selectivity of different reaction products. Data presented in Table 4.8 again prove that the conversions and the selectivity of products differ on varying the reagents and the best reaction conditions (entry 10) for the maximum oxidative bromination of 10 mmol of thymol with 92% conversion are: catalyst (0.003 g, 4.8×10^{-3} mmol), H_2O_2 (3.39 g, 30 mmol), KBr (1.19 g, 10 mmol) and HClO_4 (4.29 g, 30 mmol) in 20 mL water i.e. substrate : oxidant : catalyst : KBr : HClO_4 ratios (in mmol) of 10 : 30 : 4.8×10^{-3} : 10 : 30. Under these conditions, only two products, 4-bromothymol and 2,4-dibromothymol with the selectivity percent of 1 and 99% were obtained. Turn over frequency calculated at 2 h under this condition is 956 which is much less than that obtained for molybdenum catalyst. The overall conversion is also less than molybdenum complex.

Table 4.8. Conversion of 10 mmol (1.5 g) thymol using $[\text{U}^{\text{VI}}\text{O}_2(\text{pip-2,4-dmp})(\text{MeOH})]$ (4.2) as a catalyst for 2 h of reaction time under different reaction conditions.

Sr. No.	KBr [g (mmol)]	H_2O_2 [g (mmol)]	HClO_4 [g (mmol)]	Catalyst [mg (mmol)]	Conv (%)	TOF (h^{-1})	2-Brth	4-BrTh	2,4-dBrth
1	1.19 (10)	1.13 (10)	1.43 (10)	0.5 (8.03×10^{-4})	57	3549	13	4	82
2	1.19 (10)	1.13 (10)	1.43 (10)	1.0 (1.60×10^{-3})	62	1937	10	9	80
3	1.19 (10)	1.13 (10)	1.43 (10)	2.0 (3.2×10^{-3})	57	890	11	3	85
4	1.19 (10)	1.13 (10)	1.43 (10)	3.0 (4.8×10^{-3})	80	831	6	14	78
5	1.19 (10)	2.27 (20)	1.43 (10)	3.0 (4.8×10^{-3})	82	852	13	15	71
6	1.19 (10)	3.39 (30)	1.43 (10)	3.0 (4.8×10^{-3})	88	914	8	43	48
7	2.38 (20)	3.39 (30)	1.43 (10)	3.0 (4.8×10^{-3})	87	904	4	17	78
8	3.57 (30)	3.39 (30)	1.43 (10)	3.0 (4.8×10^{-3})	86	893	10	18	72
9	2.38 (20)	3.39 (30)	2.86 (20)	3.0 (4.8×10^{-3})	90	935	-	4	96
10	2.38 (20)	3.39 (30)	4.29 (30)	3.0 (4.8×10^{-3})	92	956	-	1	99
12	2.38 (20)	3.39 (30)	4.29 (30)	-	42	-	35	31	44

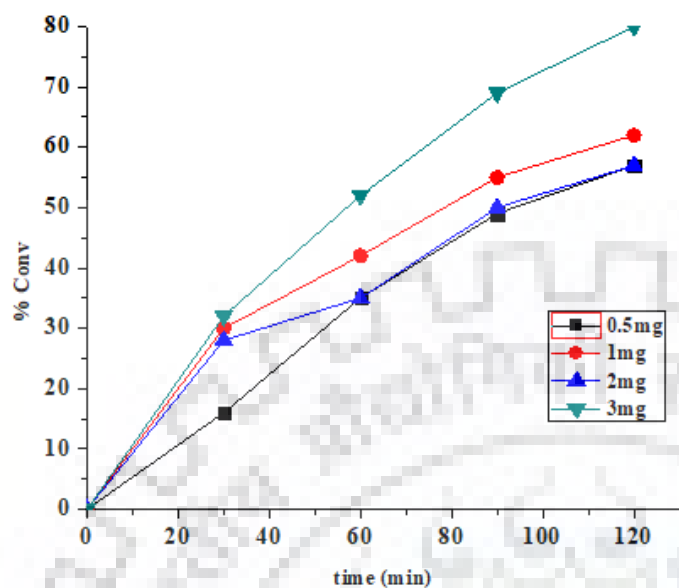


Fig. 4.13. Conversion of thymol with varying amounts of $[U^{VI}O_2(\text{pip-2,4-dmp})(\text{MeOH})]$ (4.2) as catalyst. Other reactions, Other reaction conditions (in mmol), substrate : H_2O_2 : KBr : $HClO_4$ ratios of 10 : 10 : 10 : 10.

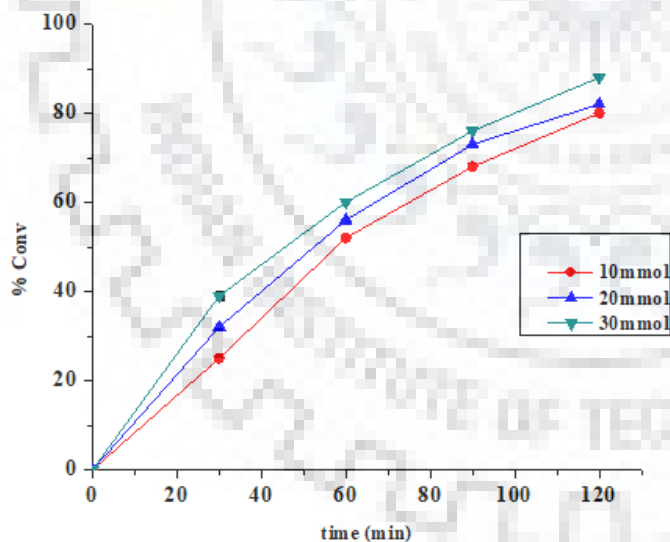


Fig. 4.14. Effect of oxidant on the oxidative bromination of thymol using $[U^{VI}O_2(\text{pip-2,4-dmp})(\text{MeOH})]$ (4.2) as a catalyst. Other reaction conditions (in mmol), substrate : catalyst : KBr : $HClO_4$ ratios of 10 : 4.8×10^{-3} : 10 : 10.

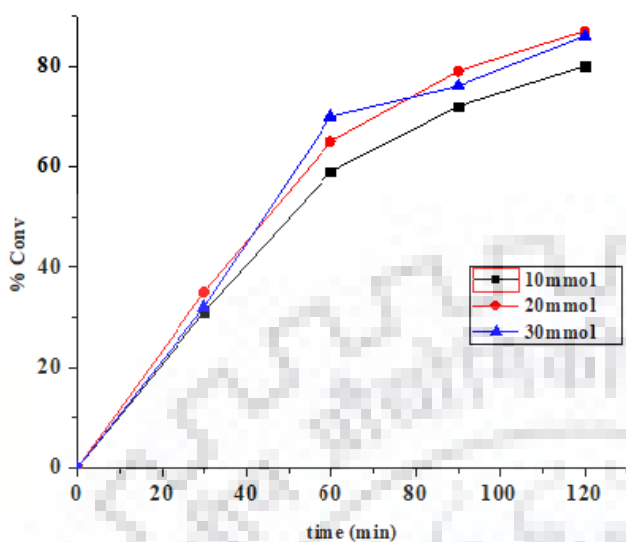


Fig. 4.15. Effect of variation of KBr on the oxidative bromination of thymol using $[U^{VI}O_2(\text{pip-2,4-dmp})(\text{MeOH})]$ (**4.2**) as catalyst. Other reaction conditions (in mmol), substrate : catalyst : KBr : HClO_4 ratios of 10 : 4.8×10^{-3} : 10 : 10.

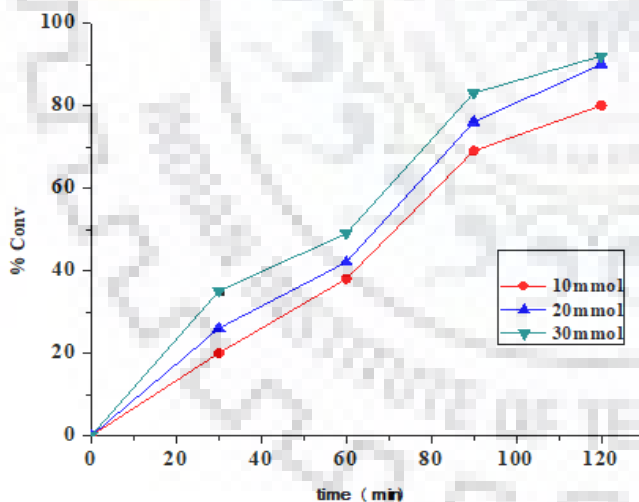


Fig. 4.16. Effect of variation of HClO_4 on the oxidative bromination of thymol using $[U^{VI}O_2(\text{pip-2,4-dmp})(\text{MeOH})]$ (**4.2**) complex as catalyst. Other reaction conditions (in mmol), substrate : oxidant : catalyst : KBr ratios of 10 : 4.8×10^{-3} : 10 : 10.

The catalytic oxidative bromination of uranium complex is relatively low but of molybdenum complex reported here is very well comparable with those reported for

dioxidomolybdenum(VI) complexes (94-99%) of Schiff base ligands derived from 8-formyl-7-hydroxy-4-methylcoumarin and hydrazides [103]. However, the selectivity of 2,4-dibromothymol varies within these two complexes reported here as well as within those reported in literature. The vanadium complex $[V^VO(OMe)(MeOH)(L)]$ [$H_2L = 6,6'-(2-(pyridin-2-yl)ethylazanediyl)bis(methylene)bis(2,4-di-tert-butylphenol)$] under the optimised reaction conditions (i.e. substrate : H_2O_2 : KBr : $HClO_4$ of 1 : 2 : 2 : 2 for 10 mmol of thymol) gave as high as 99% conversion with 57 % selectivity towards 2,4-dibromothymol, followed by 37% towards the 4-bromothymol and rest towards 2-bromothymol isomer [138]. Complexes, $[W^{VI}O_2(hap-hyz)(MeOH)]$ ($H_2hap-hyz =$ Schiff bases derived from 2-hydroxy acetophenone and hydrazides) show conversion between 91-96% [156] which is again better than uranium complex but almost same like molybdenum complex.

4.3.8. Reactivity of uranium complex with H_2O_2 and possible reaction mechanism

As observed in *cis*- $[MO_2]$ - complexes ($M = V, Mo$) [54, 163], KBr in the presence of H_2O_2 and $HClO_4$, catalytically generate HOBr and/or Br^+ , Br_2 , which are the brominating reagent for the substrates. Conte *et al.* have identified an oxidomonoperoxidovanadium(V) complex as the oxidant of the Br^- ion to HOBr/ Br_2 by spectroscopic techniques [160]. It was also observed recently by ^{51}V NMR study that the $[VO(O_2)(L)]$ -type species is an active intermediate during catalytic study of oxidative bromination of thymol in the presence of oxidant H_2O_2 [138]. In order to generate information for such an intermediate in *trans*- $[UO_2]$ -complexes, we have also treated uranium complex **4.2** with H_2O_2 and monitored the changes by UV-Vis spectroscopy. Thus, the successive addition of one drop portion of 30% H_2O_2 (0.108 g, 0.95 mmol) dissolved in 5 mL of MeCN to 25 mL of 4.8×10^{-3} M solution of **4.2** in MeCN resulted in the continuous decrease in the intensity of 502 and 383 nm bands to almost flat (Fig. 4.17). The UV region (not shown here) is not much affected. These spectral changes suggest the reaction of H_2O_2 with uranium complex and the formation of possibly peroxido species in solution. Such peroxido intermediate, as observed in vanadium and molybdenum complexes, is responsible for the generation of brominating reagent from KBr catalytically.

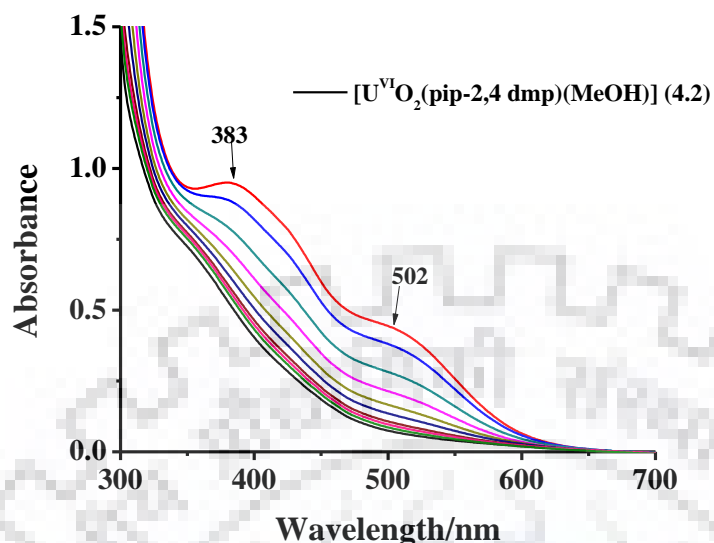


Fig. 4.17. Plots representing the spectral changes observed during the titration of $[\text{U}^{\text{VI}}\text{O}_2(\text{pip-2,4 dmp})(\text{MeOH})]$ (**4.2**) with H_2O_2 . Spectra were obtained after successive addition of one drop portion of 30% H_2O_2 (0.108 g, 0.95 mmol) dissolved in 5 mL of MeCN to 25 mL of 4.8×10^{-3} M solution of **4.2** in MeCN.

4.4. Conclusions

Dioxidomolybdenum (VI) and dioxidouranium (VI) complexes of piperazine derived tetradentate (ONNO) donor ligand, bis{(2,4-dmp)CH₂}(μ₂-piperazine)] ($\text{H}_2\text{pip-2,4-dmp}$) were prepared successfully and characterized by UV, IR, NMR, elemental analysis and TGA, and single crystal X-ray study of uranium complex. Based on the characterization data it has been concluded that molybdenum in complex $[\text{Mo}^{\text{VI}}\text{O}_2(\text{pip-2,4-dmp})]$ is hexacoordinated while uranium in $[\text{U}^{\text{VI}}\text{O}_2(\text{pip-2,4-dmp})(\text{MeOH})]$ is hepta-coordinated. The catalytic activity of these complexes for the oxidative bromination of thymol, a reaction generally observed by vanadium dependent halo peroxidases, was studied by gas chromatography and it has been observed that these complexes show very good conversion and enhanced selectivity towards the products in the order: 2,4-dibromothymol > 4-bromothymol > 2-bromothymol, under the optimized reaction conditions. Thus, these complexes mimic similar catalytic reactivity as shown by vanadium based halo peroxidases.